

**THE SYNTHESIS AND KINETIC EVALUATION OF LYSOSOMOTROPIC SUBSTRATE-BASED PROBES  
FOR CATHEPSINS B AND L**

By

Brady Garitt Vigliarolo

A thesis submitted to

The Department of Chemistry

Faculty of Science and Environmental Studies, Lakehead University

in partial fulfillment of the requirements for the degree of

Master of Science

August 2014

© Brady Garitt Vigliarolo, 2014

## Abstract

Members of the cathepsin family of cysteine proteases are gaining interest as potential imaging biomarkers and drug targets due to their multifunctional roles in a range of diseases such as cancer, asthma and arthritis. Cathepsins are also involved in important regulatory processes such as cell recycling, prohormone activation, and wound healing. Developing imaging agents with the ability to assess cathepsin activity *in vivo* is important for identifying the specific roles these enzymes have in disease processes. We report here novel prodrug-inspired probes for Cathepsins B and L that employ weakly basic aminoquinoline reporter groups intended to be lysosomotropic once released from the enzyme, meaning they are expected to be retained in the acidic lysosome where the majority of cysteine cathepsins are primarily active. To evaluate this approach to probe design we first synthesized a series of prodrug inspired substrates using the self-immolative linker *p*-aminobenzyl alcohol conjugated to four different aminoquinolines as potential reporters of enzyme activity. We then developed a convenient HPLC method to estimate  $k_{\text{cat}}/K_{\text{M}}$  values for well-established fluorogenic substrates to first validate our new HPLC method. Once a reliable HPLC method was developed for fluorogenic substrates consistent with data obtained on a plate reader, we then determined  $k_{\text{cat}}/K_{\text{M}}$  values for all novel quinoline-based probe candidates. All compounds were excellent substrates of both CTB and CTL, and three candidates were hydrolyzed with particularly efficient  $k_{\text{cat}}/K_{\text{M}}$  values by CTL. This suggests that efficiently hydrolyzed prodrug-inspired probes bearing aminoquinoline reporters could potentially be adapted into substrate-based PET imaging agents which offer an amplification of signal and reporter immobilization in the lysosomes of cancer cells overexpressing CTL.

## Acknowledgements

Endless thanks and appreciation is extended to Dr. Chris Phenix, who has been a source of inspiration and support while being a fantastic supervisor. His passion, patience, and knowledge have been essential throughout this process - my gratitude and admiration are lifelong. I would also like to thank Dr. Morshed Chowdhury and Dr. Ignace Moya for providing synthetic and enzymatic expertise crucial in developing and assaying the novel probe candidates. I have also had the opportunity to work alongside other great coworkers, namely Ben Adams and Dr. Shusheng Wang, who have been helpful and friendly while in the lab. I am thankful for being part of such a supportive Chemistry Department; in particular I would like to thank my committee Dr. Christine Gottardo and Dr. Justin Jiang for their knowledge, support and feedback. TBRRRI has been an incredible place to work due to the culture and interdisciplinary nature of the scientists. I would also like to thank the Canadian Cancer Society and NSERC-cMIP for the opportunities to attend conferences and workshops pertaining to cancer research and PET imaging. Importantly, I would like to thank my mother, father, and brother for their love and support when away from the lab and school.

# Table of Contents

|   |             |
|---|-------------|
| <b>Abstract</b> .....   | <b>ii</b>   |
| <b>Acknowledgements</b> .....                                     | <b>iii</b>  |
| <b>Table of Contents</b> .....                                    | <b>iv</b>   |
| <b>List of Tables</b> .....                                       | <b>vi</b>   |
| <b>List of Figures</b> .....                                      | <b>vii</b>  |
| <b>List of Schemes</b> .....                                      | <b>viii</b> |
| <b>Chapter 1: Introduction</b> .....                              | <b>1</b>    |
| <b>Chapter 2: Literature Review</b> .....                         | <b>2</b>    |
| 2.1: Molecular Imaging .....                                      | 2           |
| 2.1.1: Overview .....   | 2           |
| 2.1.2: Nuclear Imaging and PET .....                              | 3           |
| 2.1.3: PET Imaging Agents and Applications.....                   | 5           |
| 2.2: Cysteine Cathepsins as Biomarkers for Aggressive Cancer..... | 10          |
| 2.2.1: Proteases and Cysteine Cathepsins .....                    | 10          |
| 2.2.2: Cathepsin B and Aggressive Cancer .....                    | 14          |
| 2.2.3: Cathepsin B as a Targeted Biomarker .....                  | 16          |
| 2.2.4: Our Approach to Imaging Cathepsins .....                   | 22          |
| 2.3: Summary and Scope of Project.....                            | 29          |
| 2.4: References .....   | 30          |
| <b>Chapter 3: Methodology</b> .....                               | <b>42</b>   |
| 3.1: Synthesis of Probe Candidates.....                           | 42          |
| 3.2: Kinetic Evaluation of Probe Candidates.....                  | 47          |
| 3.3: References .....   | 51          |
| <b>Chapter 4: Manuscript</b> .....                                | <b>53</b>   |
| 4.1: Abstract.....  | 53          |
| 4.2: Introduction .....   | 54          |
| 4.3: Results and discussion .....                                 | 58          |
| 4.3.1: Probe Design .....   | 58          |
| 4.3.2: Synthesis .....  | 62          |

|   |            |
|---|------------|
| 4.3.3: Enzymatic Assays .....                       | 64         |
| 4.4: Conclusions .....                              | 74         |
| 4.5: Experimental .....                             | 75         |
| 4.7: References .....                               | 78         |
| Supporting Information .....                        | 82         |
| <b>Chapter 5: Conclusions and Future Work .....</b> | <b>112</b> |

## List of Tables

|  |    |
|--|----|
| Table 1: Structures and yields for the deprotected probe candidates.....                       | 64 |
| Table 2: Kinetic results for novel probe candidates and commercial fluorogenic substrates..... | 73 |

## List of Figures

|  |    |
|--|----|
| Figure 1: Imaging glucose metabolism using FDG-PET .....   | 9  |
| Figure 2: Schechter and Berger nomenclature for a protease active site and complimentary substrate. 12                               | 12 |
| Figure 3: The role of Cathepsins B and L at the invading edge of an aggressive tumor .....   | 16 |
| Figure 4: Lysosomotropism of a lipophilic amine .....  | 21 |
| Figure 5: Prodrug-inspired substrate based approach for cathepsin probes .....   | 23 |
| Figure 6: The general structure of the novel prodrug-inspired probe candidates reported herein .....                                 | 24 |
| Figure 7: The four quinoline isomers used as reporter groups in our substrate-based probes .....                                     | 28 |
| Figure 8: Michaelis-Menten curve .....   | 49 |
| Figure 9: Prodrug-inspired substrate based approach for CTB and CTL probes.....  | 59 |
| Figure 10: The general structure of the novel prodrug-inspired probe candidates reported herein .....                                | 60 |
| Figure 11: The four quinoline isomers used as reporter groups in our substrate-based probes .....                                    | 62 |
| Figure 12: Comparative results of the CTB plate reader assay and HPLC estimation .....   | 67 |
| Figure 13: Comparative results of the CTL plate reader assay and HPLC estimation .....   | 68 |
| Figure 14: Linear relationship between Cathepsin concentration and initial velocity of commercial and quinoline substrates.....      | 70 |
| Figure 15: Linear fits of $v_0/[S]$ used in the estimation of $k_{cat}/K_M$ for the quinoline probes when assayed with CTB .....     | 71 |
| Figure 16: Linear fits of $v_0/[S]$ used in the estimation of $k_{cat}/K_M$ for the Z-FK quinoline probes when assayed with CTL..... | 71 |
| Figure 17: Linear fits of $v_0/[S]$ used in the estimation of $k_{cat}/K_M$ for the Z-KK quinoline probes when assayed with CTL..... | 72 |

## List of Schemes

|  |    |
|--|----|
| Scheme 1: Hydrolysis of a peptide bond by cysteine proteases.....  | 11 |
| Scheme 2: Covalent labeling of cathepsin active sites using AOMK inhibitors .....  | 19 |
| Scheme 3: Synthetic scheme of precursor peptides Z-FK-PAB-OH (7) and Z-KK-PAB-OH (12).....   | 43 |
| Scheme 4: Conjugation of the four aminoquinoline reporter groups to 7 and 12.....  | 46 |
| Scheme 5: General scheme for Michaelis-Menten Kinetics .....   | 48 |
| Scheme 6: Formation of precursor peptides 3 and 4 .....  | 63 |
| Scheme 7: General scheme for conjugation of the quinoline reporters to the peptide precursors 3 and 4 via stable carbamate linkages..... | 63 |

## **Chapter 1: Introduction**

The theme of this thesis is the synthesis and enzymatic assay of substrate-based probe candidates for imaging cathepsins involved in aggressive cancer. The results of the project are provided as a Manuscript in Chapter 4, along with specific procedural details and supporting information. Preceding Chapter 4 is a Literature Review providing background information which contextualizes the thesis and explains the purpose and utility of substrate-based probes for molecular imaging of cathepsin activity. Theory, methodology, and rationale not covered in the Literature Review or Manuscript are provided in the Methodology section. Finally, the Conclusions and Future Work section summarizes the results and suggests directions for continuing research of this project.

## Chapter 2: Literature Review

### 2.1: Molecular Imaging

#### 2.1.1: Overview

Molecular imaging is a rapidly growing field with significant implications of how researchers and clinicians understand, predict, and respond to disease.<sup>1</sup> While anatomical imaging has always been crucial in providing macroscopic physical information in relation to health and disease, molecular imaging (MI) provides important information on biochemical processes. Anatomical imaging techniques such as X-Ray, computed tomography (CT), and magnetic resonance imaging (MRI) provide important spatial information on size, shape, and density of organs and tissues. In contrast, molecular imaging can noninvasively provide functional, quantitative, and even kinetic information of biochemical characteristics.<sup>1</sup> These biochemical characteristics are referred to as biomarkers and can serve as diagnostic or prognostic indicators, but they can also predict or reveal *in vivo* response to targeted therapies in both the preclinical and clinical settings. Molecular imaging provides researchers with a tool for understanding disease-promoting processes and developing targeted therapies<sup>2,3</sup>, while helping clinicians to characterize the pathology of a given individual or their response to treatment early on at the biochemical level.<sup>4</sup> Key biochemical changes typically happen prior to anatomical changes<sup>1</sup>, central to the diagnostic and prognostic power of molecular imaging.<sup>5</sup> The ability to noninvasively quantify biochemical processes *in vivo* is the essence of molecular

imaging and the reason for its growing importance in predicting and evaluating therapeutic response early after initiating therapy.

### **2.1.2: Nuclear Imaging and PET**

The nuclear imaging techniques single photon computed tomography (SPECT) and positron emission tomography (PET) are the most clinically relevant of the MI modalities.<sup>4,6,7</sup> While functional MRI (fMRI) is emerging as a tool for molecular imaging, the use of fMRI remains largely preclinical due to limited sensitivity in the detection of molecular contrast agents and limited temporal resolution.<sup>8</sup> Optical imaging using near-infrared fluorescent (NIRF) tags is also used preclinically and to a less extent clinically, but due to poor imaging depth it is largely limited to shallow imaging of small animals or *ex vivo* imaging of tissues or organs.<sup>1</sup> Functional ultrasound (fUS) is currently limited to the use of contrast microbubbles preclinically, and has yet to be translated for use in imaging molecular markers.<sup>4</sup> PET and SPECT offer unlimited depth penetration and are also the most sensitive of the molecular imaging techniques.<sup>7,9</sup> The picomolar sensitivity of PET means it is not only clinically powerful but also minimally invasive since only trace amounts of imaging agent are required to produce high contrast images.

Highly sensitive molecular imaging with PET is similar in premise to SPECT, but the two modalities differ in the radionuclides used.<sup>7</sup> A sub-microgram amount of radiolabeled imaging agent, also known as a tracer, is injected into the bloodstream. The tracer travels throughout the body but is designed to interact with a biomolecular target or metabolic pathway involved in disease.<sup>10</sup> This results in an accumulation of the tracer in connection with a functional

biochemical process, and the tracer is quantitatively detected by means of the attached radionuclide. While both methods employ biologically active tracers tagged with radionuclides, the isotopes used in PET decay differently than those used in SPECT.

The positron-emitting radionuclides used in PET decay to release positrons which travel a negligible distance to annihilate with an electron. As a result of this annihilation, two 511 keV gamma rays are emitted 180° from one another and are coincidentally detected by a gamma camera.<sup>10</sup> The single-photon emitting radionuclides used in SPECT decay to emit a single 140 keV gamma ray directly. In both cases, detection of the gamma rays using 360° cameras allows for reconstruction of a three-dimensional image.<sup>11</sup> The gamma rays have unlimited tissue depth penetration and allow the tracers to be detected with picomolar sensitivity<sup>9</sup>, meaning that only trace amounts of the imaging agent need to be injected. Toxicity issues are therefore less of a concern when compared to other imaging modalities, meaning that the endogenous biochemistry is unaltered by the tracer. This nontoxic and non-invasive nature is important for true insight into the underlying biochemistry of a given pathology.

While both PET and SPECT offer very high sensitivity and are minimally invasive, PET offers important advantages.<sup>12</sup> To begin, the two coincident gamma rays emitted in opposing directions make it easier for PET cameras to define the precise location of the biomarker or radiolabeled tracer in three-dimensional space than does the single gamma ray emitted by SPECT radionuclides.<sup>13</sup> The resulting spatial resolution for clinical PET is typically 3-4 mm, while that for  $\mu$ PET is approximately 1-2 mm.<sup>14</sup> While the SPECT radionuclide  $^{99m}\text{Tc}$  is currently used in 80% of nuclear medicine procedures owing to its convenient formation from the long-lived isotope  $^{99}\text{Mo}$ , the common isotopes used in PET ( $^{15}\text{O}$ ,  $^{13}\text{N}$ ,  $^{11}\text{C}$ , and  $^{18}\text{F}$ ) are more biologically

compatible and are easier to chemically incorporate into small biologically active tracers when compared to large atoms like  $^{99m}\text{Tc}$  or  $^{123}\text{I}$ .<sup>15</sup> Worldwide supply of the primary SPECT isotope  $^{99m}\text{Tc}$  has also been notoriously unreliable in recent years and alternatives are being sought due to reliance on weapons-grade uranium and five increasingly old reactors for its production.<sup>16,17</sup> Proximity to expensive cyclotron and radiopharmacy facilities is necessitated by the short half lives of PET isotopes, leading to challenges in tracer development and use. The resulting main disadvantage of PET imaging is the current limited availability of clinically approved imaging agents.

### **2.1.3: PET Imaging Agents and Applications**

New biomarkers are constantly being identified as important indicators of disease, especially in recent years.<sup>18</sup> This has created great demand for the development of novel imaging agents intended to target new biomarkers for research and clinical purposes. Biomarkers can include biomolecular protein markers overexpressed in association with disease such as receptors, integrins, enzymes, or antibodies.<sup>14</sup> Biomarkers can also include physiochemical or phenotype characteristics such as oxygenation, perfusion, and amyloid plaques.<sup>9,19-21</sup> Inspiration for the design of novel imaging agents is based on structural biochemistry of the target or microenvironment, endogenous substrates of the biomarker, computational chemistry, or current probes and drugs.<sup>14</sup> Any combination of these approaches may be used to rationally design probes specific to their target. The probe must also be chemically and metabolically stable prior to reaching the target, and must overcome delivery

barriers such as cell membranes, antibody recognition, rapid excretion, and phagocytosis.<sup>22</sup>

Also important to the design of tracers is the radioisotope used for labelling.

The most commonly used PET isotopes are  $^{15}\text{O}$ ,  $^{13}\text{N}$ ,  $^{11}\text{C}$ , and  $^{18}\text{F}$ , with half lives of 2, 10, 20, and 110 minutes respectively.<sup>15</sup> With the exception of  $^{18}\text{F}$ , their clinical utility largely comes from the fact that they are radionuclides of elements with naturally occurring isotopes and can therefore replace the stable nuclide in naturally occurring compounds. The isotope  $^{18}\text{F}$  however can be employed in tracers as an isostere for hydroxyl groups, and because of its small size it can be incorporated into high affinity ligands or substrates for protein biomarkers. As a result of the short half lives of PET isotopes however, there are important practical considerations in the development of imaging agents. The half-life of the radionuclide used must be suitable for practical considerations of synthesis, shipping, administration, and the pharmacokinetic profile of the tracer.<sup>14,23,24</sup> Interest has grown in the longer-lived PET isotopes  $^{64}\text{Cu}$  and  $^{89}\text{Zr}$  due to the ability to ship them to distant locations and their potential to be incorporated into imaging agents with longer serum half-lives such as antibodies. PET tracers however generally need to be synthesized, purified, and analyzed within minutes, while most synthetic reactions used in medicinal chemistry occur on the hour or day time scale and are therefore impractical in radiotracer synthesis. The short half lives of positron emitters therefore not only create the need for proximity to a cyclotron and radiopharmacy, but strategic approaches to tracer design and synthesis are needed as well. Although these factors make tracer development a great challenge, there are both preclinical and clinical applications of PET.

Strategically designed tracers that target specific biomolecules can be used in the preclinical setting to help understand the underlying biochemistry of disease. Not only are new

biomarkers and tracers constantly being investigated for their utility in understanding disease characteristics, MI can also be used for therapeutic target validation and drug assessment at the preclinical stage.<sup>2,3,25</sup> Many drugs and chemotherapeutic agents that target markers associated with disease have been radiolabeled for PET studies, allowing for the noninvasive assessment of their biodistribution and pharmacokinetics preclinically. Examples include <sup>68</sup>Ga-Trastuzumab which targets epidermal growth factor receptor type II (HER2) positive breast cancer, <sup>11</sup>C-Tarceva which targets epidermal growth factor receptor, and <sup>18</sup>F-Tamoxifen which targets the oestrogen receptor.<sup>4</sup> Few drug candidates are ever translated for clinical use, and most fail during clinical trials. This results in fruitless drug development costs and has led to an increased demand for early noninvasive screening procedures in humans<sup>2</sup>. So not only are new biomarkers and imaging agents constantly being investigated for the purpose of understanding disease, PET will also continue to play an increasingly important role in the development of novel therapeutics for the clinic.

PET currently has clinical applications in oncology, neurology, and cardiology,<sup>26-28</sup> where it is involved in diagnosis, prognosis, staging, and the prediction and evaluation of therapeutic response.<sup>13</sup> PET imaging has been used to diagnose malignant cancer, and it has been used to differentiate between recurring tumors and necrosis due to radiation therapy.<sup>29,30</sup> Cardiac function, perfusion, and viability have all been assessed using PET.<sup>31,32</sup> A patient's risk of developing coronary heart disease (CAD) can be determined, and PET can also help determine which patients are likely to benefit from heart bypass surgery. PET has also been used in monitoring response to therapy as demonstrated using [<sup>18</sup>F]Fluoromisonidazole to image the

hypoxic environment of tumors in response to chemotherapy, and fluorodeoxyglucose ( $^{18}\text{F}$ -FDG) to gauge therapeutic response in patients suffering from lymphoma.

$^{18}\text{F}$ -FDG is the most widely-used PET radiopharmaceutical in the world.<sup>33</sup> It is used to assess glycolytic metabolism, especially in growing tumors that have an increased demand for glucose due to the Warburg effect<sup>34</sup>. It is a radiolabeled derivative of glucose, employing the positron emitting radionuclide  $^{18}\text{F}$  in the 2' position in lieu of the hydroxyl group as seen in Figure 1. FDG is rapidly taken up by tumor cells by the GLUT transport proteins and phosphorylated by hexokinase in the same way that glucose is in the first step of glycolysis. Phosphoglucose isomerase, the second enzyme involved in the glycolytic pathway, cannot isomerize  $^{18}\text{F}$ -FDG-6-phosphate since the 2' hydroxyl group has been replaced by  $^{18}\text{F}$ . By virtue of being phosphorylated,  $^{18}\text{F}$ -FDG-6-phosphate is ionically charged and can no longer be pumped out of the cell by the GLUT transport proteins nor can it passively diffuse across cell membranes. As a consequence,  $^{18}\text{F}$ -FDG-6-phosphate is cell impermeable and accumulates in hyperglycolytic tissues and organs. Indeed, FDG uptake in suspected cancer lesions is correlated with poor patient prognosis and is used to help differentiate responders from nonresponders following therapy.<sup>34</sup>

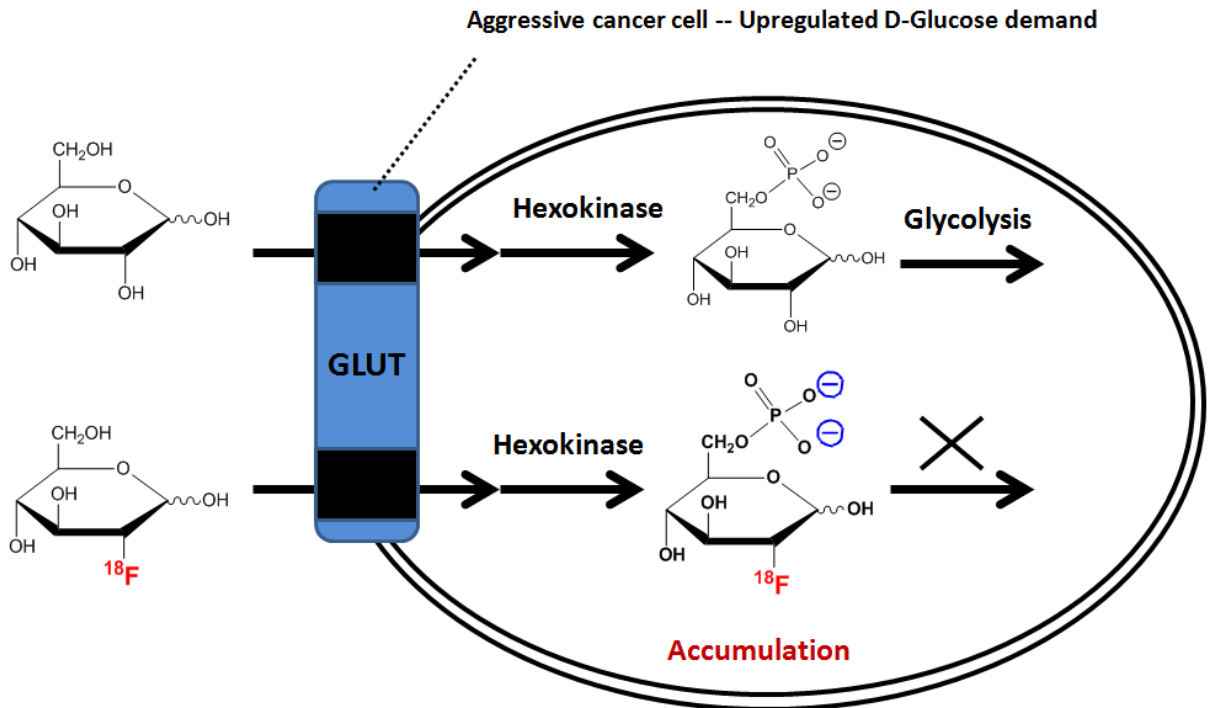


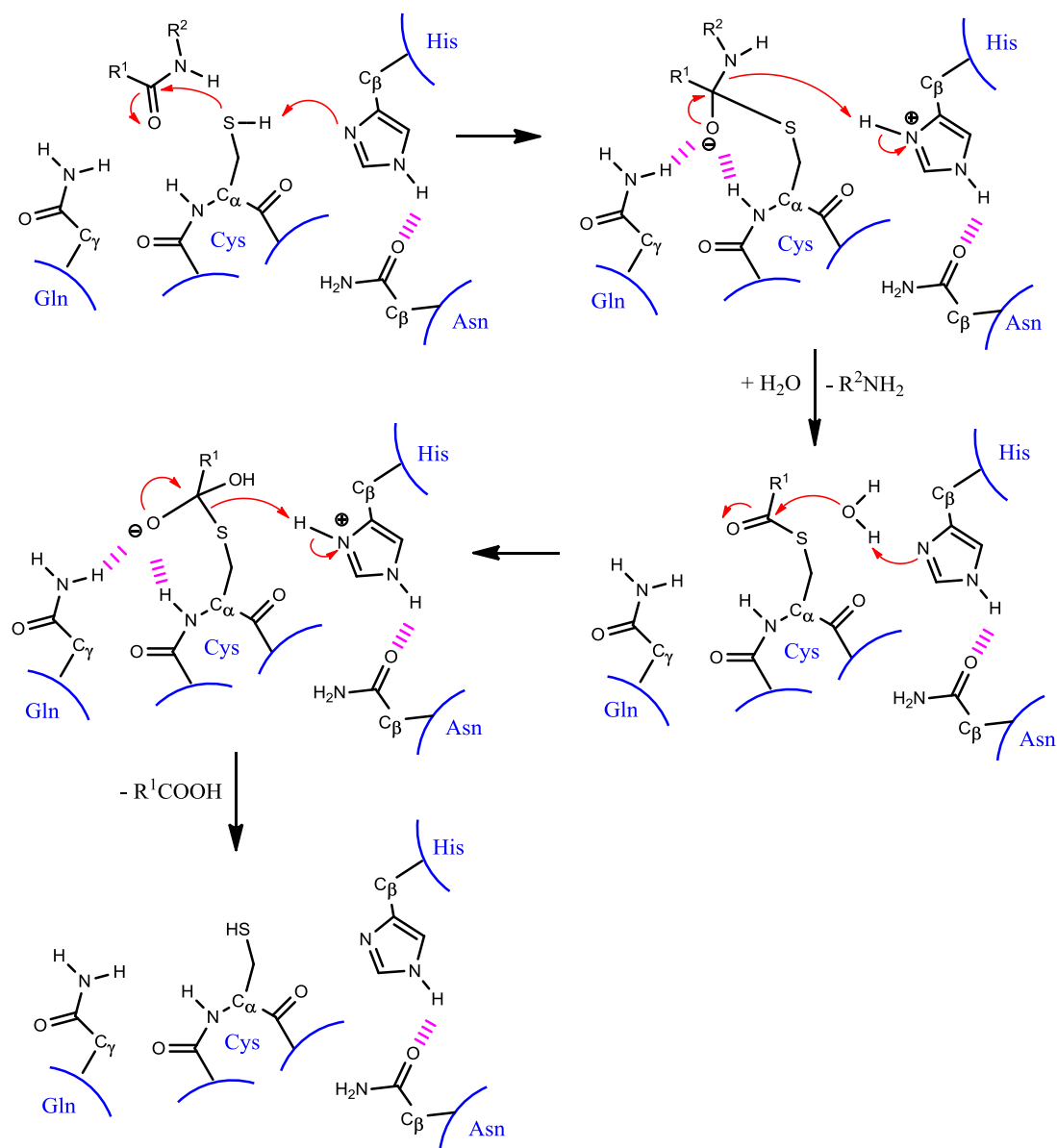
**Figure 1: Imaging glucose metabolism using FDG-PET.** Highly metabolic tumor cells have a high demand for glucose relative to other cells.  $^{18}\text{F}$ -FDG is rapidly influxed by the GLUT transporter proteins and phosphorylated by hexokinase in a similar manner to glucose.  $^{18}\text{F}$ -FDG-6P is ionically charged and therefore cell impermeable, allowing for PET imaging of aggressive cancer.

The many applications of FDG-PET are due to its ability to image glycolytic activity, which is an aberrant metabolic process in many pathologies. However to understand how specific pathways or biomolecules contribute to other diseases and disease processes, new tracers targeting other potential biomarkers are urgently needed. FDG, however, demonstrates the utility in designing tracers to be efficient substrate-based probes which release radioactive products that accumulate at the site of enzyme activation without inhibiting the target enzyme.

## 2.2: Cysteine Cathepsins as Biomarkers for Aggressive Cancer

### 2.2.1: Proteases and Cysteine Cathepsins

Protein hydrolysis is a key process in all living cells carried out by a diverse class of enzymes called proteases that are involved in many aspects of health and disease.<sup>35</sup> Due to the diverse nature of proteins as ubiquitous biomolecules, there are many preclinical and clinical implications of proteolytic activity.<sup>35,36</sup> There are five general protease classes; serine, cysteine, aspartyl, threonine, and metalloproteases, all of which are grouped according to the mechanism of catalysis employed in the enzyme active sites.<sup>37</sup> Within the active site of aspartyl and metalloproteases, a water molecule is promoted as the nucleophile in hydrolysis of the peptide bond. However in the case of serine, threonine and cysteine proteases, the respective eponymous residues themselves are involved in nucleophilic attack of the peptide bond, promoted by one or more amino acids acting as general bases in close proximity to the active residue.<sup>36</sup> The catalytic mechanism employed by cysteine proteases is shown in Scheme 1.



**Scheme 1: Hydrolysis of a peptide bond by cysteine proteases.** Histidine increases the nucleophilicity of the cysteine thiol group, which upon nucleophilic attack of the peptide carbonyl carbon forms a tetrahedral intermediate prior to forming the acetylated enzyme. The thioester is subsequently hydrolyzed, releasing the remaining fragment of the substrate as a carboxylic acid.

According to Schechter and Berger nomenclature<sup>38</sup>, peptides are cleaved between the  $P_1$  and  $P_1'$  amino acid residues by definition, which relative to the scissile bond are located toward the amino- and carboxy-terminus of the peptide respectively. The amino acid residues of the peptide are termed  $P_1, P_2, P_3...$  as counted toward the N-terminus from the scissile bond and  $P_1', P_2', P_3'...$  as counted toward the carboxy-terminus.<sup>36</sup> The corresponding recognition subsites within the protease that accept the substrate residues are deemed  $S_1, S_2, S_3...$  or  $S_1', S_2', S_3'...$  in a complementary fashion to the P and P' residues of the peptide as shown in Figure 2. The affinity of these noncovalent interactions depends on how well the subsites accept the particular residues of the peptide. Within the cysteine cathepsin family of proteases, structural homology and similarity in specificity is seen across most of the enzymes.

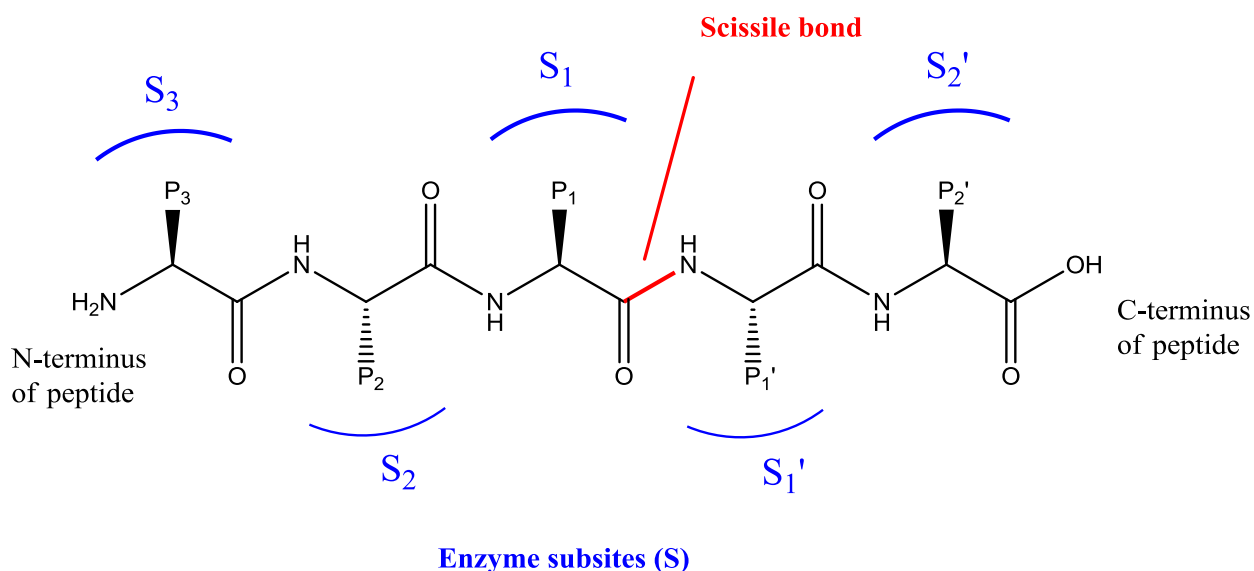


**Figure 2: Schechter and Berger nomenclature for a protease active site and complimentary substrate.** Both the enzyme subsites (S) and peptide residue (P) are numbered relative to the scissile bond. The  $S_1'...S_N'$  subsites and corresponding  $P_1'...P_N'$  residues are numbered ascendingly toward to C-terminus of the peptide from the scissile bond, while the  $S_1...S_N$  subsites and  $P_1...P_N$  residues are numbered ascendingly toward the N-terminus of the peptide.

The papain family of cysteine proteases is a well-studied group of hydrolases which encompasses eleven human enzymes known as cathepsins. Cathepsins B, C, F, H, K, L, O, S, V, W, and X are all involved in intracellular proteolysis, and the majority of these cysteine cathepsins evolved to be located within small organelles dedicated to catabolism and cellular debris recycling called lysosomes.<sup>39</sup> Cathepsin activity is therefore largely dependent on and limited to the acidic milieu of the lysosome, which has a pH ranging from approximately 4-5.<sup>40,41</sup> Cysteine cathepsins are also active to a certain extent in the acidic endosomes, which transport extracellular material engulfed by endocytosis to the lysosome.<sup>42</sup> They all have important physiological functions and are involved in such processes as immune response, hormone processing, catabolism, and even bone development.<sup>39,43</sup>

As with most proteases, the regulation of endogenous activity is not only dependent on location, but other posttranslational processes as well. At the expression level, cysteine cathepsins are synthesized as "proenzymes" or zymogens which are mainly inactive until undergoing protease activation within the lysosome. Activation of the proenzymes to their mature fully-active counterparts can be executed by the residually active proenzymes themselves, known as autocatalysis, or by other proteases. The activity of subsequently mature cathepsin is further controlled by differential expression of endogenous inhibitors, including the small protein competitive inhibitors of the cystatin, thyropin, and serpin families. The functional activity of these important enzymes is therefore largely regulated at the posttranslational level and is seclused to lysosomes under normal conditions. In association with numerous pathologies however, their aberrant expression, activity or delocalization can lead to or promote diseases such as aggressive cancer, arthritis, and atherosclerosis.<sup>44,45</sup> This highlights

the importance of techniques that image functional cathepsin activity in disease-promoting processes and not just expression levels alone.

### **2.2.2: Cathepsin B and Aggressive Cancer**

There is growing evidence that the overexpression of cathepsins in various cancers is associated with tumor metastasis, the primary cause of death among cancer patients.<sup>46</sup> Metastasis is the spread of cancer to distant tissues and organs from the original location, and the likelihood of a tumor to spread from its primary site is referred to as its metastatic potential. Metastasis of a tumor to a secondary location involves several steps.<sup>47,48</sup> The first step is invasion, where invasive tumor cells break away from the primary aggressive tumor and eventually migrate toward blood vessels.<sup>49,50</sup> The tumor cells must then enter the bloodstream or lymphatic system, termed intravasation, which serves as their primary means of migration to other organs. Upon surviving circulation and arresting at a given location the tumor cells must extravasate, or exit the bloodstream or lymphatic system. Depending on their ability to invade and proliferate in the new tissue, the cancer cells can then colonize to form a secondary tumor.<sup>51</sup> This spread of cancer from one location to another is believed to account for 90% of all cancer deaths, as opposed to tumor cells residing at one inopportune site for a prolonged period of time.<sup>48</sup> Therefore the ability to characterize the metastatic potential or aggressiveness of a patient's tumor at an early stage would have valuable prognostic applications and could aid in determining the aggressiveness of therapy required.<sup>52,53</sup>

The overexpression and delocalization of cathepsin B is believed to be involved in invasion as seen in Figure 3, the earliest stage of metastasis.<sup>46</sup> Like most cathepsins, CTB is

optimally active in and isolated to the lysosome under healthy conditions. However its increased activity at the invading edge of a tumor and within the extracellular matrix is known to contribute to a tumor's ability to become invasive and reach the bloodstream.<sup>54</sup> While CTB is known to degrade collagen and fibronectin of the extracellular matrix (ECM) producing a permissive region for cancer cells to invade, it is also believed to indirectly contribute to ECM degradation through the activation of other proteases and the degradation of protease inhibitors. Extracellular CTB is believed to cleave cell adhesion proteins, resulting in tumor cell mobility. An increase in extracellular CTB activity has been correlated with metastatic potential and poor patient prognosis.<sup>55-57</sup> Further complicating is the fact that CTB can not only blunt tumor response to chemotherapy<sup>58</sup>, but actually induce tumor growth in reaction to chemotherapy.<sup>59</sup> On the contrary, aberrant intracellular CTB activity is known to promote apoptosis in tumor cells and is associated with favorable patient prognosis.<sup>60-62</sup> Given the apparent role CTB has in promoting the invasion of aggressive cancer, great efforts have been made to develop CTB-targeted prodrugs as potential anti-cancer therapeutics. The ability to PET image cathepsin activity would therefore be valuable not only in validating CTB as a legitimate therapeutic target, but also in developing a diagnostic or prognostic test for aggressive or chemotherapy-resistant tumors.

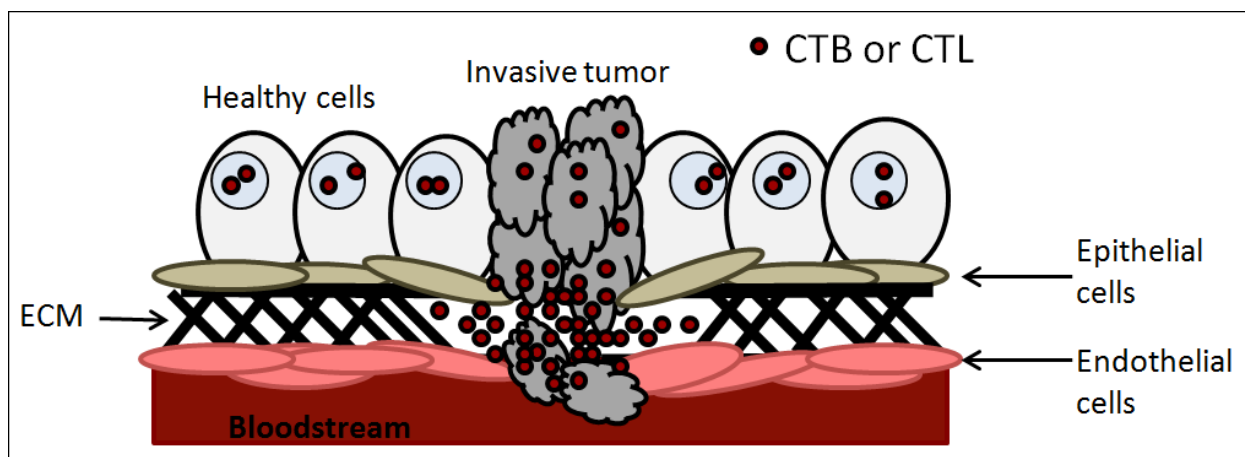


**Figure 3: The role of Cathepsins B and L at the invading edge of an aggressive tumor.** While CTB and CTL activity is normally isolated to the lysosome in healthy cells, their aberrant expression and activity in the tumor microenvironment is known to promote invasion, the first step in tumor metastasis to a secondary site. CTB and CTL are known to degrade the extracellular matrix (ECM) and cell adhesion proteins, creating a permissive path for intravasation to the bloodstream.

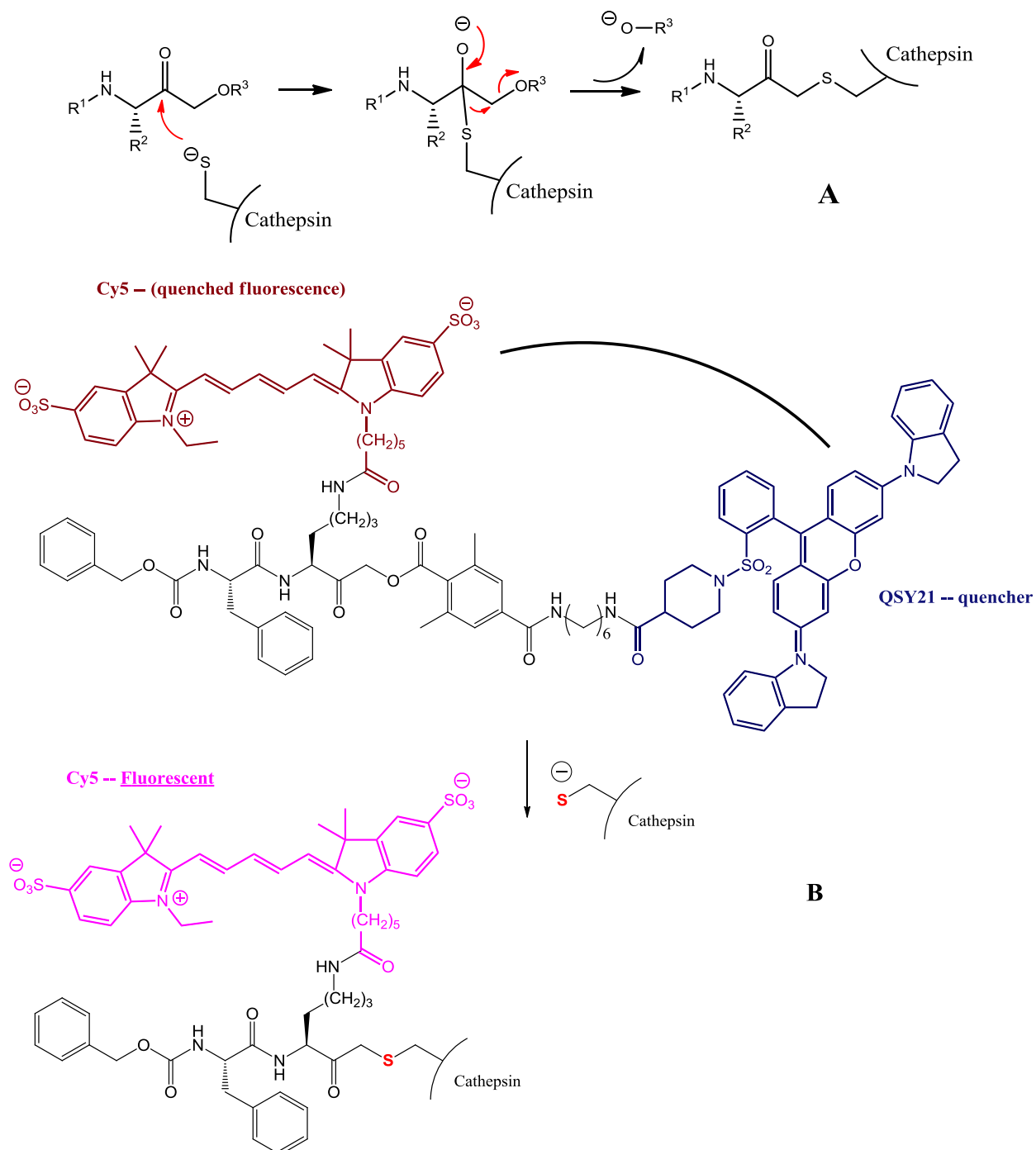
### 2.2.3: Cathepsin B as a Targeted Biomarker

To evaluate functional cathepsin activity *in vitro* and *in vivo* as opposed to relying on expression levels alone, two strategies have emerged. The first approach uses activity-based inhibitors that are designed to covalently label the target active site of catalytically active enzymes in a 1:1 ratio. They contain a targeting moiety that provides affinity for the target active site linked to a reactive group (or "warhead") and either a fluorescent tag or PET radioisotope. By virtue of alkylating the active site, mechanism-based probes inherently offer a means of signal localization, therefore accumulating in the immediate local tissues and organs that have high enzyme activity. A drawback of the activity-based approach is that covalent labelling of the enzyme active site prevents further enzyme processing of more probe molecules by the same enzyme. This could result in a decrease in contrast since physiological levels of enzyme may not be high enough to generate sufficient signal-to-noise for detailed PET

images. Substrate-based probes, on the other hand, are not covalently retained in the active site but rather are recognized and catalytically processed by the target enzyme.<sup>63</sup> This potentially offers an amplification of signal as one active site is capable of turning over thousands of tracer molecules per minute. Once freely released from the active site however, substrate-based probes must rely on different mechanisms of local retention than the covalent nature of activity-based probes.

Activity-based probes (ABPs) for the purpose of imaging cysteine cathepsin activity were first reported by Bogoy and coworkers who developed fluorogenic mechanism-based inhibitors employing the reactive acyloxymethyl ketone (AOMK) group.<sup>64</sup> Until the AOMK group reacts with the cysteine active site through the mechanism shown in Scheme 2(a), the fluorescent signal of the probe is inherently quenched as shown in Scheme 2(b). In other words, the probes become fluorescent only after being recognized and hydrolyzed by the target protease. The inherent fluorescence of probes is low since the Cy5 fluorophore and internal QSY21 quencher are held in close proximity to each other but on opposite sides of the cathepsin-recognized bond.<sup>64</sup> The QSY21 quencher is conjugated to the aryl leaving group of the AOMK warhead and diffuses from the vicinity of the Cy5-labelled active site once released by the cysteine protease. Despite the elegance of these "smart" fluorescent probes that turn on only once activated, they lacked specificity for either CTB or CTL, and fluorescent probes are intrinsically limited to small animal studies<sup>64</sup> and tissue surfaces<sup>65</sup> due to very poor imaging depth. Nonetheless, derivatives of these quenched activity-based probes (qABPs) were radiolabeled for PET studies in animal models of cancer. Along with removal of the QSY21 quencher group to yield an underivatized AOMK warhead, 1,4,7,10-tetraazacyclododecane-1,4,7,10-tetraacetic acid (DOTA) was

conjugated either at the N-terminus of the peptide or in lieu of the Cy5 moiety to allow for coordination of the  $^{64}\text{Cu}$  radiolabel by chelation.<sup>66</sup> Although the derivative employing the N-terminus DOTA- $^{64}\text{Cu}$  provided modest tumor uptake, both tracers exhibited high liver uptake and hepatobiliary clearance resulting in poor images since the entire abdomen of the mouse was radioactive. This is likely due to the high lipophilicity of these tracers which is typically avoided in most PET probes since renal clearance and elimination of the radiotracer in the bladder is preferable. While demonstrating the ability to PET image cysteine cathepsins with an AOMK warhead, these tracers were not shown to be specific for any given cathepsin and lacked signal amplification by virtue of being activity-based probes that bound to the enzyme with 1:1 stoichiometry.



**Scheme 2: Covalent labeling of cathepsin active sites using AOMK inhibitors.** (A) Mechanism of inhibition by AOMK inhibitors; (B) Quenched activity-based probes as employed by Bogoy and coworkers. Prior to enzymatic labelling, the fluorescence of the Cy5 moiety is quenched due to proximity of the QSY21 quencher on the opposite end of the cathepsin-recognized linkage. An enzyme labelled in such a way is incapable of further probe turnover, limiting the signal to a 1:1 ratio of inhibitor to enzyme.

To evaluate a signal amplifying substrate-based approach to NIR fluorogenic probes, Kim and coworkers developed a polymer nanoprobe composed of repeating glycol chitosan monomers which are conjugated to either a tumor-targeting hormone or CTB-targeting peptide substrate in an alternating fashion.<sup>67</sup> At the N-terminus of the CTB-targeting peptide is the Cys5.5 fluorophore which is quenched by the BHQ-3 quencher toward the C-terminus on the other side of the scissile bond. The scissile bond is hydrolyzed by CTB to free the fluorophore from close proximity to the quencher, activating the fluorescent signal. This occurs at multiple locations along the polymer to yield strong fluorescence in correlation with CTB activity. Unfortunately, due to poor blood clearance and poor cell permeability, a nanoparticle approach is largely dependent on the enhanced permeability and retention (EPR) effect of the tumor environment.<sup>68</sup> That is, the enhanced permeability of tumor vasculature and the suppression of lymphatic filtration can improve the ability of macromolecules to spontaneously enter and reside in tumors. However, heterogeneity of the EPR effect within and between tumor types has hampered the development and utility of imaging agents and drugs employing a nanoparticle design.<sup>68</sup> So while substrate-based polymers such as those explored by Kim might offer greater sensitivity over activity-based inhibitors, small molecule probes typically have superior pharmacodynamic properties for clinical imaging and are easier to prepare and purify, satisfying the strict regulations associated with PET tracers intended for human use.

Small molecule SBPs such as the ones reported herein potentially offer the advantage of signal amplification, but a major drawback commonly encountered is the rapid diffusion of the reporter molecules from the site of activation. Cathepsins, however, are primarily active in the acidic lysosomes of cells, and this low pH can potentially be exploited to enhance the retention

of reporter groups released within this environment. Not long after discovering the lysosome six decades ago, deDuve reported that weakly basic amines spontaneously accumulate at high concentration after becoming ionically charged in the acidic environment.<sup>69,70</sup> This ionic trapping in the lysosome, as seen in Figure 4, results from membrane impermeability and has come to be known as lysosomotropism.<sup>71</sup> SBPs bearing lysosomotropic amine reporter molecules that are freely released from the enzyme upon hydrolysis of the substrate could potentially offer a means of signal localization in addition to an amplification of signal.

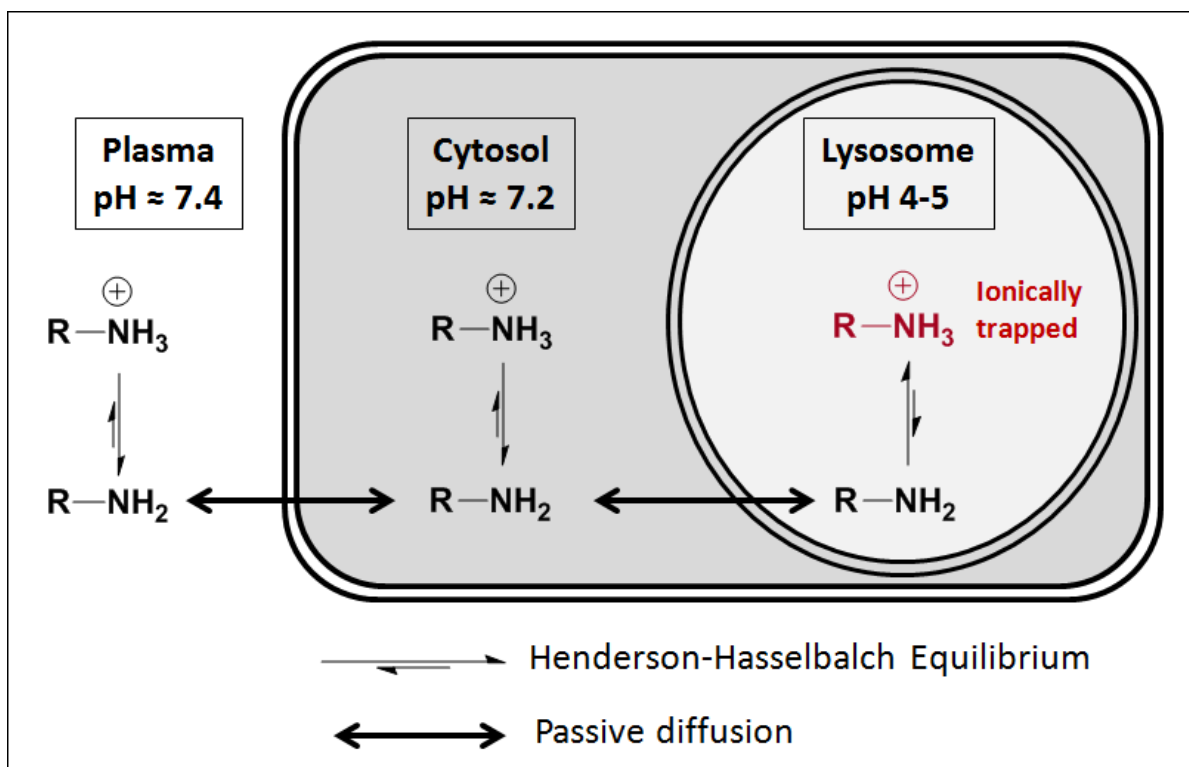


**Figure 4: Lysosomotropism of a lipophilic amine.** A lipophilic amine has the ability to passively diffuse across membranes, but depending on its pK<sub>a</sub> a weakly basic amine may become primarily protonated once reaching the acidic lysosome and therefore retained. The R group can also be a lysosome-targeting drug or a radiolabeled PET imaging agent which targets lysosomal enzymes.

#### 2.2.4: Our Approach to Imaging Cathepsins

Indeed small molecular probes tend to have rapid biodistribution and clearance properties and are easier to prepare and purify when compared to nanoparticles.<sup>68,72,73</sup> In addition to superior biodistribution and clearance properties, small molecules are also less prone to elicitation of immune response.<sup>74</sup> Ease in preparation is important for optimizing the structures of probe candidates, and the radiolabelling process is typically more direct and rapid for small molecules with relatively few functional groups.<sup>74</sup> In particular, small molecular substrate-based probes that release locally retained species as opposed to activity-based probes that inhibit the enzymatic target potentially offer the advantage of signal amplification. To this end, we have developed small molecule probes that are designed to release retained reporters at the target site only after being processed and released by CTB or CTL, rather than functioning as activity-based inactivators that achieve retention by means of covalently inhibiting the active site of the target.

Designed to be selective for CTB or CTL, we chose to synthesize probe candidates employing a three-component design. One of various aminoquinoline reporter groups is connected to a dipeptide substrate via the self-immolative linker PABA. Analogous to prodrugs that are activated to release a drug as seen in Figure 5, the substrate-based probes reported herein are efficiently hydrolyzed by CTB and CTL to release one of various aminoquinolines which should be ionically charged and retained within the lysosome. Only upon enzymatic cleavage of the dipeptide from the linker-reporter unit does the PABA linker spontaneously decompose to release a locally retained reporter. The PABA linker is commonly used in the design of prodrugs, and until recognition and cleavage by CTB within the lysosome of the cell,

the intact probe should be cell permeable and travel throughout the body to reach the target site.  $^{18}\text{F}$ -labelled lysosomotropic reporter groups could prove useful toward developing cathepsin substrate-based PET agents that are retained in their immediate environment.

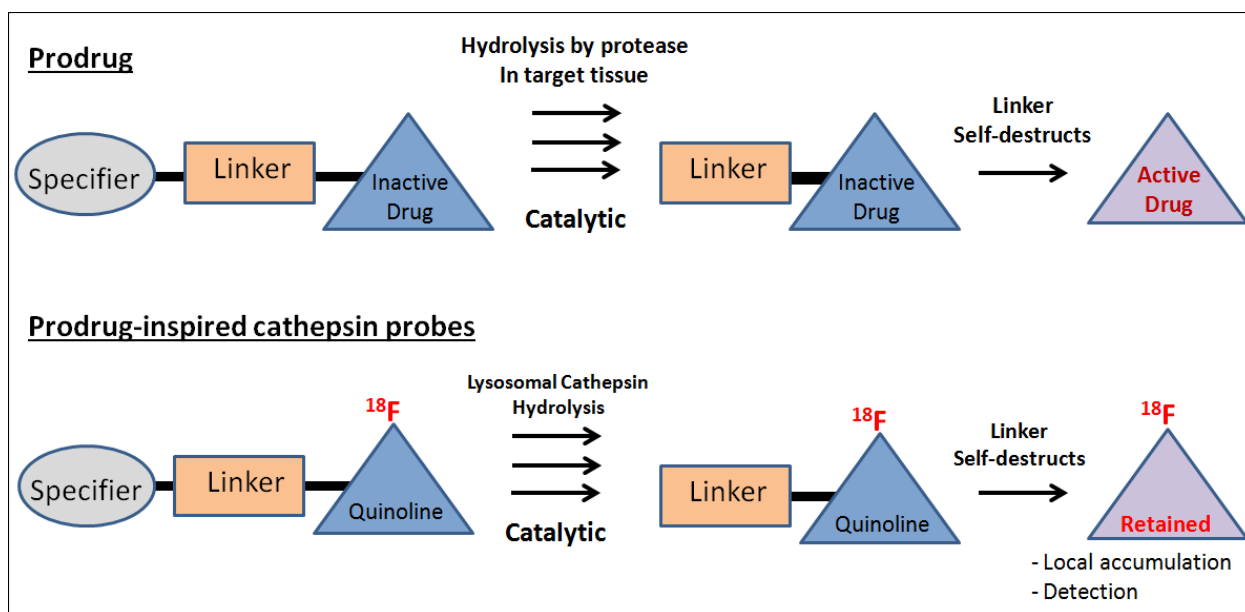


**Figure 5: Prodrug-inspired substrate based approach for cathepsin probes.** Prodrugs are enzymatically processed at a target site to release an active drug. In an analogous fashion, the prodrug-inspired probe candidates employed herein are efficiently hydrolyzed by CTB and CTL to release one of various aminoquinoline isomers, which are all expected to accumulate in the cathepsin-occupied lysosome and can foreseeably be  $^{18}\text{F}$ -radiolabeled. Such substrate-based probes offer an amplification of signal compared to activity-based inactivators while still potentially offering a mechanism of signal localization.

The dipeptide portion of the probe is designed to provide affinity and specificity for CTB or CTL. There are eleven human cathepsins and achieving specificity to any of them is a challenge due to structural homology within the family. The majority of cathepsins prefer a positively charged species at the  $P_1$  position of the substrate and a hydrophobic species at the  $P_2$  position<sup>75</sup>, however CTB is unique in that it can also accept a positively charged amino acid at the top of its  $S_2$  pocket. This is due to the presence of a glutamic acid residue at the top of its  $S_2$  pocket. To take advantage of this substrate preference, we designed probes with lysine as the

amino acid in both the P<sub>1</sub> and P<sub>2</sub> positions as seen in Figure 6. Analogs employing phenylalanine at the P<sub>2</sub> position were also prepared to be substrates of CTB and CTL. The probes are protected at the N-terminus using carboxybenzyl (Z) as this has been shown in literature to be well accepted by the P<sub>3</sub> pocket of CTB. Using lysine in lieu of arginine, which is employed in the commercial substrates Z-FR-AMC and Z-RR-AMC, is advantageous for synthetic reasons as discussed in Chapter 3.

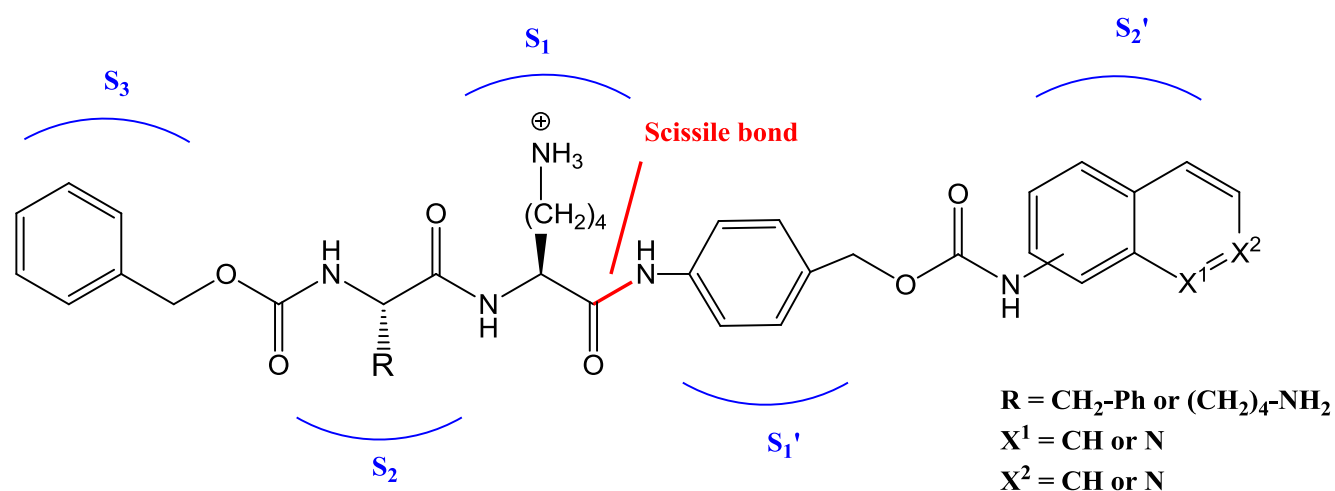


**Figure 6: The general structure of the novel prodrug-inspired probe candidates reported herein.** At the P<sub>1</sub> and P<sub>3</sub> positions of the peptidic probe candidates are lysine and carboxybenzyl respectively, both shown to be well accepted by the S<sub>1</sub> and S<sub>3</sub> subsites of the enzyme. At the P<sub>2</sub> position is either phenylalanine, known to be well-tolerated by most cathepsins, or lysine, hopefully exploiting the unique ability of CTB to accept positively charged groups within the S<sub>2</sub> site. The PABA linker conjugates the dipeptides to one of various aminoquinolines (3-AMQ, 4-AMQ, 5-AIQ, or 6-AMQ).

The PABA linker has been used in the design of prodrugs<sup>76-78</sup> and fluorogenic<sup>79,80</sup> enzymatic substrates. The amine of PABA can be condensed with the carboxy-terminus of a peptide specifier to form an amide linkage, and phenol- or aniline-based drugs can be subsequently conjugated to the benzylic alcohol of PABA via stable phenolic or carbamate linkages. Following hydrolysis of the specifier-PABA amide bond, self-immolation of a PABA-

drug carbamate bond occurs spontaneously and rapidly.<sup>81</sup> The spontaneous hydrolysis of the benzyl-carbamate bond following enzymatic cleavage of the specifier-linker bond is due to conversion of the weakly electron-donating acyl-amido group to the relatively strong electron-donating amine group. This extra electron density within the  $\pi$  system promotes the development of a *para*-azaquinone-methide through a 1,6-elimination<sup>82</sup>, allowing for spontaneous immolation of the benzyl-carbamate linkage. The resulting carbamic acid is unstable and spontaneously decomposes to rapidly yield carbon dioxide and the aniline-based drug. This rapid self-immolation has been taken advantage of in both prodrugs and profluorophore substrates.

In the case of prodrugs, a linker such as PABA has been used to conjugate a specifier to a drug in order to improve intermolecular bond stability or provide the prodrug with greater affinity for the target enzyme.<sup>79,81,83</sup> In the design of fluorogenic enzymatic substrates, the use of PABA in conjugating phenol- or aniline-based fluorophores by means of phenolic or carbamate linkages may inherently quench their fluorescence prior to enzymatic recognition.<sup>79</sup> Our group has previously demonstrated that when introduced into fluorogenic peptides, PABA improves recognition and cell permeability while maintaining efficient turnover of profluorophore probes by CTB.<sup>84</sup>

There are several advantages of incorporating the prodrug-inspired PABA linker into three-component probe candidates for CTB. The prodrug inspired PABA linker enables the conjugation of the aniline based aminoquinoline reporters through a chemically and metabolically stable carbamate linkage. Without PABA, a peptide directly derivatized with an aminoquinoline reporter would form a reactive amide that is likely to be processed by a

number of proteases or esterase enzymes. Furthermore, PABA can extend into the active cleft of CTB, preserving recognition when bulky substituents such as drugs or contrast agents are placed at the P<sub>2</sub>' position. Indeed, prodrugs employing PABA as a self-immolative linker have not only been shown to be efficiently processed by cathepsins to release an active drug, but are serum stable as well.<sup>76,85</sup>

The novel probe candidates herein are designed to release a reporter molecule that is retained in the lysosome where cathepsins primarily reside. We hypothesize that using a substrate-based approach will take advantage of the catalytic power of the target protease while also using aminoquinolines as lysosomotropic reporter molecules that will accumulate within the lysosome where most cysteine cathepsins are located. This approach will potentially provide both amplification of signal and reporter retention compared to an activity-based approach which inactivates the target enzyme.

Indeed, there are examples of PET imaging agents and therapeutics that have taken advantage of lysosomotropism for increased sensitivity or selectivity toward their given targets. Lysosomal trapping as a mechanism of signal amplification in PET is demonstrated by [<sup>11</sup>C]N-desmethyl-loperamide, which enters brain cells and accumulates in lysosomes therein only when the blood-brain barrier efflux protein P-glycoprotein is not functioning.<sup>86</sup> The effect of lysosomotropism on drug biodistribution has been reported by several investigators<sup>71</sup>, and lysosomal sequestration of anticancer agents has been shown to promote cancer cell selectivity at least *in vitro*.<sup>87</sup> The lysosomotropic epoxide-based cathepsin probe reported by Wright and coworkers<sup>88</sup> is an activity-based inhibitor of the enzyme and therefore lack a mechanism of signal amplification similar to other activity-based probes mentioned. In addition, they would

potentially provide poor signal to noise if radiolabeled for PET studies because they accumulate in lysosomes regardless of cathepsin recognition. Although most cysteine proteases reside primarily in the lysosome, cathepsin substrate-based probes that employ lysosomotropic reporters have yet to be developed.

The four quinoline reporter groups we chose as reporter molecules and expected to be retained in the lysosomes are 3-aminoquinoline (3-AMQ), 4-aminoquinoline (4-AMQ), 5-aminoisoquinoline (5-AIQ), and 6-aminoquinoline (6-AMQ), as seen in Figure 7. The approximate pH range of the lysosome is 4-5<sup>41</sup>, while the weakly basic quinoline isomers 3-AMQ, 4-AMQ, 5-AIQ, and 6-AMQ have pKa values of 4.95-5.0, 9.0-9.17, 5.59-6.0 and 5.63 respectively.<sup>89,90</sup> The lysosomotropic properties of 3-AMQ, 4-AMQ, and 5-AIQ have been reported in literature, determined by treating living cells with low concentrations of each amine.<sup>90</sup> The ratio of [lysosomal]/[cytosolic] accumulation for 4-AMQ was reported as approximately 60, while that for 5-AIQ and 3-AMQ was approximately 25 and 4 respectively.<sup>90</sup> The pKa values of the individual quinolines correlate with these results and were hypothesized to determine the degree to which each accumulates in the low pH of the lysosome. Although 6-AMQ is not reported in literature as being lysosomotropic, its pKa of 5.6 suggests that it is also likely to be ionized and retained within the lysosome. Employing lysosomotropic reporter molecules in such a way is a novel approach, and it is currently unclear how lysosomotropic behaviour would be influenced when each aminoquinoline is released by an enzyme directly within the lysosome. To evaluate this approach, a series of small molecule substrate-based probes bearing aminoquinoline reporter groups was developed along with a convenient HPLC method for estimating kinetic turnover of the substrates by cathepsins B and L.

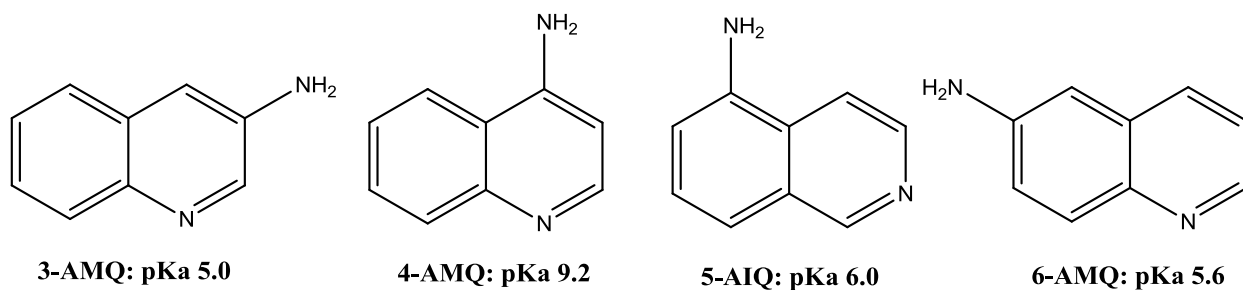


**Figure 7: The four quinoline isomers used as reporter groups in our substrate-based probes.** For the purpose of assessing the ability to detect cathepsin activity using lysosomotropic reporter groups, amines with varying pKa were chosen which can all be conjugated to peptide substrates using similar chemistry. 3-AMQ, 4-AMQ, and 5-AIQ have been reported as being lysosomotropic when incubated with cells, and because 6-AMQ has a pKa > 5, it is also likely to be mainly protonated and retained in the acidic lysosome.

### 2.3: Summary and Scope of Project

Given the multifunctional roles of cathepsins in health and disease, imaging agents with the ability to specifically assess cathepsin activity *in vivo* would be important for validating individual cathepsins as biomarkers of disease or drug targets. We report herein a series of novel prodrug-inspired peptidic probes for CTB and CTL that employ aminoquinoline reporter groups intended to be lysosomotropic once released from the enzyme, meaning they are expected to be locally retained where the majority of cysteine cathepsins are primarily active. These substrate-based probes do not covalently label the enzyme active site but rather are freely released upon hydrolysis, potentially offering a means of signal amplification in addition to signal retention. To evaluate this approach to probe design we developed a convenient HPLC method for determining  $k_{\text{cat}}/K_{\text{M}}$  values for commercial fluorogenic substrates. The kinetic values of  $k_{\text{cat}}/K_{\text{M}}$  obtained using the HPLC method were consistent with a fluorospectrophotometer-based continuous assay using the well-established fluorogenic substrates. The same HPLC method was used to determine  $k_{\text{cat}}/K_{\text{M}}$  for each quinoline-based probe candidate reported herein. We hypothesize that this approach to probe design could be used to detect other enzyme families, and the HPLC assay developed could be conveniently applied to other biological mediums such as lysates, homogenates, and blood.

## 2.4: References

1. James ML, Gambhir SS. A molecular imaging primer: Modalities, imaging agents, and applications. *Physiol Rev.* 2012;92(2):897-965.
2. Cunha L, Szigeti K, Mathe D, Metello LF. The role of molecular imaging in modern drug development. *Drug Discov Today.* 2014;19(7):936-948.
3. Willmann JK, van Bruggen N, Dinkelborg LM, Gambhir SS. Molecular imaging in drug development. *Nat Rev Drug Discov.* 2008;7(7):591-607.
4. Pysz MA, Gambhir SS, Willmann JK. Molecular imaging: Current status and emerging strategies. *Clin Radiol.* 2010;65(7):500-516.
5. Desar IM, van Herpen CM, van Laarhoven HW, Barentsz JO, Oyen WJ, van der Graaf WT. Beyond RECIST: Molecular and functional imaging techniques for evaluation of response to targeted therapy. *Cancer Treat Rev.* 2009;35(4):309-321.
6. Pither R. PET and the role of in vivo molecular imaging in personalized medicine. *Expert Rev Mol Diagn.* 2003;3(6):703-713.
7. Rahmim A, Zaidi H. PET versus SPECT: Strengths, limitations and challenges. *Nucl Med Commun.* 2008;29(3):193-207.
8. Constable RT. Challenges in fMRI and its limitations. In: *Functional MRI.* Springer US; 2006:75-

9. Ametamey SM, Honer M, Schubiger PA. Molecular imaging with PET. *Chem Rev.* 2008;108(5):1501-1516.
10. Phelps ME. PET: The merging of biology and imaging into molecular imaging. *J Nucl Med.* 2000;41(4):661-681.
11. Mariani G, Bruselli L, Kuwert T, et al. A review on the clinical uses of SPECT/CT. *Eur J Nucl Med Mol Imaging.* 2010;37(10):1959-1985.
12. Hicks RJ, Hofman MS. Is there still a role for SPECT-CT in oncology in the PET-CT era? *Nat Rev Clin Oncol.* 2012;9(12):712-720.
13. Fahim-UI-Hassan, Cook GJ. PET/CT in oncology. *Clin Med.* 2012;12(4):368-372.
14. Serdons K, Verbruggen A, Bormans GM. Developing new molecular imaging probes for PET. *Methods.* 2009;48(2):104-111.
15. Miller PW, Long NJ, Vilar R, Gee AD. Synthesis of <sup>11</sup>C, <sup>18</sup>F, <sup>15</sup>O, and <sup>13</sup>N radiolabels for positron emission tomography. *Angew Chem Int Ed Engl.* 2008;47(47):8998-9033.
16. Lewis DM. (99)mo supply--the times they are a-changing. *Eur J Nucl Med Mol Imaging.* 2009;36(9):1371-1374.
17. Ballinger JR. 99Mo shortage in nuclear medicine: Crisis or challenge? *J Label Compd Radiopharm.* 2010;53(4):167-168.

18. van der Meel R, Gallagher WM, Oliveira S, O'Connor AE, Schiffelers RM, Byrne AT. Recent advances in molecular imaging biomarkers in cancer: Application of bench to bedside technologies. *Drug Discov Today*. 2010;15(3-4):102-114.
19. Krohn KA, Link JM, Mason RP. Molecular imaging of hypoxia. *J Nucl Med*. 2008;49 Suppl 2:129S-48S.
20. Di Carli MF, Dorbala S, Meserve J, El Fakhri G, Sitek A, Moore SC. Clinical myocardial perfusion PET/CT. *J Nucl Med*. 2007;48(5):783-793.
21. Quigley H, Colloby SJ, O'Brien JT. PET imaging of brain amyloid in dementia: A review. *Int J Geriatr Psychiatry*. 2011;26(10):991-999.
22. Massoud TF, Gambhir SS. Molecular imaging in living subjects: Seeing fundamental biological processes in a new light. *Genes Dev*. 2003;17(5):545-580.
23. Hooker JM. Modular strategies for PET imaging agents. *Curr Opin Chem Biol*. 2010;14(1):105-111.
24. Pimlott SL, Sutherland A. Molecular tracers for the PET and SPECT imaging of disease. *Chem Soc Rev*. 2011;40(1):149-162.
25. Hargreaves RJ. The role of molecular imaging in drug discovery and development. *Clin Pharmacol Ther*. 2008;83(2):349-353.

26. Herholz K, Heiss WD. Positron emission tomography in clinical neurology. *Mol Imaging Biol.* 2004;6(4):239-269.
27. Di Carli MF, Hachamovitch R. Should PET replace SPECT for evaluating CAD? the end of the beginning. *J Nucl Cardiol.* 2006;13(1):2-7.
28. Papathanassiou D, Bruna-Muraille C, Liehn JC, Nguyen TD, Cure H. Positron emission tomography in oncology: Present and future of PET and PET/CT. *Crit Rev Oncol Hematol.* 2009;72(3):239-254.
29. Lizarraga KJ, Allen-Auerbach M, Czernin J, et al. (18)F-FDOPA PET for differentiating recurrent or progressive brain metastatic tumors from late or delayed radiation injury after radiation treatment. *J Nucl Med.* 2014;55(1):30-36.
30. Rohren EM, Turkington TG, Coleman RE. Clinical applications of PET in oncology. *Radiology.* 2004;231(2):305-332.
31. Kobylecka M, Maczewska J, Fronczewska-Wieniawska K, Mazurek T, Plazinska MT, Krolicki L. Myocardial viability assessment in 18FDG PET/CT study (18FDG PET myocardial viability assessment). *Nucl Med Rev Cent East Eur.* 2012;15(1):52-60.
32. Plein S, Sivananthan M. The role of positron emission tomography in cardiology. *Radiography.* 2001;7(1):11-20.

33. Zanoni L, Abdulaziz S, Stefano F. Clinical applications of 18F fluoro-2-deoxy-D-glucose (FDG) positron emission tomography-computed tomography (PET/CT). *Nuclear Medicine Review*. 2012;15:48-51.
34. Alford R, Ogawa M, Choyke PL, Kobayashi H. Molecular probes for the in vivo imaging of cancer. *Mol Biosyst*. 2009;5(11):1279-1291.
35. Lopez-Otin C, Bond JS. Proteases: Multifunctional enzymes in life and disease. *J Biol Chem*. 2008;283(45):30433-30437.
36. Turk B. Targeting proteases: Successes, failures and future prospects. *Nat Rev Drug Discov*. 2006;5(9):785-799.
37. Choi KY, Swierczewska M, Lee S, Chen X. Protease-activated drug development. *Theranostics*. 2012;2(2):156-178.
38. Schechter I, Berger A. On the size of the active site in proteases. I. papain. *Biochem Biophys Res Commun*. 1967;27(2):157-162.
39. Turk V, Stoka V, Vasiljeva O, et al. Cysteine cathepsins: From structure, function and regulation to new frontiers. *Biochim Biophys Acta*. 2012;1824(1):68-88.
40. McGrath ME. The lysosomal cysteine proteases. *Annu Rev Biophys Biomol Struct*. 1999;28:181-204.

41. Ashoor R, Yafawi R, Jessen B, Lu S. The contribution of lysosomotropism to autophagy perturbation. *PLoS One*. 2013;8(11):e82481
42. Guha S, Padh H. Cathepsins: Fundamental effectors of endolysosomal proteolysis. *Indian J Biochem Biophys*. 2008;45(2):75-90.
43. Turk B, Turk D, Turk V. Lysosomal cysteine proteases: More than scavengers. *Biochim Biophys Acta*. 2000;1477(1-2):98-111.
44. Reiser J, Adair B, Reinheckel T. Specialized roles for cysteine cathepsins in health and disease. *J Clin Invest*. 2010;120(10):3421-3431.
45. Mohamed MM, Sloane BF. Cysteine cathepsins: Multifunctional enzymes in cancer. *Nat Rev Cancer*. 2006;6(10):764-775.
46. Tan GJ, Peng ZK, Lu JP, Tang FQ. Cathepsins mediate tumor metastasis. *World J Biol Chem*. 2013;4(4):91-101.
47. Gupta GP, Massague J. Cancer metastasis: Building a framework. *Cell*. 2006;127(4):679-695.
48. Chaffer CL, Weinberg RA. A perspective on cancer cell metastasis. *Science*. 2011;331(6024):1559-1564.
49. Quail DF, Joyce JA. Microenvironmental regulation of tumor progression and metastasis. *Nat Med*. 2013;19(11):1423-1437.

50. Chambers AF, Groom AC, MacDonald IC. Dissemination and growth of cancer cells in metastatic sites. *Nat Rev Cancer*. 2002;2(8):563-572.
51. Nguyen DX, Bos PD, Massague J. Metastasis: From dissemination to organ-specific colonization. *Nat Rev Cancer*. 2009;9(4):274-284.
52. Winnard PT, Jr, Pathak AP, Dhara S, Cho SY, Raman V, Pomper MG. Molecular imaging of metastatic potential. *J Nucl Med*. 2008;49 Suppl 2:96S-112S.
53. Yang Y, Hong H, Zhang Y, Cai W. Molecular imaging of proteases in cancer. *Cancer Growth Metastasis*. 2009;2:13-27.
54. Victor BC, Anbalagan A, Mohamed MM, Sloane BF, Cavallo-Medved D. Inhibition of cathepsin B activity attenuates extracellular matrix degradation and inflammatory breast cancer invasion. *Breast Cancer Res*. 2011;13(6):R115.
55. Nouh MA, Mohamed MM, El-Shinawi M, et al. Cathepsin B: A potential prognostic marker for inflammatory breast cancer. *J Transl Med*. 2011;9(1).
56. Niedergethmann M, Wostbrock B, Sturm JW, Willeke F, Post S, Hildenbrand R. Prognostic impact of cysteine proteases cathepsin B and cathepsin L in pancreatic adenocarcinoma. *Pancreas*. 2004;29(3):204-211.
57. Gong F, Peng X, Luo C, et al. Cathepsin B as a potential prognostic and therapeutic marker for human lung squamous cell carcinoma. *Mol Cancer*. 2013;12(1):125.

58. Shree T, Olson OC, Elie BT, et al. Macrophages and cathepsin proteases blunt chemotherapeutic response in breast cancer. *Genes Dev.* 2011;25(23):2465-2479.
59. Bruchard M, Mignot G, Derangere V, et al. Chemotherapy-triggered cathepsin B release in myeloid-derived suppressor cells activates the Nlrp3 inflammasome and promotes tumor growth. *Nat Med.* 2013;19(1):57-64.
60. Repnik U, Stoka V, Turk V, Turk B. Lysosomes and lysosomal cathepsins in cell death. *Biochim Biophys Acta.* 2012;1824(1):22-33.
61. Droga-Mazovec G, Bojic L, Petelin A, et al. Cysteine cathepsins trigger caspase-dependent cell death through cleavage of bid and antiapoptotic bcl-2 homologues. *J Biol Chem.* 2008;283(27):19140-19150.
62. Blomgran R, Zheng L, Stendahl O. Cathepsin-cleaved bid promotes apoptosis in human neutrophils via oxidative stress-induced lysosomal membrane permeabilization. *J Leukoc Biol.* 2007;81(5):1213-1223.
63. Chen L, Li J, Du L, Li M. Strategies in the design of small-molecule fluorescent probes for peptidases. *Med Res Rev.* 2014;0(0):1-25.
64. Blum G, von Degenfeld G, Merchant MJ, Blau HM, Bogoy M. Noninvasive optical imaging of cysteine protease activity using fluorescently quenched activity-based probes. *Nat Chem Biol.* 2007;3(10):668-677.

65. Cutter JL, Cohen NT, Wang J, et al. Topical application of activity-based probes for visualization of brain tumor tissue. *PLoS One*. 2012;7(3):e33060.
66. Ren G, Blum G, Verdoes M, et al. Non-invasive imaging of cysteine cathepsin activity in solid tumors using a <sup>64</sup>Cu-labeled activity-based probe. *PLoS One*. 2011;6(11):e28029.
67. Ryu JH, Kim SA, Koo H, et al. Cathepsin B-sensitive nanoprobe for in vivo tumor diagnosis. *J Mater Chem*. 2011;21(44):17631-17634.
68. Prabhakar U, Maeda H, Jain RK, et al. Challenges and key considerations of the enhanced permeability and retention effect for nanomedicine drug delivery in oncology. *Cancer Res*. 2013;73(8):2412-2417.
69. de Duve C. Lysosomes revisited. *Eur J Biochem*. 1983;137(3):391-397.
70. de Duve C, de Barse T, Poole B, Trouet A, Tulkens P, Van Hoof F. Commentary. lysosomotropic agents. *Biochem Pharmacol*. 1974;23(18):2495-2531.
71. Kaufmann AM, Krise JP. Lysosomal sequestration of amine-containing drugs: Analysis and therapeutic implications. *J Pharm Sci*. 2007;96(4):729-746.
72. Takakura Y, Hashida M. Macromolecular carrier systems for targeted drug delivery: Pharmacokinetic considerations on biodistribution. *Pharm Res*. 1996;13(6):820-831.
73. Yuan F, Dellian M, Fukumura D, et al. Vascular permeability in a human tumor xenograft: Molecular size dependence and cutoff size. *Cancer Res*. 1995;55(17):3752-3756.

74. Reshef A, Shirvan A, Akselrod-Ballin A, Wall A, Ziv I. Small-molecule biomarkers for clinical PET imaging of apoptosis. *J Nucl Med*. 2010;51(6):837-840.
75. Choe Y, Leonetti F, Greenbaum DC, et al. Substrate profiling of cysteine proteases using a combinatorial peptide library identifies functionally unique specificities. *J Biol Chem*. 2006;281(18):12824-12832.
76. Shao LH, Liu SP, Hou JX, et al. Cathepsin B cleavable novel prodrug ac-phe-lys-PABC-ADM enhances efficacy at reduced toxicity in treating gastric cancer peritoneal carcinomatosis: An experimental study. *Cancer*. 2012;118(11):2986-2996.
77. Zhong YJ, Shao LH, Li Y. Cathepsin B-cleavable doxorubicin prodrugs for targeted cancer therapy (review). *Int J Oncol*. 2013;42(2):373-383.
78. Kumar SK, Williams SA, Isaacs JT, Denmeade SR, Khan SR. Modulating paclitaxel bioavailability for targeting prostate cancer. *Bioorg Med Chem*. 2007;15(14):4973-4984.
79. Meyer Y, Richard JA, Delest B, Noack P, Renard PY, Romieu A. A comparative study of the self-immolation of para-aminobenzylalcohol and hemithioaminal-based linkers in the context of protease-sensitive fluorogenic probes. *Org Biomol Chem*. 2010;8(8):1777-1780.
80. Richard JA, Meyer Y, Jolivel V, et al. Latent fluorophores based on a self-immolative linker strategy and suitable for protease sensing. *Bioconjug Chem*. 2008;19(8):1707-1718.
81. Carl PL, Chakravarty PK, Katzenellenbogen JA. A novel connector linkage applicable in prodrug design. *J Med Chem*. 1981;24(5):479-480.

82. Erez R, Shabat D. The azaquinone-methide elimination: Comparison study of 1,6- and 1,4-eliminations under physiological conditions. *Org Biomol Chem*. 2008;6(15):2669-2672.
83. Alley SC, Benjamin DR, Jeffrey SC, et al. Contribution of linker stability to the activities of anticancer immunoconjugates. *Bioconjug Chem*. 2008;19(3):759-765.
84. Chowdhury MA, Moya IA, Bhilocha S, et al. Prodrug-inspired probes selective to cathepsin B over other cysteine cathepsins. *J Med Chem*. 2014;57(14):6092-6104.
85. Dubowchik GM, Firestone RA. Cathepsin B-sensitive dipeptide prodrugs. 1. A model study of structural requirements for efficient release of doxorubicin. *Bioorg Med Chem Lett*. 1998;8(23):3341-3346.
86. Kannan P, Brimacombe KR, Kreisl WC, et al. Lysosomal trapping of a radiolabeled substrate of P-glycoprotein as a mechanism for signal amplification in PET. *Proc Natl Acad Sci U S A*. 2011;108(6):2593-2598.
87. Ndolo RA, Luan Y, Duan S, Forrest ML, Krise JP. Lysosomotropic properties of weakly basic anticancer agents promote cancer cell selectivity in vitro. *PLoS One*. 2012;7(11):e49366.
88. Wiedner SD, Anderson LN, Sadler NC, et al. Organelle-specific activity-based protein profiling in living cells. *Angew Chem Int Ed Engl*. 2014;53(11):2919-2922.
89. Singerman GM. Cinnolines. In: *Chemistry of heterocyclic compounds*. John Wiley & Sons, Inc; 1973:1-321.

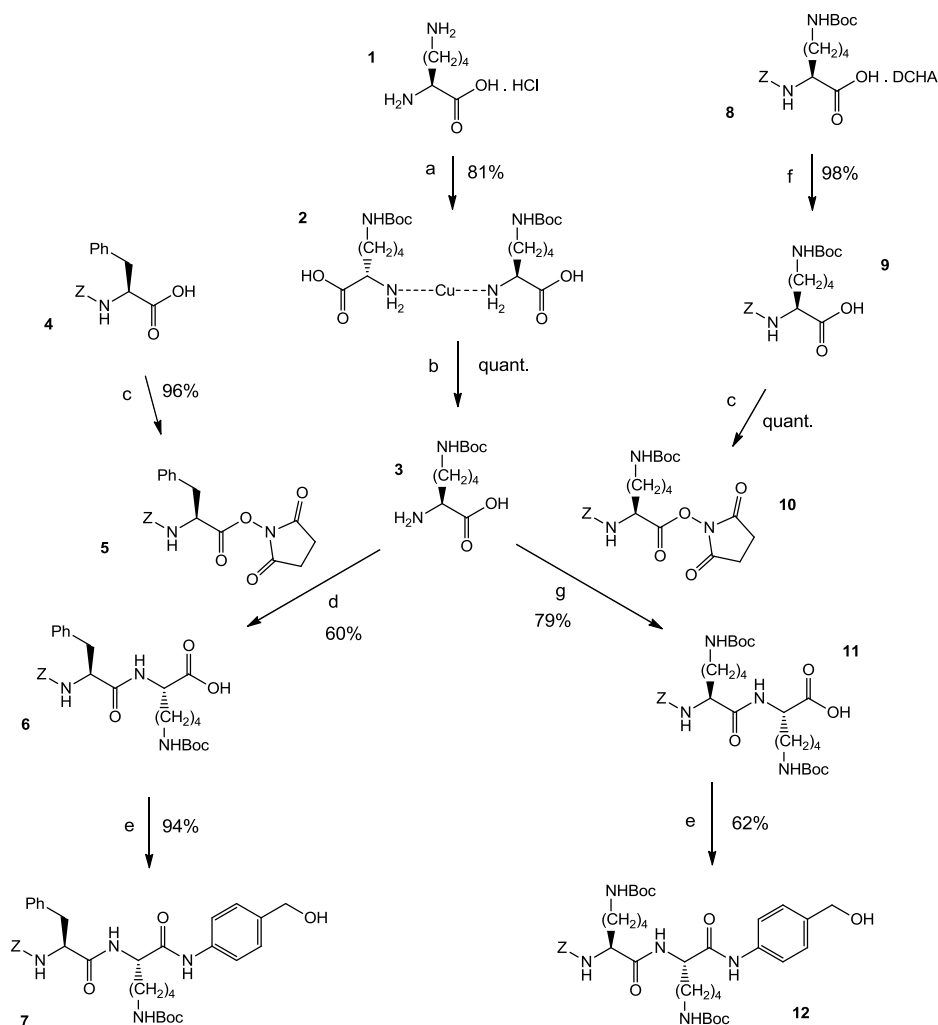
90. Duvvuri M, Konkar S, Funk RS, Krise JM, Krise JP. A chemical strategy to manipulate the intracellular localization of drugs in resistant cancer cells. *Biochemistry*. 2005;44(48):15743-15749.

## Chapter 3: Methodology

This chapter reviews the methods used in the following manuscript, with a focus on the underlying rationale and theory not covered therein. Specific procedural details are provided in the following manuscript of Chapter 4.

### 3.1: Synthesis of Probe Candidates

For the purpose of evaluating a series of substrate-based molecular probes bearing aminoquinoline reporter groups, we sought a common route for their preparation. First, the two substrate-linker peptides Z-Phe-Lys(BOC)-PAB-OH and Z-Lys(BOC)-Lys(BOC)-PAB-OH are prepared using well-established peptide chemistry<sup>1</sup>. Each quinoline was then conveniently conjugated by means of isocyanation and subsequent coupling to the acidic hydroxyl group of PABA through a stable carbamate linkage. The quinolines 3-AMQ, 5-AIQ, and 6-AMQ are all converted to their respective isocyanates by phosgenations, while 4-quinolinecarboxylic acid (4-QCA) is converted to its respective isocyanate by means of a Lossen rearrangement for incorporation as the 4-AMQ reporter group.<sup>2</sup> Deprotection of the BOC groups was achieved rapidly in quantitative or high yield using 50% TFA:DCM. The use of lysine instead of arginine, an amino acid preferred at the S<sub>1</sub> site of CTB and CTL, was chosen due to the convenient installation and removal of BOC protecting groups from the  $\epsilon$ -amine versus protection and deprotection of the arginine guanidinium group.



**Scheme 3: Synthetic scheme of precursor peptides Z-FK-PAB-OH (7) and Z-KK-PAB-OH (12).** (a)  $\text{CuSO}_4 \cdot 5\text{H}_2\text{O}$ ,  $\text{BOC}_2\text{O}$ ,  $\text{H}_2\text{O}/\text{acetone}$ , RT, 12h; (b) 8-hydroxyquinoline,  $\text{H}_2\text{O}$ , RT, 5h; (c) HO-Su, DCC, THF,  $0^\circ\text{C}$ -RT, 12h; (d)  $\text{NaHCO}_3$ , THF/ $\text{H}_2\text{O}$ , RT, 16h; (e) EEQD, THF, RT, 16h; (f)  $\text{H}_2\text{SO}_4$ , ethyl acetate, RT, 1h; (g)  $\text{Et}_3\text{N}$ , DMF,  $0^\circ\text{C}$ -RT, 16h

The activated precursors Z-Phe-O-succinimide (5) and Z-Lys-N- $\epsilon$ -BOC-O-succinimide (10) were prepared according to literature<sup>3</sup> as seen in reaction (c) of Scheme 3. Commercially available Z-Lys(BOC)-OH·DCHA (8) was extracted to the free acid (9) using  $\text{H}_2\text{SO}_2$ , and along with commercially available Z-Phe-OH, the two were both converted to their respective succinimides using N-hydroxysuccinimide and DCC. For the purpose of being coupled to the

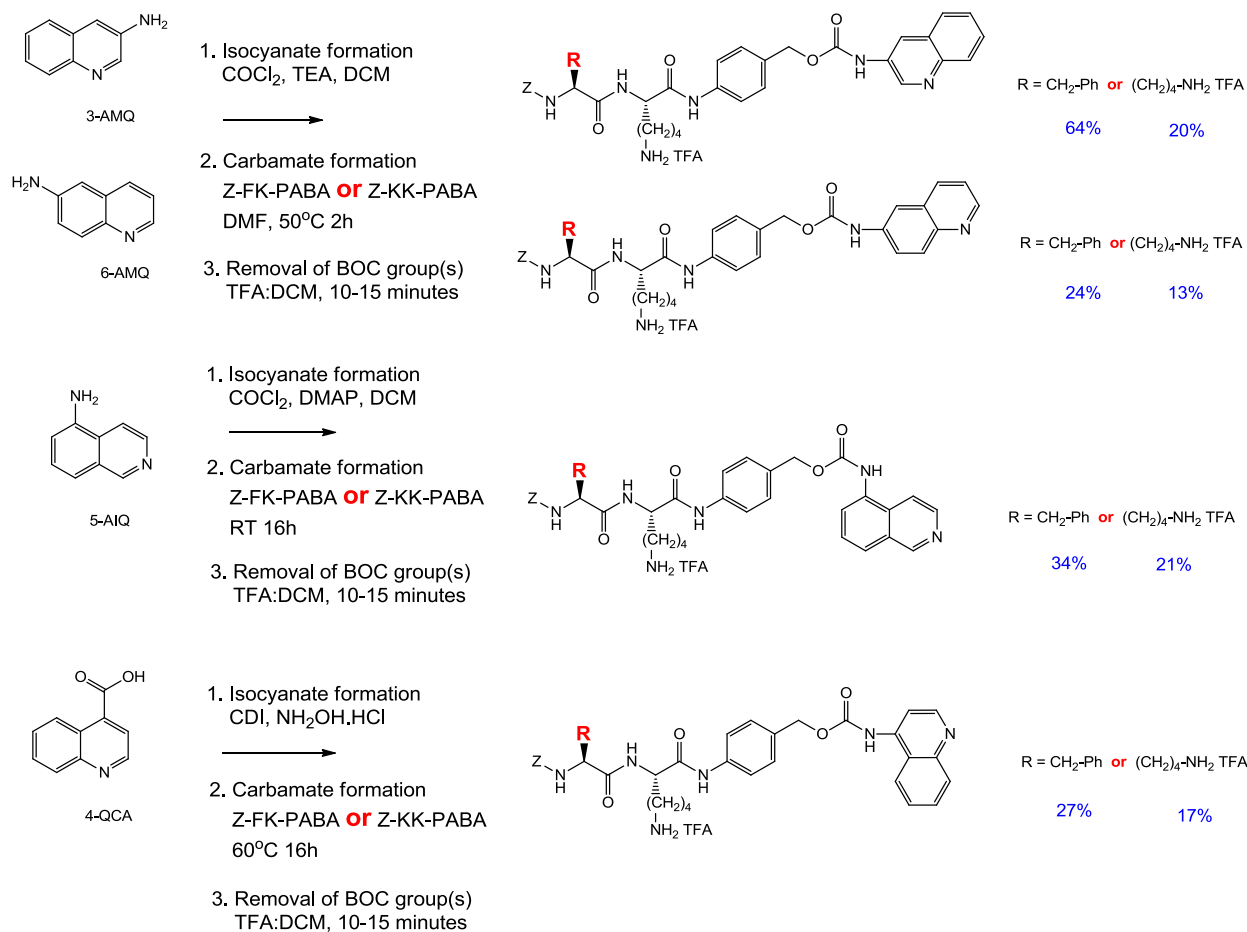
activated precursors (5) and (10) as the P<sub>1</sub> moiety of all probe candidates, Lys(BOC)-OH (3) was also conveniently and inexpensively prepared according to literature<sup>4</sup>, although it can be purchased commercially if desired. Lys•HCl was converted to Lys<sub>2</sub>Cu as an intermediate using CuSO<sub>4</sub>•5H<sub>2</sub>O, followed by addition of excess di-*tert*-butyl dicarbonate in a one-pot procedure to yield (2). The unreacted pyrocarbonate is decomposed using methanol prior to filtering the precipitated [Lys(BOC)]<sub>2</sub>Cu product, after which the copper is quantitatively removed using 8-quinolinol to furnish (3).

Coupling of (3) with either (5) or (10) was performed to provide either Z-Phe-Lys(BOC)-OH (6) or Z-Lys(BOC)-Lys(BOC)-OH (11) respectively. Coupling of (3) with (5) was performed using NaHCO<sub>3</sub> in water and THF<sup>5</sup>, while (3) was coupled to (10) using TEA as the base and DMF as the solvent<sup>6</sup>. Both of the resulting peptides (6) and (11) were coupled with PABA using EEDQ in THF<sup>1</sup>, providing Z-Phe-Lys(BOC)-PAB-OH (7) and Z-Lys(BOC)-Lys(BOC)-PAB-OH (12).

Phosgenation of 5-AIQ in the presence of 4-dimethylaminopyridine was carried out overnight in a procedure adapted from literature, and following extraction of the isocyanate it was coupled to 7 and 12 in yields of 34% and 21% respectively. While this procedure provided modest yields for 5-AIQ, it was ineffective in the coupling of 6-AMQ and 3-AMQ to 7 and 12. Isocyanation and subsequent coupling of both 6-AMQ and 3-AMQ is performed using a shared procedure adapted from literature<sup>7</sup> as shown in Scheme 4. Conversion of either 6-AMQ or 3-AMQ to their respective isocyanates is achieved using phosgene in the presence of triethylamine, and subsequent coupling to either 7 or 12 is performed in a one-pot fashion within hours. In this manner, 6-AMQ was coupled to 7 and 12 in yields of 24% and 16% respectively, while 3-AMQ was coupled to 7 and 12 in yields of 64% and 20% respectively. 4-

quinolinecarboxylic acid (4-QCA) is converted to its respective isocyanate through a Lossen Rearrangement using carbonyldiimidazole and hydroxyl amine<sup>2</sup>, so as to be incorporated as the 4-aminoquinoline (4-AMQ) reporter group. We chose 4-QCA as it is commercially inexpensive relative to its 4-AMQ counterpart yet is still conveniently coupled in a one-pot procedure with 7 and 12 with yields of 27% and 19% respectively. 8-aminoquinoline failed to be converted to its isocyanate counterpart for coupling, probably due to the low nucleophilicity of its amine.

All resulting BOC-protected carbamates were deprotected using 50% TFA:DCM at ice bath temperature, rapidly providing the final probe candidates seen in Scheme 4. Deprotection was quantitative in all cases except in furnishing Z-K(TFA)K(TFA)-PABA-6AMQ and Z-K(TFA)K(TFA)-PABA-4AMQ, which were obtained in yields of 82% and 88% respectively from their BOC-protected counterparts.



**Scheme 4: Conjugation of the four aminoquinoline reporter groups to 7 and 12.** 3-AMQ, 6-AMQ, and 5-AIQ are all converted to their respective isocyanates via phosgenation for convenient coupling to the acidic hydroxyl of 7 and 12. 4-quinolinecarboxylic acid (4-QCA) is converted to its isocyanate via a Lossen Rearrangement for incorporation as the 4-aminoquinoline reporter group. All BOC-protected carbamates are deprotected in quantitative or high yield using TFA:DCM. Yields are based on precursor peptides 7 and 12.

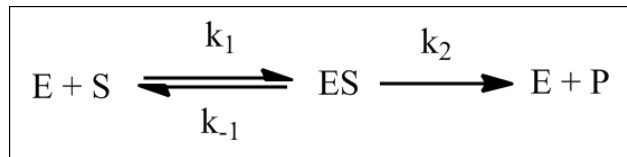
### 3.2: Kinetic Evaluation of Probe Candidates

There are two common methods for determining kinetic parameters associated with enzymatic activity, although both rely on quantifying the formation of product or the consumption of substrate over a given amount of time. The first type of enzymatic assay is an end-point assay, where samples of the enzymatic reaction are stopped after given time points and the concentration of substrate or product is quantified. This is in contrast to a continuous assay, which employs a continuous or "live" reading of substrate turnover during the course of the reaction. Quantification of substrate turnover is typically based on the generation of a fluorescent signal as a result of enzymatic processing, or spectrophotometric detection of the product as a result of UV or visible light absorption. Fluorescent detection of product is typically more sensitive, but in either case there must be no interference between materials in the assay matrix and the optical properties of the analyte if a continuous assay is to be employed. That is, the optimal wavelengths of excitation or emission must not be absorbed or emitted by other materials in the assay matrix such as excess substrate. In the case of prodrugs or PET imaging agents that are potential substrate-based probes of specific enzymes, the drugs or reporter groups are not chosen based on their optical properties but rather their biological properties. As a result, there are cases where a stopped assay in combination with techniques other than spectrophotometry must be employed for the detection of reporter groups.

Since the quinoline reporter groups employed in our probe candidates do not have suitable optical properties for detection by means of a continuous assay, a convenient end-point assay was established, employing high-performance liquid chromatography (HPLC) in the resolution and detection of the quinoline reporter groups. In addition, poor solubility of probe

candidates was noted prior to achieving enzyme-saturating concentrations of substrate and therefore a value of  $k_{\text{cat}}/K_M$  could not be derived from full Michaelis-Menten curves. As a result, a commonly used mathematical estimation of  $k_{\text{cat}}/K_M$  using low substrate concentrations was employed, based on an alternative representation of the Michaelis-Menten equation.

The Michaelis-Menten model of enzyme kinetics describes substrate binding and catalysis in terms of reaction rate constants as seen in Scheme 5.



**Scheme 5: General scheme for Michaelis-Menten Kinetics**

Where  $k_1$  and  $k_{-1}$  are equilibrium constants representing the rate of formation of the enzyme-substrate complex [ES] for a given substrate S, and  $k_2$  represents the rate of catalysis (or  $k_{\text{cat}}$ ) to product P. The effective rate of hydrolysis is represented by the following relationship:

$$v_0 = \frac{[S]}{K_M + [S]} V_{\text{max}}$$

**Equation 1**

Where  $v_0$  represents the initial rate of hydrolysis, the term  $[S]/(K_M + [S])$  represents the ratio of enzyme bound to ligand, and  $V_{\text{max}}$  represents the maximum velocity under saturating concentrations of substrate. As seen in a Michaelis-Menten plot (Figure 8),  $K_M$  represents the concentration of substrate at which half of the maximal velocity  $V_{\text{max}}$  is achieved. The equation demonstrates that  $v_0$  is proportional to  $[S]$  at low concentrations of substrate, noted by the

linear portion of the plot. However upon saturating concentrations of substrate, when  $[S] \gg K_M$ ,  $v_0 \approx V_{\max}$  and the velocity is independent of substrate concentration as observed by the plateau. The  $k_{\text{cat}}$  term of  $k_{\text{cat}}/K_M$  is derived from such a plot by dividing  $V_{\max}$  by total enzyme concentration ( $[E]_{\text{total}} = [ES] + [E]$ ).

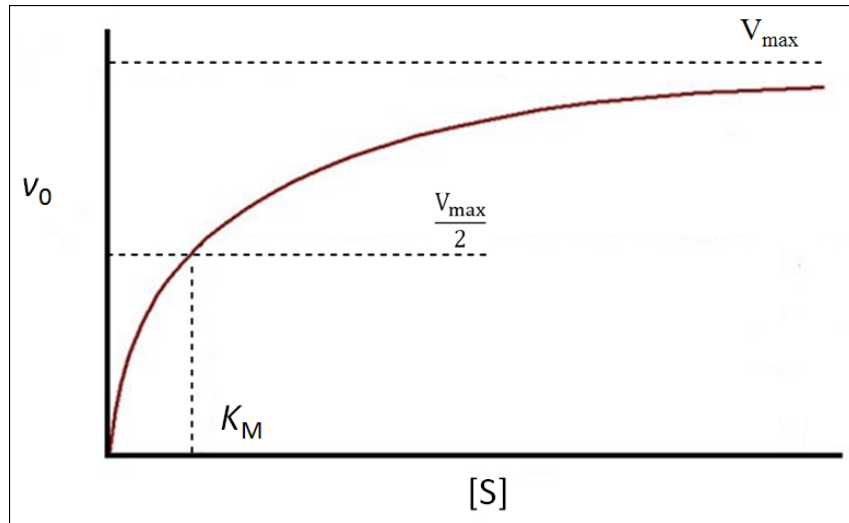


**Figure 8: Michaelis-Menten curve.** The initial rate of reaction  $v_0$  is represented along the y-axis while substrate concentration  $[S]$  is represented along the x-axis.  $K_M$  represents the substrate concentration at which half the maximal velocity  $V_{\max}$  is achieved, and the two values are used to elucidate a  $k_{\text{cat}}/K_M$  value for a given substrate and enzyme.

When saturating concentrations of substrate cannot be achieved due to solubility, availability, time, or cost of precious substrates, the linear portion of the curve at low  $[S]$  can be used to estimate the combined  $k_{\text{cat}}/K_M$  term<sup>8-12</sup>. By substituting  $V_{\max} = k_2[E]_{\text{total}} = k_{\text{cat}}[E]_{\text{total}}$  into Equation 1, the following is obtained:

$$v_0 = \frac{[S][E]_{\text{total}}k_{\text{cat}}}{K_M + [S]}$$

Equation 2

When  $[S] \ll K_M$  as represented by the linear portion of a Michaelis-Menten curve,

$$v_0 \approx \frac{[S][E]_{\text{total}}k_{\text{cat}}}{K_M}$$

Equation 3

or

$$v_0/[S] \approx \frac{k_{\text{cat}}}{K_M} [E]_{\text{total}}$$

Equation 4

Equation 3 represents a second order rate equation with units  $\mu\text{M}^{-1}\text{Sec}^{-1}$  and is rearranged to provide Equation 4. In this representation of the Michaelis-Menten equation,  $v_0/[S]$  represents the slope of the linear fit while  $[E]_{\text{total}}$  represents the enzyme concentration used for the assay. In other words, by dividing the slope of the linear fit  $v_0/[S]$  by enzyme concentration, an estimation of  $k_{\text{cat}}/K_M$  can theoretically be obtained. Not only is this a useful method when encountering solubility issues at relatively high  $[S]$ , it also proved to be valuable in streamlining the process of screening probes candidates using automated HPLC. Specific procedural details are provided in the following manuscript, and the resulting kinetic studies for all probe candidates are presented and discussed therein.

### 3.3: References

1. Chowdhury MA, Moya IA, Bhilocha S, et al. Prodrug-inspired probes selective to cathepsin B over other cysteine cathepsins. *J Med Chem*. 2014;57(14):6092-6104.
2. Dube P, Nathel NF, Vetelino M, et al. Carbonyldiimidazole-mediated lossen rearrangement. *Org Lett*. 2009;11(24):5622-5625.
3. Firestone RA, Dubowchik GM. Lysosomal enzyme-cleavable antitumor drug conjugates. Bristol-Myers Squibb Company, Patent EP0624377A2. 1994.
4. Wiejak S, Masiukiewicz E, Rzeszotarska B. A large scale synthesis of mono- and di-urethane derivatives of lysine. *Chem Pharm Bull*. 1999;47(10):1489-1490.
5. Felix AM, Gillessen G, Lergier W, Meienhofer JA, Trzeciak AF. Intermediates for thymosin alpha 1. Hoffmann-La Roche & Co, Patent EP0123951A2. 1984.
6. Rauber P, Walker B, Stone S, Shaw E. Synthesis of lysine-containing sulphonium salts and their properties as proteinase inhibitors. *Biochem J*. 1988;250(3):871-876.
7. Lee MR, Baek KH, Jin HJ, Jung YG, Shin I. Targeted enzyme-responsive drug carriers: Studies on the delivery of a combination of drugs. *Angew Chem Int Ed Engl*. 2004;43(13):1675-1678.
8. Rothlisberger D, Khersonsky O, Wollacott AM, et al. Kemp elimination catalysts by computational enzyme design. *Nature*. 2008;453(7192):190-195.

9. Gordon SR, Stanley EJ, Wolf S, et al. Computational design of an alpha-gliadin peptidase. *J Am Chem Soc.* 2012;134(50):20513-20520.
10. Moroz OV, Moroz YS, Wu Y, et al. A single mutation in a regulatory protein produces evolvable allosterically regulated catalyst of nonnatural reaction. *Angew Chem Int Ed Engl.* 2013;52(24):6246-6249.
11. James TW, Frias-Staheli N, Bacik JP, et al. Structural basis for the removal of ubiquitin and interferon-stimulated gene 15 by a viral ovarian tumor domain-containing protease. *Proc Natl Acad Sci U S A.* 2011;108(6):2222-2227.
12. Barrett AJ. Fluorimetric assays for cathepsin B and cathepsin H with methylcoumarylamide substrates. *Biochem J.* 1980;187(3):909-912.

## Chapter 4: Manuscript

### 4.1: Abstract

Members of the cathepsin family of cysteine proteases are gaining interest as potential imaging biomarkers and drug targets due to their multifunctional roles in regulatory processes such as cell recycling and wound healing, but also due to their multifunctional roles in diseases such as cancer, asthma and arthritis. Developing imaging agents with the ability to assess cathepsin activity *in vivo* is important for identifying specific roles in disease and ultimately guiding therapy and drug development. We report here novel prodrug-inspired substrates that release lysosomotropic reporter groups upon activation by CTB and CTL. We hypothesize that aminoquinolines may be retained in the lysosome where the majority of cysteine cathepsins are primarily active. To evaluate this approach we first synthesized a variety of substrates bearing various aminoquinoline isomers connected to CTL and CTB recognition peptides derivatized with the prodrug linker *p*-aminobenzyl alcohol. Then, a convenient HPLC method was developed to estimate  $k_{\text{cat}}/K_M$  values first using commercial fluorogenic substrates then using the novel quinoline-modified probe candidates. Three of the candidates were hydrolyzed by CTL with very efficient  $k_{\text{cat}}/K_M$  values, suggesting that prodrug-inspired probes bearing AMQ reporters could potentially be adapted into PET imaging agents that are efficient substrates of CTB and CTL, releasing a reporter that is retained in the lysosome of cancer cells overexpressing cysteine cathepsins.

## 4.2: Introduction

The cysteine cathepsins have various roles in healthy cell function, but their aberrant expression has been linked to aggressive cancer, arthritis, and various respiratory and lysosomal storage diseases<sup>1,2</sup>. There are 11 human cysteine cathepsins and interest has grown in cathepsins as biomarkers of disease or drug targets<sup>3</sup>. Most cysteine cathepsins are ubiquitously expressed, but by virtue of being involved in many normal and disease processes, their *in vivo* expression and activity varies greatly. The majority of cysteine cathepsins are found sequestered in lysosomes and to a lesser extent endosomes, and therefore a reducing, acidic environment is needed for optimal activity. However in addition to the physiochemical environment and localization, catalytic activity is controlled by interaction with a complex system of other biological molecules. To begin, cathepsins are synthesized as mainly inactive proenzymes, and activation to their respectively mature counterparts can be carried out by the residually active proenzymes themselves, known as autocatalysis, or by other proteases operating in the lysosome. Inhibition of activity to prevent unwanted proteolysis can be controlled by diverse reversible small protein inhibitors called cystatins, thyropins, and serpins<sup>1</sup>. Variability in expression, proenzyme activation, and endogenous inhibition results in great variation in the catalytic activity of the cathepsins dependent on location in tissues and cells. Techniques which can assess the functional activity of cathepsins as opposed to expression levels alone are therefore needed to fully understand the role that each enzyme has in disease-promoting processes.

The increased expression and activity of cathepsins in various cancers, in combination with their involvement in various stages of tumor progression, has led to interest in cathepsins as imaging biomarkers and drug targets<sup>3</sup>. Overexpression and localization at the invading edge of a tumor or in the tumor microenvironment is linked with aggressive cancers<sup>4</sup>, while intracellular CTB has been shown to indirectly induce apoptosis in tumor cells<sup>5</sup>. CTB has also been reported to not only blunt tumor response to chemotherapy, but actually promote tumor growth in response to chemotherapy<sup>6,7</sup>. Although there is evidence suggesting that CTB has important roles in cancer and its prognosis, probes capable of evaluating CTB activity *in vivo* are needed to specifically define these roles and determine if CTB is a legitimate biomarker of aggressive cancer or a potential therapeutic target.

The first reported strategy for visualizing cysteine protease activity in cells and animals originated with Bogoy and coworkers, who developed fluorescently quenched activity-based probes (qABPs) employing an acyloxymethyl ketone (AOMK) warhead<sup>8</sup>. The AOMK warhead, which is conjugated to a fluorophore-derivatized dipeptide, alkylates the active site cysteine residue to form a covalent thioether ketone linkage. Although efficient at visualizing cathepsin activity *in vitro*, the qABPs lacked specificity as both CTB and CTL were efficiently labelled. And while these smart ABPs yield a fluorescent signal only upon reacting with and attaching to the cysteine active site, a potential drawback results from the 1:1 stoichiometry, limiting signal accumulation and image contrast.

To improve signal contrast by exploiting the catalytic power of the cysteine proteases, Kim and coworkers designed substrate-based probes (SBPs) using a polymer composed of

monomers conjugated to either a tumor-targeting hormone or a CTB-targeting substrate in an alternating fashion. Each cathepsin-targeting peptide was derivatized with a Cy5.5 fluorophore and the BHQ-3 quencher at opposite termini of the CTB-hydrolyzable bond, allowing the fluorophore to be released to yield strong fluorescence in correlation with CTB activity. Although SBPs may increase contrast since a single enzyme can hydrolyze and release thousands of probe molecules per minute, nanoparticles typically have poor cell permeability and long circulation times meaning that images can often only be taken days after injection. In addition, nanoparticle imaging probes depend heavily on the enhanced permeability and retention (EPR) of tumor vasculature for tumor delivery. However heterogeneity of the EPR effect within and between tumor types has hampered the development and utility of imaging agents and drugs employing a nanoparticle design. In contrast, small molecule substrate-based probes could potentially offer better pharmacokinetic properties while still offering a mechanism for signal amplification.

Although SBPs offer the advantage of signal amplification, a major drawback commonly encountered is the rapid diffusion of the reporter molecules from the site of enzyme activation. However cathepsins are primarily active in the acidic lysosome of cells, and a low pH may potentially be used to enhance the retention of reporter groups within this environment by using basic amines that become protonated and membrane impermeable once enzymatically released. Not long after discovering the lysosome six decades ago, deDuve reported that weakly basic amines spontaneously accumulate to high concentrations after becoming ionically charged in the acidic environment of the lysosomes, a phenomenon called lysosomotropism<sup>9</sup>. Indeed, there are examples of imaging agents and therapeutics that have taken advantage of

lysosomotropic properties for increased sensitivity or selectivity toward their given targets. Lysosomal trapping as a mechanism of signal amplification in PET was demonstrated by Hall and coworkers, who established that [<sup>11</sup>C]N-desmethyl-loperamide enters brain cells and accumulates in lysosomes therein<sup>10</sup>. Lysosomotropic anticancer agents have been shown to promote cancer cell selectivity at least *in vitro*<sup>11</sup>, and a number of investigators have reported on the effects of lysosomotropism on drug biodistribution in tissue<sup>12</sup>. Although a lysosomotropic epoxide-based inhibitory cathepsin probe was reported by Wright and coworkers<sup>13</sup>, the design causes it to be retained in the lysosome regardless of cathepsin recognition. Since most cysteine proteases reside primarily in the lysosome, SBPs that employ lysosomotropic amines would have the advantages of rapid turnover while trapping the reporter in the lysosome.

We report here the synthesis and *in vitro* kinetic analysis of eight novel three-component SBPs consisting of a dipeptide substrate, a prodrug linker, and one of four aminoquinoline reporter groups. Three of the four quinoline reporter groups used (3-AMQ, 4-AMQ and 5-AIQ) have previously been reported as lysosomotropic<sup>14</sup> but have yet to be used as reporter groups of enzymatic activity. All probes were easily prepared and through a convenient HPLC method shown to be efficiently hydrolyzed by cathepsins B and L. Importantly, three of the eight probes were very efficiently hydrolyzed by CTL and are therefore excellent lead compounds for the design of future PET imaging probes. This work is a significant step toward the development of substrate-based probes that provide an amplification of signal through catalytic activity while also immobilizing the reporter molecule at the site of enzyme activity.

## 4.3: Results and discussion

### 4.3.1: Probe Design

Rather than functioning as activity-based inactivators that are covalently retained in the active site of the target, we desired substrate-based probes that would be catalytically processed by CTB or CTL to release a lysosomotropic reporter molecule where cysteine cathepsins primarily reside. We hypothesize that our substrate-based approach will take advantage of the catalytic power of the target protease while still locking the reporter molecule at the site of hydrolysis, thus providing an amplification of signal compared to an activity-based approach which inactivates the target enzyme. Designed to be efficient substrates for CTB and CTL, these prodrug-inspired peptidic probe candidates employ a three-component design consisting of a dipeptide substrate that provides high affinity and specificity to CTB and/or CTL, a self-immolative linker that spontaneously releases a reporter upon its enzymatic hydrolysis from the peptide, and one of various aminoquinoline reporters that are expected to be locally retained in the cathepsin-laced lysosome. Analogous to prodrugs that are processed to release an active drug as seen in Figure 9, these substrate-based probes are designed to be efficiently hydrolyzed by CTB to release one of various aminoquinoline isomers that should be retained within the lysosome. The PABA linker has been used in the design of prodrugs, and until recognition and cleavage by CTB within the lysosome of the cell, the intact probe should be cell permeable and travel throughout the body to reach the target site. <sup>18</sup>F-labelled lysosomotropic reporter groups could prove useful toward developing cathepsin substrate-based PET agents that are retained in their immediate environment.

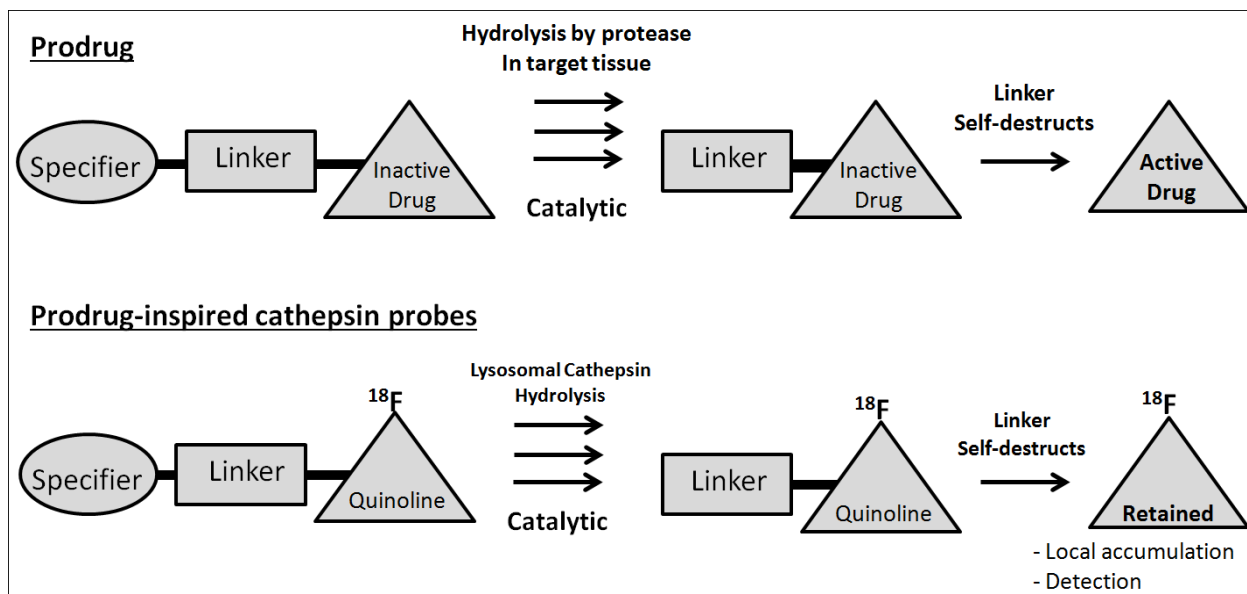


**Figure 9: Prodrug-inspired substrate based approach for CTB and CTL probes.** Prodrugs are enzymatically processed at a target site to release an active drug. In an analogous fashion, the prodrug-inspired probe candidates employed herein are efficiently hydrolyzed by CTB and CTL to release one of various aminoquinoline isomers, which are all expected to accumulate in the cathepsin-occupied lysosome and can foreseeably be <sup>18</sup>F-radiolabeled. Such substrate-based probes offer an amplification of signal compared to activity-based inactivators while still potentially offering a mechanism of signal localization.

To evaluate lysosomotropic amines in the context of potential PET imaging reporter molecules for lysosomal enzymes, we first synthesized substrates that are likely to be rapidly hydrolyzed by several cysteine cathepsins. The majority of cysteine cathepsins prefer a positively charged species in the P<sub>1</sub> position of the peptide substrate and a hydrophobic species in the P<sub>2</sub> position<sup>15</sup>. We therefore synthesized derivatives employing (s)-lysine and (s)-phenylalanine at the P<sub>1</sub> and P<sub>2</sub> positions respectively (Figure 10), while protected at the N-terminus using carboxybenzyl (Z) as this has been shown in literature to be well accepted by the P<sub>3</sub> pocket of many cysteine cathepsins. However, we also desired probes that had selectivity to CTB over other cysteine cathepsins. CTB is unique in that it can accept a positively charged amino acid at the top of its P<sub>2</sub> pocket. This is due to the presence of a glutamic acid residue at



not only been shown to be efficiently processed by cathepsins to release an active drug, but are serum stable as well.

The four quinoline reporter groups employed in our prodrug substrates are 3-aminoquinoline (3-AMQ), 4-aminoquinoline (4-AMQ), 5-aminoisoquinoline (5-AIQ), and 6-aminoquinoline (6-AMQ), as shown in Figure 11. The approximate pH range of the lysosome is 4 - 5<sup>16</sup>, while the quinoline isomers 3-AMQ, 4-AMQ, 5-AIQ, and 6-AMQ have pKa values of 5.0, 9.2, 6.0 and 5.6 respectively<sup>14,17</sup>. These quinolines are thus expected to be mostly ionic and retained in the acidic lysosome where CTB and CTL primarily reside. The lysosomotropic properties of 3-AMQ, 4-AMQ, and 5-AIQ have been reported as the ratio of [lysosomal]/[cytosolic] accumulation, with 4-AMQ having a value of approximately 60, while that for 5-AIQ and 3-AMQ was approximately 25 and 4 respectively<sup>14</sup>. The pKa values of the individual quinolines correlate with lysosomotropic results and likely determine the degree to which each becomes retained in the low pH of the lysosome. Although 6-AMQ is not reported in literature as being lysosomotropic, its pKa of 5.6 means it is also likely to be charged and retained within the lysosome. It is important to acknowledge that the ratio of lysosomal to cytosolic accumulation was obtained by treating live cells with each aminoquinoline isomer. In such a case, each quinoline must cross several lipid bilayers in contrast to being released directly into the acidic lysosome by the cysteine cathepsin enzyme. Therefore, lysosomal retention of an enzymatically released aminoquinoline may differ from lysosomal accumulation in cells treated with each quinoline. In order to first assess the potential utility of cysteine cathepsin SBPs bearing lysosomotropic reporter groups, we synthesized a series of eight probe

candidates bearing aminoquinoline isomers as reporters and determined the  $k_{\text{cat}}/K_M$  values of each using recombinant CTB and CTL.

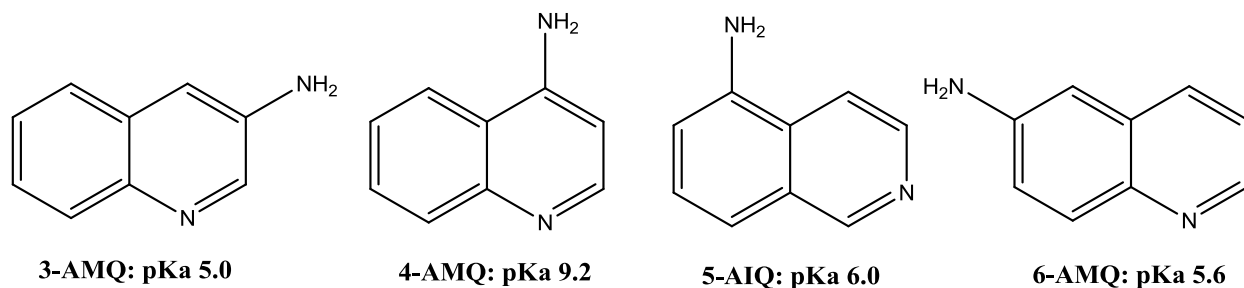


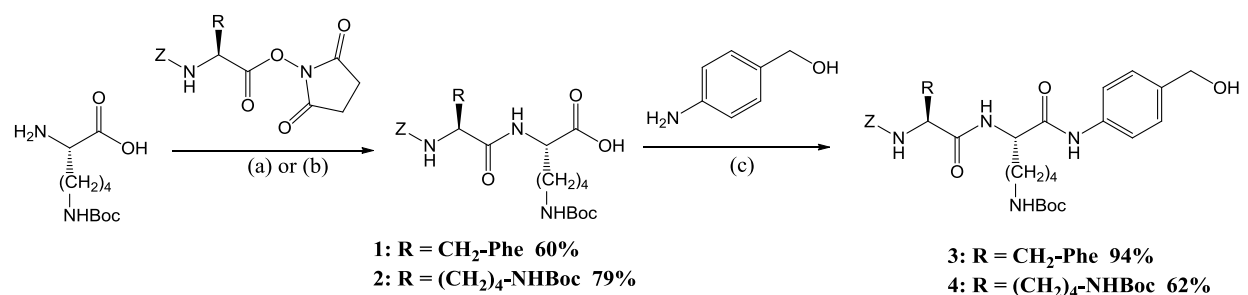
**Figure 11: The four quinoline isomers used as reporter groups in our substrate-based probes.** For the purpose of assessing the ability to image cathepsins using lysosomotropic reporter groups, amines with varying pKa were chosen which can all be conjugated to our substrates via similar chemistry. 3-AMQ, 4-AMQ, and 5-AIQ have been reported as being lysosomotropic when incubated with cells, and because 6-AMQ has a pKa > 5, it is also likely to be mainly protonated in the acidic lysosome.

#### 4.3.2: Synthesis

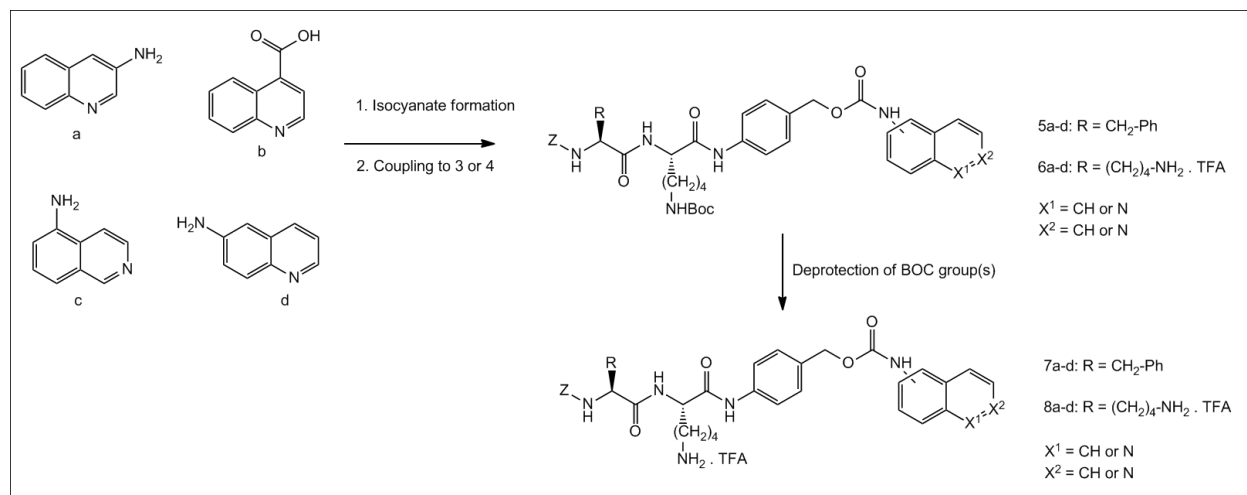
In order to evaluate the suitability of lysosomotropic amines as reporter molecules of substrate-based molecular probes, we first sought a convenient route for their preparation. To begin, the two substrate-linker peptides Z-Phe-Lys(BOC)-PAB-OH and Z-Lys(BOC)-Lys(BOC)-PAB-OH were prepared using well-established peptide chemistry as seen in Scheme 6<sup>18</sup>.

Incorporation of the 3-AMQ, 4-AMQ, 5-AIQ, and 6-AMQ reporter groups by means of a carbamate linkage was carried out by reacting their respective isocyanoquinolines with the acidic hydroxyl group of PAB-OH as seen in Scheme 7. 3-AMQ, 5-AIQ, and 6-AMQ are all converted to their respective isocyanates by means of phosgenation in the presence of either TEA or DMAP. 4-quinolinecarboxylic acid (4-QCA) was converted to its respective isocyanate through a Lossen Rearrangement using CDI and hydroxyl amine<sup>19</sup>, so as to be incorporated as the 4-AMQ reporter group. We chose 4-QCA as it is commercially inexpensive relative to its 4-

AMQ counterpart and is conveniently coupled to PABA using a Lossen Rearrangement in a one-pot procedure. Isocyanation and subsequent coupling of 3-AMQ and 6-AMQ to Z-FK-PABA and Z-KK-PABA was achieved within 6 hours while 4-AMQ and 5-AIQ were coupled overnight. All BOC-protected carbamates 5a-d and 6a-d were deprotected quantitatively or in high yield using 50% TFA:CH<sub>2</sub>Cl<sub>2</sub>, providing the final probes 7a-d and 8a-d.



**Scheme 6: Formation of precursor peptides 3 and 4.** (a) Z-Phe-OSu, NaHCO<sub>3</sub>, THF-H<sub>2</sub>O, rt, 16h; (b) Z-Lys-OSu, Et<sub>3</sub>N, DMF, 0°C to rt, 16 h; (c) PABA, THF, EEDQ, rt, 16 h



**Scheme 7: General scheme for conjugation of the quinoline reporters to the peptide precursors 3 and 4 via stable carbamate linkages.**

| Z-FK Probes<br>Yield% | Structure | Z-KK Probes<br>Yield% | Structure |
|-----------------------|-----------|-----------------------|-----------|
| 7a<br>64%             |           | 8a<br>20%             |           |
| 7b<br>27%             |           | 8b<br>17%             |           |
| 7c<br>34%             |           | 8c<br>21%             |           |
| 7d<br>24%             |           | 8d<br>13%             |           |

**Table 1: Structures and yields for the deprotected probe candidates.** Yields are based on starting peptides 3 and 4.

#### 4.3.3: Enzymatic Assays

Enzyme kinetic studies are ideally performed using chromogenic or fluorogenic substrates, where continuous turnover of substrate is conveniently quantified using spectrophotometry. However, continuous plate reader assays cannot always be used due to high concentrations of substrate interfering with the optical wavelengths of the reporter. Although the optical properties of the aminoquinoline reporters are not suitable for detection using a continuous plate reader assay, we show that 3-AMQ, 4-AMQ, and 6-AMQ have strong fluorescence when resolved and detected using HPLC. While 5AIQ was not fluorescent under any conditions, it has strong UV absorbance. Therefore,  $k_{cat}/K_M$  values can be estimated using a convenient stopped HPLC method monitoring the release of aminoquinolines. In addition, poor

solubility of probe candidates was noted prior to achieving enzyme-saturating concentrations of substrate and therefore values of  $k_{\text{cat}}/K_M$  could not be derived from full Michaelis-Menten curves. To estimate  $k_{\text{cat}}/K_M$  values, the slope of the linear fit of  $v_0$  vs  $[S]$  at low substrate concentrations was fitted to the linear relationship of  $[v_0/(S)]/[E] = k_{\text{cat}}/K_M$ <sup>20-24</sup>. In this representation of the Michaelis-Menten equation,  $v_0/S$  represents the slope of the linear fit while  $[E]$  represents the final enzyme concentration.

In order to verify that  $k_{\text{cat}}/K_M$  values of our probe candidates can be accurately predicted using HPLC and this representation of the Michaelis-Menten equation, benchmark kinetic values for two commercial substrates were determined using a continuous assay and compared to values obtained using the stopped HPLC method. Enzymatic turnover was stopped at known times using sodium chloroacetate, a potent inhibitor of cysteine proteases. This is a shelf-stable, inexpensive water-soluble inhibitor which alkylates all cysteine active sites immediately. Although CTB and CTL were never assayed at concentrations exceeding 3 nM, sodium chloroacetate was used in 50 mM excess. This ensured saturation and complete inactivation while still maintaining solubility of the stopped solutions. 8-aminoquinoline was conveniently included in the stopping solution as the HPLC internal standard for all assays. The efficacy of the stopping method was confirmed using plate reader assays of Z-RR-AMC and Z-FR-AMC, noting instantaneous inactivation of each enzyme.

As shown in Figures 12 and 13,  $k_{\text{cat}}/K_M$  values can be accurately estimated for commercial substrates Z-RR-AMC and Z-FR-AMC as substrates for CTB and CTL respectively. To ensure data points were within the linear range of the Michaelis-Menten curve, a four-fold

substrate concentration range was used to provide  $R^2$  values of at least 0.95 in all cases. To ensure that  $v_0$  was accurately measured up to the 10 minute stopping point, the wells containing the lowest substrate concentration were stopped after 20 and 30 minutes and were shown to be within the linear portion of the reaction. Not only is this a useful method when encountering solubility issues at relatively high  $[S]$ , but it also proved to be valuable in streamlining the process of screening probe candidates using HPLC. Once we were confident that the  $k_{cat}/K_M$  values obtained via HPLC was consistent with plate reader data using the established fluorescent substrates, we then assayed the aminoquinoline and PABA derived substrates.

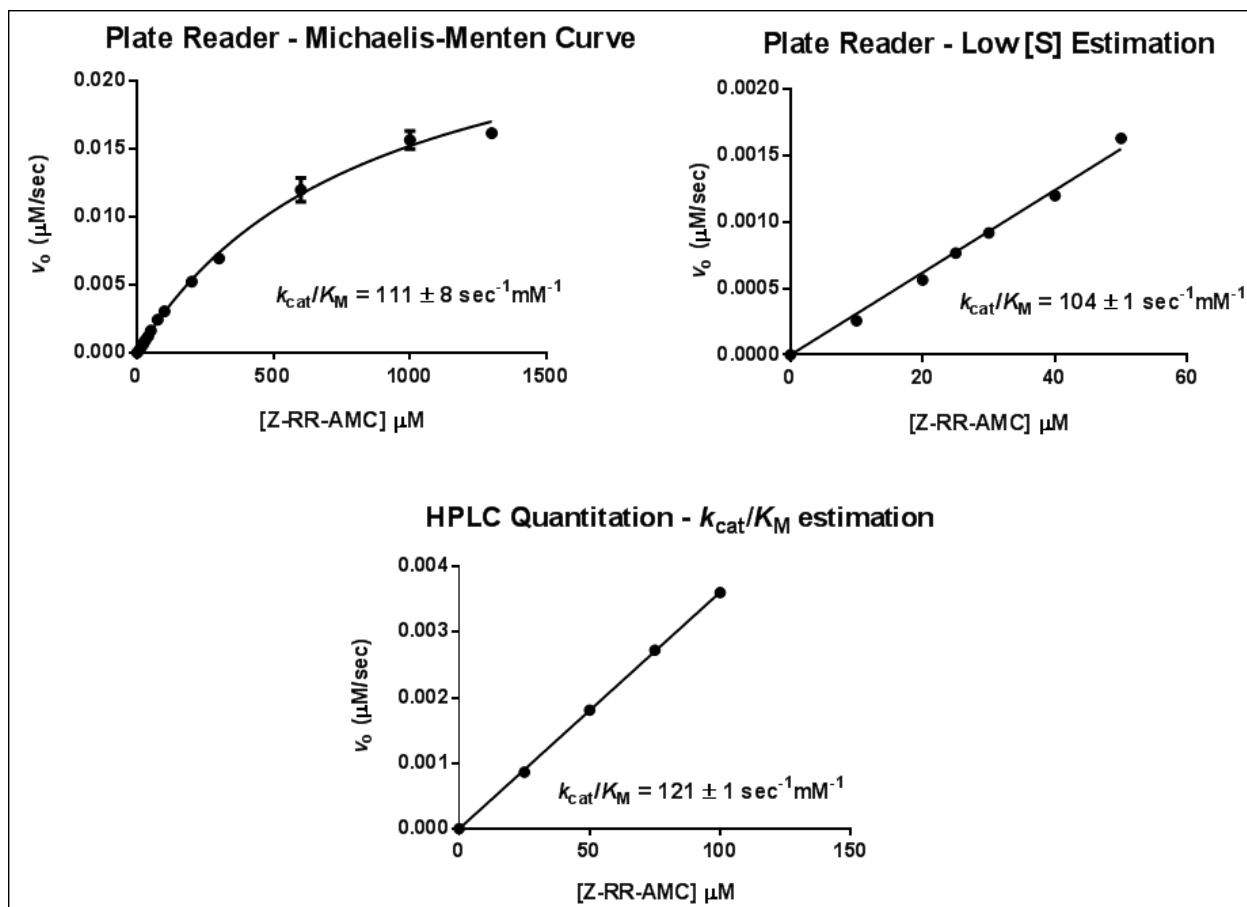


**Figure 12: Comparative results of the CTB plate reader assay and HPLC estimation.** The similar  $k_{\text{cat}}/K_M$  values obtained in all cases indicate that an HPLC-quantified stopped assay can be used to estimate the catalytic efficiency of CTB for a given substrate.

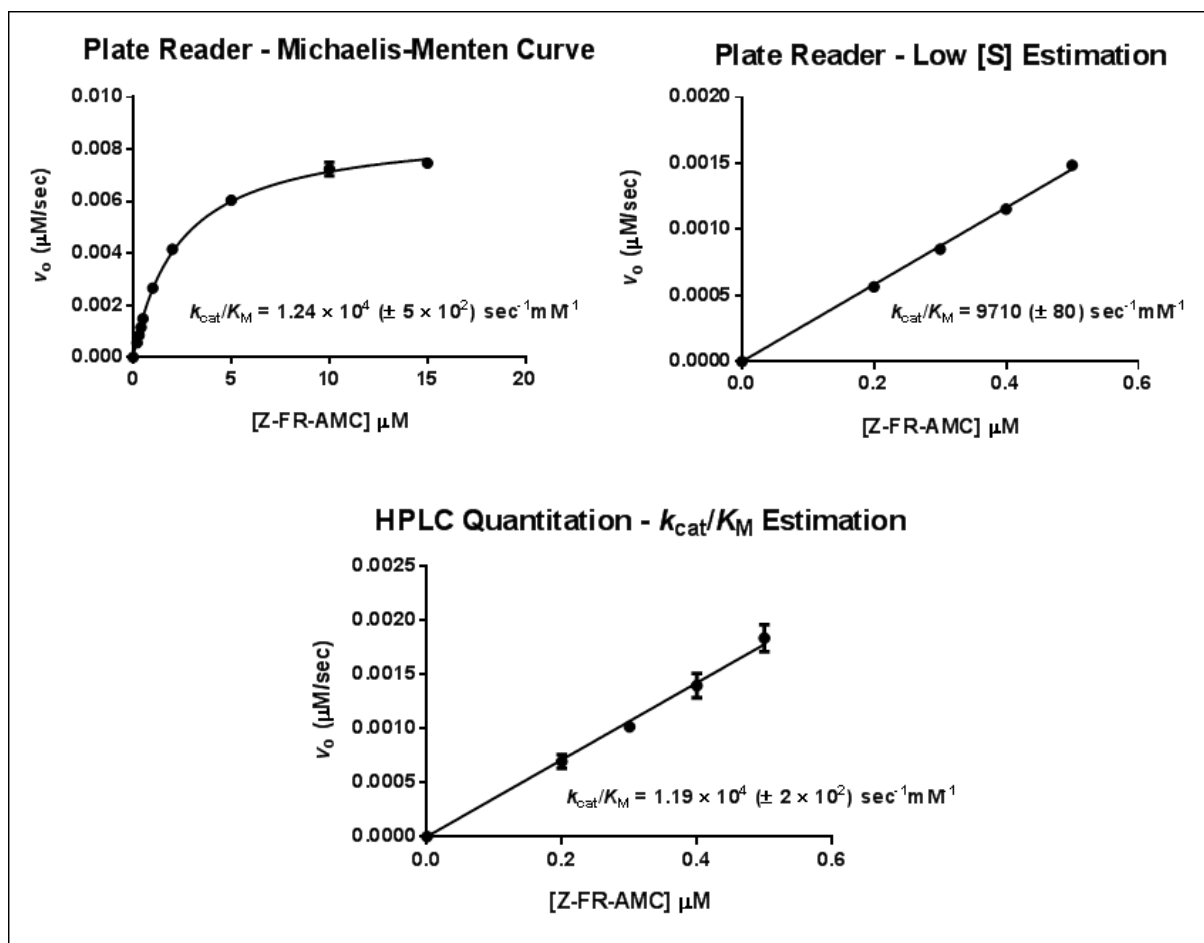


**Figure 13: Comparative results of the CTL plate reader assay and HPLC estimation.** The similar  $k_{cat}/K_M$  values obtained in all cases indicate that an HPLC-quantified stopped assay can be used to estimate the catalytic efficiency of CTL for a given substrate.

For convenience and consistency in screening the quinoline probe candidates, a standardized HPLC elution method was desired for resolving all of the quinolines from other assay materials including substrate, buffer and internal standard. The standardized HPLC elution method that is used in all cases is also in unison with the optimal optical conditions of the quinoline reporter groups. While 3-AMQ, 4-AMQ, and 5-AIQ have yet to be used as reporter groups of enzymatic activity, 6-AMQ has been employed as a reporter of hydrolase activity. The wavelengths of maximum excitation and emission for unconjugated 6-AMQ have previously been shown to be unaffected by pH, however the resulting fluorescence intensity is optimal in

acidic conditions. We therefore employed 0.1% TFA (pH < 2) as a solvent system to improve peak separation and resolution, fortuitously increasing the fluorescent yield of 6-AMQ. Surprisingly, 3-AMQ and 4-AMQ were also optimally fluorescent when resolved under the same HPLC conditions and 5-AIQ showed strong absorbance in the UV range. In order of increasing fluorescence intensity, 6-AMQ, 4-AMQ, and 3-AMQ all proved to be highly sensitive reporters by means of HPLC. All quinolines are eluted and detected within 9 minute retention times and virtually no baseline noise is observed on either the VWD or FLD.

We proceeded to verify that the PABA linker does not influence the release rate of reaction products from the active sites of CTB and CTL prior to kinetic studies. Due to the varying pKa of the quinolines used herein, it was necessary to assess how PABA affects the release of aminoquinolines following hydrolysis of the substrate. To demonstrate that enzymatic hydrolysis of each substrate was a slower kinetic process than PABA decomposition and AMQ release, we demonstrated that the initial rate of hydrolysis was proportional to a 10 fold range in concentration of CTB and CTL and seen in Figure 14.

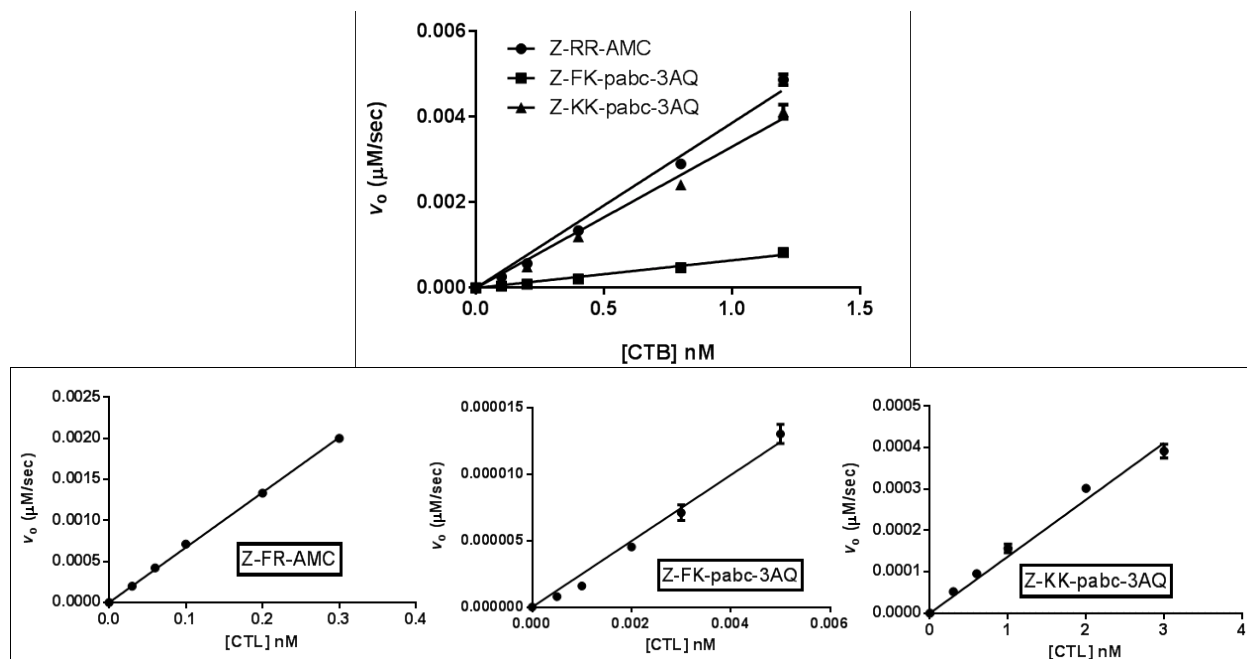


**Figure 14: Linear relationship between Cathepsin concentration and initial velocity of commercial and quinoline substrates.** All substrates were assayed at  $40\mu\text{M}$ , Z-RR-AMC and Z-FR-AMC were assayed using the continuous plate reader method, while the quinoline-derived substrates were assayed using the HPLC method. The linearity in all cases suggests that the release of product is faster than enzymatic hydrolysis of substrate.

The slope of the linear fit  $v_0/[S]$  is shown for each probe candidate in Figures 15, 16 and 17 for CTB and CTL, used to estimate  $k_{\text{cat}}/K_M$  using the same HPLC method as used for the commercial fluorogenic substrates. As seen in Table 2, the aminoquinoline-based probes are efficient substrates of CTB and CTL, however CTL hydrolysis suffered drastically with the use of the Z-KK-PABA-AQ probes. Interestingly, CTL has significantly higher  $k_{\text{cat}}/K_M$  values for the Z-FK-PABA-AQ probes than does CTB. This is not surprising as CTL is considered a more potent enzyme having much lower  $K_M$  values than CTB.

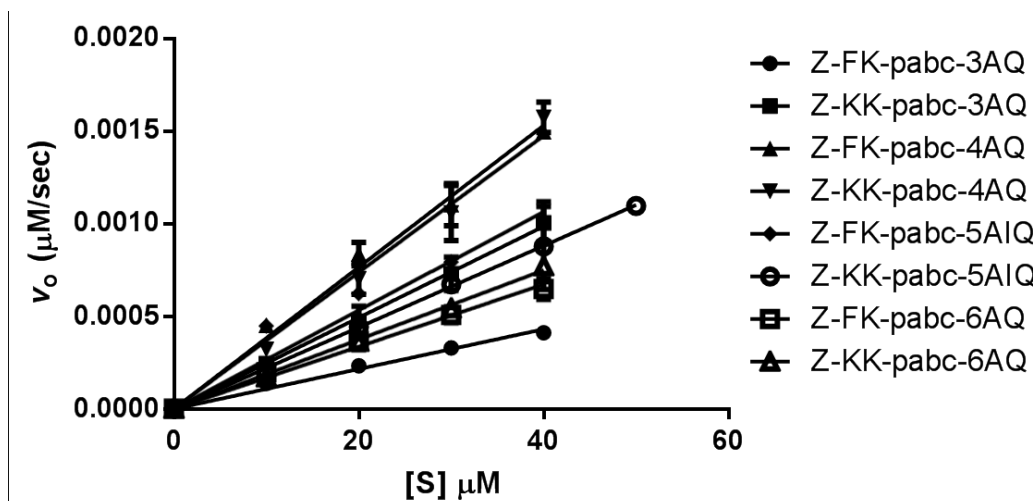


Figure 15: Linear fits of  $v_0/[S]$  used in the estimation of  $k_{\text{cat}}/K_M$  for the quinoline probes when assayed with CTB. CTB was assayed at 0.3 nM and the resulting  $k_{\text{cat}}/K_M$  for 7a, 8a, 7b, 8b, 7c, 8c, 7d, and 8d are  $36 \pm 1$ ,  $82 \pm 2$ ,  $128 \pm 4$ ,  $123 \pm 3$ ,  $89 \pm 4$ ,  $72 \pm 1$ ,  $56 \pm 1$ , and  $62 \pm 2 \text{ sec}^{-1}\text{mM}^{-1}$  respectively.

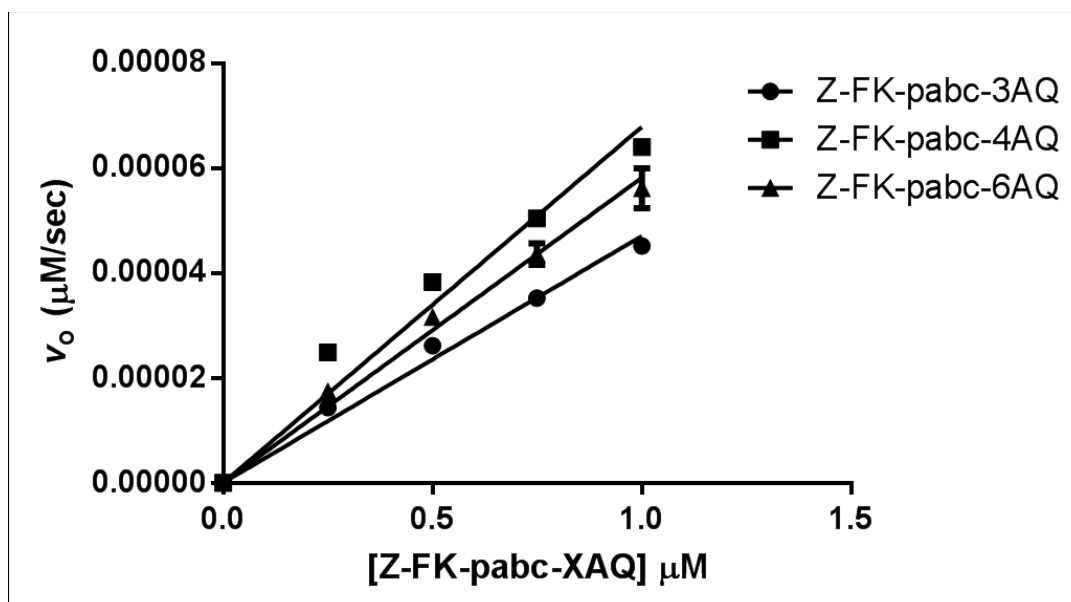
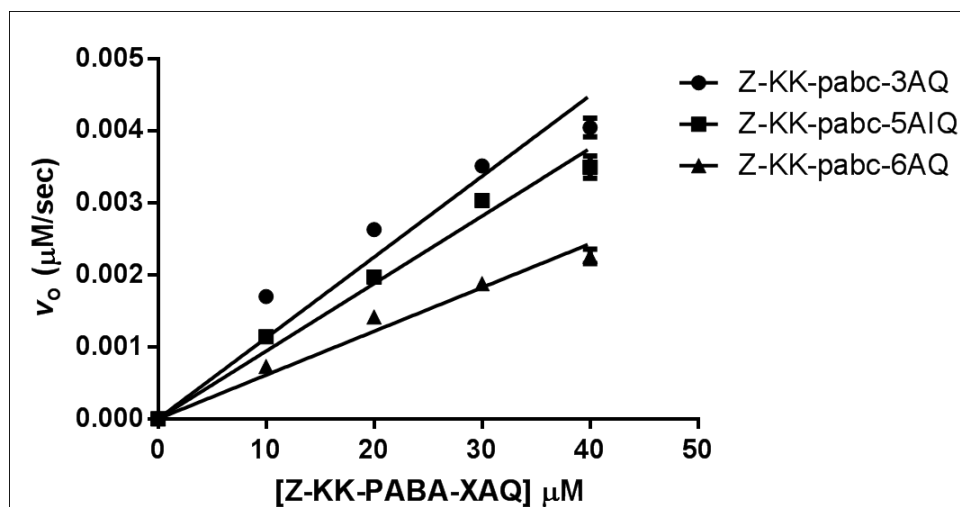


Figure 16: Linear fits of  $v_0/[S]$  used in the estimation of  $k_{\text{cat}}/K_M$  for the Z-FK quinoline probes when assayed with CTL. CTL was assayed at 0.005 nM and the resulting  $k_{\text{cat}}/K_M$  for 7a, 7b, and 7d are  $9.4 \times 10^3$  ( $\pm 2 \times 10^2$ ),  $1.4 \times 10^4$  ( $\pm 7 \times 10^2$ ), and  $1.2 \times 10^4$  ( $\pm 3 \times 10^2$ )  $\text{sec}^{-1}\text{mM}^{-1}$  respectively.



**Figure 17: Linear fits of  $v_o/[S]$  used in the estimation of  $k_{cat}/K_M$  for the Z-KK quinoline probes when assayed with CTL.** CTL was assayed at 3.0 nM and the resulting  $k_{cat}/K_M$  for 8a, 8c, and 8d are  $37 \pm 1$ ,  $31 \pm 1$ , and  $20 \pm 1 \text{ sec}^{-1}\text{mM}^{-1}$  respectively.

The high  $k_{cat}/K_M$  values of hydrolysis for Z-FK-PABA-AQ probe candidates by CTL are particularly interesting. While the stopped assay allows us to obtain estimations for  $k_{cat}/K_M$ , it does not allow us to determine the individual  $k_{cat}$  and  $K_M$ . For example, high  $k_{cat}/K_M$  values can result from an exceptionally low  $K_M$  or high  $k_{cat}$  value. However we can obtain insight into the  $K_M$  value by considering the substrate and enzyme concentrations used in each assay. All assays of quinoline-based probes involving CTB employed a substrate concentration range of 10-40  $\mu\text{M}$ , as did CTL for the Z-KK-PABA-AQ probes. The Z-FK-PABA-AQ probes however were saturating CTL at all initial concentrations employed, requiring lower concentrations of substrate in the nM range (0.25-1  $\mu\text{M}$ ). Since  $K_M$  is the concentration of substrate required to reach  $1/2V_{max}$  and nM concentrations of Z-FK-PABA-AQ substrates were required to avoid maximal velocity of CTL, the  $K_M$  values in these cases must be very low. Therefore, affinity of the Z-FK-PABA-AQ probes to the active site of CTL was high. Furthermore, a very low enzyme concentration of 0.005 nM was used compared to the 0.3 nM and 3.0 nM used in the other CTB

and CTL assays in order to stay within 10% turnover of substrate. This indicates that not only do the Z-FK-PABA-AQ probes have a low  $K_M$  value for CTL, but they are turned over rapidly as well with a high  $k_{cat}$  value, leading to the extraordinarily high  $k_{cat}/K_M$  values observed.

|   | Probe          | $k_{cat}/K_M$ (sec <sup>-1</sup> mM <sup>-1</sup> )   |  |
|---|----------------|---|--|
|   |                | CTB   | CTL  |
| Novel AMQ Probes                            | Z-FK-PABA-3AMQ | 36 ± 1  | 9.4 × 10 <sup>3</sup> (± 2 × 10 <sup>2</sup> ) |
|   | Z-KK-PABA-3AMQ | 82 ± 2  | 37 ± 1   |
|   | Z-FK-PABA-4AMQ | 128 ± 4   | 1.4 × 10 <sup>4</sup> (± 7 × 10 <sup>2</sup> ) |
|   | Z-KK-PABA-4AMQ | 123 ± 3   | ND   |
|   | Z-FK-PABA-5AIQ | 89 ± 4  | ND   |
|   | Z-KK-PABA-5AIQ | 72 ± 1  | 31 ± 1   |
|   | Z-FK-PABA-6AMQ | 56 ± 1  | 1.2 × 10 <sup>4</sup> (± 3 × 10 <sup>2</sup> ) |
|   | Z-KK-PABA-6AMQ | 62 ± 2  | 20 ± 1   |
| Commercial Probes<br>(validation of method) | Z-RR-AMC       | Michaelis: 111 ± 8<br>HPLC estim: 121 ± 1   |  |
|   | Z-FR-AMC       | Michaelis: 1.24 × 10 <sup>4</sup> (± 5 × 10 <sup>2</sup> )<br>HPLC estim: 1.19 × 10 <sup>4</sup> (± 2 × 10 <sup>2</sup> ) |  |

**Table 2: Kinetic results for novel probe candidates and commercial fluorogenic substrates.**

#### 4.4: Conclusions

We synthesized a series of substrate-based probes, and using a convenient HPLC method, four different aminoquinoline isomers have been evaluated as reporters for CTB and CTL activity. Although the Z-FK-based peptides were efficient substrates of CTB, much higher  $k_{\text{cat}}/K_M$  values were measured for CTL. In contrast, Z-KK-based probes are efficient substrates of CTB and relatively poor substrates of CTL. This suggests that a prodrug inspired approach using lysosomotropic reporters may have utility for detecting cysteine cathepsin activity *in vivo*. Future work will involve cell assays to evaluate cell permeability and specificity to cysteine cathepsin enzymes, in addition to evaluating the subsequent retention of the various aminoquinolines in lysosomes of treated cells.

## 4.5: Experimental

### General Procedures

Proton ( $^1\text{H}$ ) and carbon ( $^{13}\text{C}$ ) NMR spectra were acquired at the Lakehead University Instrumentation Laboratory (LUIL) on a Varian Unity Inova 500 MHz spectrometer and  $J$  (coupling constant) values are estimated in hertz (Hz). Thin layer chromatography (TLC) and silica gel column chromatography were performed using TLC silica gel 60 F<sub>254</sub> (EMD) and SiliaFlashP60 (SiliCycle) respectively. Human Cathepsin B was purchased from Novoprotein (Cat# C398, Accession# P07858), as was Cathepsin L (Cat# C401, Accession# P07711). Continuous kinetic studies were performed in a Biotek Synergy 4 plate reader. HPLC was performed on an Agilent 1200 Infinity LC with stopped reactions separated on an Agilent Eclipse XDB-C18 column (4.6 mm, 150 mm, 5  $\mu\text{m}$ ) and detected using a 1200 series variable wavelength detector (G1314B).

### Enzyme Kinetic Studies

The reaction mixture (300  $\mu\text{L}$  final volume) consisted of 30 mM acetate-NaOH, pH 5.5, 3.0 mM EDTA, 2.0 mM DTT, and 10% DMSO. CTB was assayed at a final concentration of 0.3 nM in all cases. When assaying CTL with the commercial substrate Z-FR-AMC, a final enzyme concentration of 0.3 nM was used. When assaying CTL with Z-FK based probe candidates a final enzyme concentration of 0.005 nM was used, while a final CTL enzyme concentration of 3.0 nM was used when assaying the Z-KK based probe candidates. Samples were prewarmed at 37°C for 15 min, and the reaction was initiated upon addition of the enzyme. For commercial substrates Z-RR-AMC and Z-FR-AMC, the activity was monitored spectrophotometrically for the release of 7-amino-4-methylcoumarin (AMC; excitation 380 nm; emission 460 nm). For novel probe candidates, reactions were stopped after 10 minutes by adding 100  $\mu\text{L}$  of reaction mixture to 50  $\mu\text{L}$  of stopping solution. Stopping solution was freshly prepared prior to each assay and consists of 50 mM sodium chloroacetate, 15% methanol, and approximately 50  $\mu\text{M}$  8-aminoquinoline as internal standard. All stopped reactions were resolved on HPLC using acetonitrile (0.1% TFA) as organic solvent and H<sub>2</sub>O (0.1% TFA) as aqueous solvent. 3-AMQ and 4-AMQ were both detected on the FLD using an excitation of 240 nm, the former having a maximum emission of 465 nm and the latter having a maximum emission of 355 nm. 6-AMQ was detected on the FLD using an excitation of 260 nm and a maximum emission of 530 nm. 5-AIQ was not fluorescent under any conditions, but exhibited maximum absorbance at 254 nm.

## Synthesis

Compounds 3 and 4 were prepared according to literature<sup>18</sup>

**7a, 7d, 8a, and 8d.** To a solution of either 6AMQ or 3AMQ (200 mg, 1.4 mmol) in DCM at ice bath temperature was added TEA (393  $\mu$ L, 2.8 mmol) dropwise followed by dropwise addition of 15% phosgene in toluene (954  $\mu$ L, 1.4 mmol). After continued stirring for 30 minutes at ice bath temperature the solution was allowed to reach room temperature, after which either 3 or 4 (0.7 mmol) was added as a solid. The mixture was brought to 50°C and DMF was then added dropwise until complete solubility was achieved, stirring for an additional 2 hours. The solution was brought to room temperature, and the solvents were removed under reduced pressure. Ethyl acetate is added and the solution is washed with 0.1 M HCl, sat. NaHCO<sub>3</sub>, and sat. NaCl. Following removal of ethyl acetate under reduced pressure, the residue is purified by silica gel column chromatography using ethyl acetate as eluent to obtain the pure BOC-protected carbamates 5a, 5d, 6a, and 6d in yields of 64%, 24%, 20%, and 16% respectively based on starting peptides 3 and 4. The BOC-protected carbamates (50 mg) are all deprotected by stirring in trifluoroacetic acid-DCM (1:1 v/v, 5 mL) for 10 minutes, followed by addition of diethyl ether to form a precipitate which is centrifuged out of suspension, successively washed with diethyl ether and ethyl acetate, and dried under high vacuum to provide title compounds 7a, 7d, 8a, and 8d in yields of 64%, 24%, 20%, and 13% respectively based on precursor peptides 3 and 4. That is, deprotection was quantitative in all cases except in furnishing 8d, which was obtained with a yield of 82% from the BOC protected counterpart 6d.

**7b and 8b.** To a solution of 4-QCA (120 mg, 0.6 mmol) in ACN (25 mL) is added CDI (120 mg, 0.7 mmol), the mixture stirred for 1 hour followed by addition of hydroxyl amine hydrochloride (55 mg, 0.7 mmol) and further stirring for 2 hours followed by a second addition of CDI (140 mg, 0.9 mmol). After stirring this mixture for 30 minutes, either 3 or 4 (0.3 mmol) is added and the reaction is stirred at 60°C for 16h. Solvents are removed, DCM is added, and the solution is washed with 0.1 M HCl, NaHCO<sub>3</sub>, and sat. NaCl. Following removal of DCM under reduced pressure, the residue is purified by silica gel column chromatography using ethyl acetate as eluent to obtain the pure BOC-protected carbamates 5b and 6b in yields of 27% and 19% respectively based on starting peptides 3 and 4. The BOC-protected carbamates (50 mg) are deprotected by stirring in trifluoroacetic acid-DCM (1:1 v/v, 5 mL) for 10 minutes, followed by addition of diethyl ether to form a precipitate which is centrifuged out of suspension, successively washed with diethyl ether and ethyl acetate, and dried under high vacuum to provide title compounds 7b and 8b in yields of 27% and 17% respectively based on precursor peptides 3 and 4. That is, BOC-protected carbamate 5b was quantitatively deprotected while 8b was obtained with a yield of 88% from the BOC protected counterpart 6b.

**7c and 8c.** To DCM (30mL) at ice bath temperature is added 15% phosgene in toluene (2.6 mL, 3.9 mmol) dropwise, followed by DMAP (1 g, 8.2 mmol) in DCM (10mL), and 5AIQ (500 mg, 3.5 mmol) in DCM (10 mL). The mixture is stirred at room temperature for 16 h, dried under reduced pressure, and the isocyanate is extracted using ether before filtering. Either 3 or 4 (0.4-0.5 mmol) is added in THF (10mL) to the ether solution, stirring for an additional 2 hours. After removing volatiles under reduced pressure, ethyl acetate was added and the crude product was washed using 0.1 M HCl, sat. NaHCO<sub>3</sub>, and sat. NaCl. Following removal of ethyl acetate under reduced pressure, the residue is purified by silica gel column chromatography using ethyl acetate as eluent to obtain the pure BOC-protected carbamates 5c and 6c in yields of 34% and 21% based on starting peptides 3 and 4. The BOC-protected carbamates (50 mg) are deprotected by stirring in trifluoroacetic acid-DCM (1:1 v/v, 5 mL) for 10 minutes, followed by addition of diethyl ether to form a precipitate which is centrifuged out of suspension, successively washed with diethyl ether and ethyl acetate, and dried under high vacuum to provide title compounds 7c and 8c in yields of 34% and 21% respectively based on precursor peptides 3 and 4. That is, both BOC protected peptides 5c and 6c are deprotected quantitatively.

## 4.7: References

1. Turk V, Stoka V, Vasiljeva O, et al. Cysteine cathepsins: From structure, function and regulation to new frontiers. *Biochim Biophys Acta*. 2012;1824(1):68-88.
2. Aerts JM, Kallemeijn WW, Wegdam W, et al. Biomarkers in the diagnosis of lysosomal storage disorders: Proteins, lipids, and inhibodies. *J Inherit Metab Dis*. 2011;34(3):605-619.
3. Reiser J, Adair B, Reinheckel T. Specialized roles for cysteine cathepsins in health and disease. *J Clin Invest*. 2010;120(10):3421-3431.
4. Victor BC, Anbalagan A, Mohamed MM, Sloane BF, Cavallo-Medved D. Inhibition of cathepsin B activity attenuates extracellular matrix degradation and inflammatory breast cancer invasion. *Breast Cancer Res*. 2011;13(6):R115.
5. Repnik U, Stoka V, Turk V, Turk B. Lysosomes and lysosomal cathepsins in cell death. *Biochim Biophys Acta*. 2012;1824(1):22-33.
6. Shree T, Olson OC, Elie BT, et al. Macrophages and cathepsin proteases blunt chemotherapeutic response in breast cancer. *Genes Dev*. 2011;25(23):2465-2479.
7. Bruchard M, Mignot G, Derangere V, et al. Chemotherapy-triggered cathepsin B release in myeloid-derived suppressor cells activates the Nlrp3 inflammasome and promotes tumor growth. *Nat Med*. 2013;19(1):57-64.

8. Blum G, von Degenfeld G, Merchant MJ, Blau HM, Bogoy M. Noninvasive optical imaging of cysteine protease activity using fluorescently quenched activity-based probes. *Nat Chem Biol.* 2007;3(10):668-677.
9. de Duve C, de Barsy T, Poole B, Trouet A, Tulkens P, Van Hoof F. Commentary. lysosomotropic agents. *Biochem Pharmacol.* 1974;23(18):2495-2531.
10. Kannan P, Brimacombe KR, Kreisl WC, et al. Lysosomal trapping of a radiolabeled substrate of P-glycoprotein as a mechanism for signal amplification in PET. *Proc Natl Acad Sci U S A.* 2011;108(6):2593-2598.
11. Ndolo RA, Luan Y, Duan S, Forrest ML, Krise JP. Lysosomotropic properties of weakly basic anticancer agents promote cancer cell selectivity in vitro. *PLoS One.* 2012;7(11):e49366.
12. Kaufmann AM, Krise JP. Lysosomal sequestration of amine-containing drugs: Analysis and therapeutic implications. *J Pharm Sci.* 2007;96(4):729-746.
13. Wiedner SD, Anderson LN, Sadler NC, et al. Organelle-specific activity-based protein profiling in living cells. *Angew Chem Int Ed Engl.* 2014;53(11):2919-2922.
14. Duvvuri M, Konkar S, Funk RS, Krise JM, Krise JP. A chemical strategy to manipulate the intracellular localization of drugs in resistant cancer cells. *Biochemistry.* 2005;44(48):15743-15749.

15. Choe Y, Leonetti F, Greenbaum DC, et al. Substrate profiling of cysteine proteases using a combinatorial peptide library identifies functionally unique specificities. *J Biol Chem*. 2006;281(18):12824-12832.
16. Ashoor R, Yafawi R, Jessen B, Lu S. The contribution of lysosomotropism to autophagy perturbation. *PLoS One*. 2013;8(11):e82481.
17. Singerman GM. Cinnolines. In: Castle RN, ed. *Chemistry of heterocyclic compounds*. John Wiley & Sons, Inc; 1973:1-321.
18. Chowdhury MA, Moya IA, Bhilocha S, et al. Prodrug-inspired probes selective to cathepsin B over other cysteine cathepsins. *J Med Chem*. 2014;57(14):6092-6104.
19. Dube P, Nathel NF, Vetelino M, et al. Carbonyldiimidazole-mediated lossen rearrangement. *Org Lett*. 2009;11(24):5622-5625.
20. Rothlisberger D, Khersonsky O, Wollacott AM, et al. Kemp elimination catalysts by computational enzyme design. *Nature*. 2008;453(7192):190-195.
21. James TW, Frias-Staheli N, Bacik JP, et al. Structural basis for the removal of ubiquitin and interferon-stimulated gene 15 by a viral ovarian tumor domain-containing protease. *Proc Natl Acad Sci U S A*. 2011;108(6):2222-2227.
22. Barrett AJ. Fluorimetric assays for cathepsin B and cathepsin H with methylcoumarylamide substrates. *Biochem J*. 1980;187(3):909-912.

23. Moroz OV, Moroz YS, Wu Y, et al. A single mutation in a regulatory protein produces evolvable allosterically regulated catalyst of nonnatural reaction. *Angew Chem Int Ed Engl.* 2013;52(24):6246-6249.

24. Gordon SR, Stanley EJ, Wolf S, et al. Computational design of an alpha-gliadin peptidase. *J Am Chem Soc.* 2012;134(50):20513-20520.

## Supporting Information

**Cbz-Phe-Lys(BOC)-PABA-3AMQ:**  $^1\text{H}$  NMR (500 MHz, DMSO):  $\delta$  8.88 (bs, 1H), 8.48 (s, 1H), 8.33 (s, 1H), 7.92 (dd,  $J = 8.2, 20.3$  Hz, 2H), 7.53-7.70 (m, 4H), 7.42 (bs, 3H), 7.15-7.37 (m, 11H), 5.18 (s, 2H), 4.96 (s, 2H), 4.38-4.45 (m, 1H), 4.30-4.37 (m, 1H), 4.08 (s, 1H), 3.34 (bs, 1H), 2.98-3.10 (m, 1H), 2.83-2.95 (m, 2H), 2.75 (t,  $J = 12.5$  Hz, 1H), 1.70-1.80 (m, 1H), 1.60-1.70 (m, 1H), 1.34 (s, 9H), 1.20-1.46 (m, 4H);  $^{13}\text{C}$  NMR (125 MHz, DMSO):  $\delta$  172.07, 171.17, 156.32, 156.02, 154.19, 144.54, 144.33, 139.41, 138.55, 137.49, 133.48, 131.55, 129.71, 129.55, 129.03, 128.75, 128.69, 128.68, 128.67, 128.66, 128.47, 128.37, 128.13, 127.95, 127.89, 127.55, 126.69, 120.93, 120.91, 120.89, 119.63, 105.00, 77.78, 66.48, 65.67, 56.57, 54.06, 37.88, 32.40, 29.74, 28.72, 23.25

**Cbz-Phe-Lys(BOC)-PABA-4AMQ:**  $^1\text{H}$  NMR (500 MHz,  $\text{CDCl}_3$ ):  $\delta$  8.81 (d,  $J = 5.1$  Hz, 1H), 8.69 (bs, 1H), 8.08-8.13 (m, 2H), 7.83 (d,  $J = 8.4$  Hz, 1H), 7.68-7.72 (m, 2H), 7.58-7.63 (m, 2H), 7.51-7.55 (m, 1H), 7.10-7.40 (m, 13H), 5.23 (s, 2H), 5.06 (bs, 2H), 4.66-4.74 (m, 1H), 4.43-4.53 (m, 2H), 2.99-3.16 (m, 5H), 1.65-1.80 (m, 1H), 1.53-1.65 (m, 1H), 1.42 (s, 9H), 1.38-1.48 (m, 4H);  $^{13}\text{C}$  NMR (125 MHz, DMSO):  $\delta$  172.07, 171.12, 156.33, 156.02, 154.27, 151.18, 149.04, 142.55, 139.37, 138.51, 137.48, 131.46, 129.89, 129.68, 129.66, 129.58, 129.55, 128.75, 128.73, 128.49, 128.14, 127.89, 126.70, 126.23, 122.89, 120.98, 119.64, 110.89, 77.79, 66.76, 65.68, 65.66, 56.51, 53.96, 49.08, 32.43, 29.78, 29.76, 28.75, 28.72, 28.68, 23.24

**Cbz-Phe-Lys(BOC)-PABA-5AIQ:**  $^1\text{H}$  NMR (500 MHz, DMSO):  $\delta$  10.39 (m, 1H), 9.95 (s, 1H), 9.42 (s, 1H), 8.36-8.58 (m, 2H), 7.96-8.14 (m, 3H), 7.66-7.77 (m, 3H), 7.50-7.63 (m, 1H), 7.13-7.46 (m, 13H), 6.66-6.89 (m, 1H), 5.12-5.20 (2H), 4.93-4.97 (s, 2H), 4.39-4.46 (m, 1H), 4.29-4.36 (m, 1H), 3.00-3.10 (m, 1H), 2.82-2.94 (m, 1H), 2.71-2.79 (m, 1H), 1.71-1.82 (m, 1H), 1.60-1.71 (m, 1H), 1.34 (s, 9H), 1.26-1.44 (m, 4H);  $^{13}\text{C}$  NMR (125 MHz, DMSO):  $\delta$  172.04, 171.22, 156.31, 156.01, 155.04, 151.99, 151.96, 139.43, 138.59, 137.49, 133.78, 131.66, 130.55, 129.75, 129.36, 129.02, 128.75, 128.68, 128.67, 128.45, 128.34, 128.12, 127.88, 126.67, 125.37, 125.31, 125.30, 125.29, 125.02, 119.61, 116.97, 77.77, 66.46, 65.65, 56.68, 54.20, 45.01, 45.00, 32.38, 30.91, 29.70, 28.73, 23.24

**Cbz-Phe-Lys(BOC)-PABA-6AMQ:**  $^1\text{H}$  NMR (500 MHz,  $\text{CDCl}_3$ , drops of MeOD):  $\delta$  8.68-8.71 (m, 1H), 8.11-8.19 (m, 1H), 7.94 (d,  $J = 9.2$  Hz, 1H), 7.54-7.65 (m, 3H), 7.11-7.43 (m, 12H), 5.20 (s, 2H), 5.00-5.09 (m, 2H), 4.40-4.47 (m, 2H), 4.06 (s, 4H), 3.34-3.37 (m, 1H), 2.91-3.15 (m, 4H), 1.80-1.89 (m, 1H), 1.59-1.70 (m, 1H), 1.40 (s, 9H), 1.38-1.50 (m, 4H);  $^{13}\text{C}$  NMR (125 MHz,  $\text{CDCl}_3$ , drops of MeOD):  $\delta$  161.33, 141.83, 140.32, 140.06, 133.08, 133.00, 132.86, 132.83, 132.81, 132.79, 132.42, 132.36, 132.34, 132.33, 132.04, 131.74, 131.72, 130.84, 125.48, 125.47, 124.04, 124.03, 124.01, 70.90, 70.89, 60.11, 60.10, 57.56, 53.11, 52.94, 52.79, 52.77, 52.60, 52.42, 45.01, 42.07, 32.19, 32.16, 26.54, 26.53, 26.52, 24.88

**Cbz-Lys(BOC)-Lys(BOC)-PABA-3AMQ:**  $^1\text{H}$  NMR (500 MHz, DMSO):  $\delta$  8.83 (d,  $J = 2.5$  Hz, 2H), 8.52 (s, 1H), 7.95 (d,  $J = 8.5$  Hz, 1H), 7.83 (d,  $J = 8.1$  Hz, 1H), 7.53-7.67 (m, 4H), 7.42 (d,  $J = 8.6$  Hz, 3H), 7.25-7.38 (m, 6H), 5.22 (s, 2H), 5.10 (s, 2H), 4.46-4.51 (m, 1H), 4.11-4.16 (m, 1H), 3.50 (dd,  $J = 7.0, 14.0$  Hz, 1H), 3.32-3.34 (m, 2H), 2.99-3.07 (m, 4H), 1.59-1.98 (m, 4H), 1.36-1.55 (m, 26H);  $^{13}\text{C}$  NMR (125 MHz, DMSO):  $\delta$  172.53, 171.22, 156.48, 156.02, 156.01, 156.01, 156.00, 155.99, 154.18, 144.54, 144.53, 144.52, 144.52, 144.32, 144.31, 139.42, 137.49, 133.49, 131.50, 129.53, 129.52, 129.51, 129.03, 128.79, 128.76, 128.75, 128.37, 128.23, 128.14, 128.11, 128.08, 127.94, 127.91, 127.89, 127.53, 127.51, 119.57, 119.55, 77.79, 77.77, 66.47, 66.46, 65.86, 65.85, 65.84, 53.88, 45.00, 33.82, 32.31, 32.30, 32.06, 32.06, 25.81, 24.92, 23.32, 23.22

**Cbz-Lys(BOC)-Lys(BOC)-PABA-4AMQ:**  $^1\text{H}$  NMR (500 MHz,  $\text{CDCl}_3$ ):  $\delta$  8.77-8.80 (m, 1H), 8.22-8.33 (m, 1H), 8.01 (d,  $J = 9.1$  Hz, 1H), 7.81-7.86 (m, 2H), 7.71 (d,  $J = 8.6$  Hz, 2H), 7.55 (dd,  $J = 4.4, 8.4$  Hz, 2H), 7.50 (d,  $J = 8.5$  Hz, 4H), 7.33-7.46 (m, 5H), 5.28 (s, 2H), 5.18 (s, 2H), 4.54-4.59 (m, 1H), 4.19-4.25 (m, 1H), 3.58 (dd,  $J = 7.0, 14.1$  Hz, 1H), 3.39-3.42 (m, 2H), 3.04-3.15 (m, 4H), 1.67-2.03 (m, 4H), 1.42-1.62 (m, 26H);  $^{13}\text{C}$  NMR (125 MHz,  $\text{CDCl}_3$ ):  $\delta$  172.65, 170.03, 156.68, 156.66, 156.25, 156.25, 153.09, 151.06, 148.72, 141.08, 138.44, 135.95, 131.12, 130.33, 129.45, 129.38, 128.52, 128.40, 128.39, 128.37, 128.30, 128.26, 126.27, 120.08, 119.75, 119.54, 109.15, 67.39, 67.35, 67.30, 65.86, 55.66, 53.84, 44.99, 39.98, 39.96, 39.22, 39.20, 31.19, 31.15, 31.11, 31.06, 31.05, 31.03, 31.01, 30.32, 29.70, 29.66, 29.63, 29.46, 29.40, 28.55, 22.87, 22.24, 22.21, 22.18, 15.28, 1.02

**Cbz-Lys(BOC)-Lys(BOC)-PABA-5AIQ:**  $^1\text{H}$  NMR (500 MHz, MeOD):  $\delta$  9.23 (s, 1H), 8.44 (bs, 1H), 8.02 (bs, 1H), 7.89-7.97 (m, 2H), 7.61-7.71 (m, 3H), 7.25-7.48 (m, 9H), 5.22 (s, 2H), 5.11 (s, 2H), 4.46-4.51 (m, 1H), 4.09-4.17 (m, 2H), 3.31-3.34 (m, 2H), 2.98-3.08 (m, 5H), 1.62-1.97 (m, 4H), 1.33-1.55 (m, 26H);  $^{13}\text{C}$  NMR (125 MHz, MeOD):  $\delta$  173.75, 173.74, 171.12, 155.47, 152.04, 141.41, 138.22, 136.73, 133.01, 132.35, 128.63, 128.09, 127.64, 127.48, 127.46, 127.43, 124.42, 124.40, 119.87, 115.74, 78.46, 66.39, 55.28, 55.27, 53.90, 39.75, 39.74, 39.73, 39.59, 39.58, 31.41, 31.40, 31.39, 31.37, 31.36, 31.35, 29.20, 29.18, 29.17, 29.16, 29.14, 29.13, 29.12, 29.11, 22.82, 22.79, 22.76, 22.75, 14.06

**Cbz-Lys(BOC)-Lys(BOC)-PABA-6AMQ:**  $^1\text{H}$  NMR (500 MHz, MeOD):  $\delta$  8.69-8.72 (m, 2H), 8.23 (d, J = 8.2 Hz, 2H), 8.16 (s, 2H), 7.93 (d, J = 9.1 Hz, 2H), 7.73-7.77 (m, 1H), 7.64 (d, J = 8.3 Hz, 2H), 7.23-7.51 (m, 7H), 5.10 (s, 2H), 5.00 (s, 2H), 4.45-4.51 (m, 1H), 4.11-4.17 (m, 1H), 3.50 (dd, 7.0, 14.1 Hz, 1H), 3.30-3.35 (m, 2H), 2.96-3.08 (m, 4H), 1.59-1.96 (m, 4H), 1.31-1.56 (m, 26H);  $^{13}\text{C}$  NMR (125 MHz, MeOD):  $\delta$  173.74, 171.12, 157.27, 157.26, 157.16, 157.14, 157.13, 154.25, 148.09, 143.97, 138.18, 137.51, 136.71, 136.28, 132.39, 129.09, 128.56, 128.23, 128.10, 127.64, 127.48, 123.02, 121.49, 119.86, 119.82, 113.79, 113.78, 113.77, 113.76, 113.75, 78.46, 66.39, 66.09, 66.06, 55.28, 55.26, 55.23, 53.92, 39.75, 39.74, 39.73, 39.62, 39.59, 31.42, 31.41, 31.39, 31.37, 29.20, 29.17, 29.16, 29.14, 29.13, 29.12, 22.82, 22.79, 22.78, 22.77, 22.74

**Cbz-Phe-Lys(TFA)-PABA-3AMQ:**  $^1\text{H}$  NMR (500 MHz, DMSO):  $\delta$  10.27 (d, J = 28.5 Hz, 2H), 8.90 (s, 2H), 8.50 (s, 1H), 8.37 (bs, 1H), 7.86-8.02 (m, 3H), 7.50-7.74 (m, 4H), 7.43 (bs, 2H), 7.14-7.37 (m, 11H), 5.18 (s, 2H), 4.95 (s, 2H), 4.41-4.49 (m, 1H), 4.29-4.38 (m, 1H), 3.17 (s, 1H), 3.06 (d, J = 12.9 Hz, 1H), 2.72-2.83 (m, 3H), 1.30-1.85 (m, 6H);  $^{13}\text{C}$  NMR (125 MHz, DMSO):  $\delta$  158.85, 158.59, 156.35, 156.30, 154.19, 154.10, 144.20, 139.37, 139.26, 138.51, 137.46, 133.49, 133.37, 131.61, 129.69, 129.52, 128.92, 128.75, 128.69, 128.69, 128.47, 128.37, 128.14, 128.03, 127.96, 127.87, 127.58, 126.70, 119.66, 119.56, 66.47, 65.68, 38.96, 38.87, 37.83, 37.80, 31.98, 27.08, 27.03, 22.84

**Cbz-Phe-Lys(TFA)-PABA-4AMQ:**  $^1\text{H}$  NMR (500 MHz, MeOD):  $\delta$  8.89-8.93 (m, 2H), 8.71-8.74 (m, 2H), 8.61-8.65 (m, 2H), 8.10-8.14 (m, 2H), 7.87-7.91 (m, 1H), 7.70 (d,  $J$  = 8.7 Hz, 2H), 7.52 (d,  $J$  = 8.7 Hz, 3H), 7.11-7.36 (m, 11H), 5.37 (s, 2H), 5.05 (dd,  $J$  = 12.7, 21.0 Hz, 2H), 4.47-4.53 (m, 1H), 4.38-4.43 (m, 1H), 3.13 (dd,  $J$  = 5.9, 13.7 Hz, 1H), 2.88-2.97 (m, 3H), 1.39-1.98 (m, 6H);  $^{13}\text{C}$  NMR (125 MHz, MeOD):  $\delta$  172.97, 170.59, 157.05, 153.12, 151.74, 144.47, 139.17, 138.55, 136.83, 136.68, 134.11, 131.33, 129.20, 129.02, 128.93, 128.51, 128.14, 128.07, 127.60, 127.26, 126.42, 122.71, 120.95, 119.95, 119.17, 107.49, 67.75, 66.26, 56.67, 53.55, 39.12, 37.40, 31.03, 26.68, 22.31

**Cbz-Phe-Lys(TFA)-PABA-5AIQ:**  $^1\text{H}$  NMR (500 MHz, DMSO):  $\delta$  10.49 (s, 1H), 10.08 (s, 1H), 9.61 (s, 2H), 8.47-8.64 (m, 1H), 8.18-8.33 (m, 3H), 8.12 (bs, 2H), 7.83 (bs, 1H), 7.73 (bs, 2H), 7.09-7.59 (m, 14H), 5.17 (s, 2H), 4.95 (s, 2H), 4.41-4.49 (m, 1H), 4.29-4.38 (m, 1H), 3.10 (d,  $J$  = 13.2 Hz, 1H), 2.77 (bs, 3H), 1.28-1.87 (m, 6H);  $^{13}\text{C}$  NMR (125 MHz, DMSO):  $\delta$  172.15, 172.08, 171.16, 171.14, 171.07, 156.34, 156.28, 155.03, 154.94, 150.58, 150.56, 150.54, 139.50, 139.39, 138.63, 137.86, 137.85, 137.50, 134.07, 133.94, 131.56, 131.24, 129.83, 129.78, 129.38, 129.30, 128.76, 128.45, 128.13, 127.87, 127.26, 127.24, 126.78, 126.74, 126.73, 126.70, 126.67, 125.79, 119.60, 119.51, 118.42, 118.39, 118.37, 65.64, 65.39, 56.71, 54.06, 31.80, 31.77, 26.86, 26.81, 26.76, 22.79, 15.65

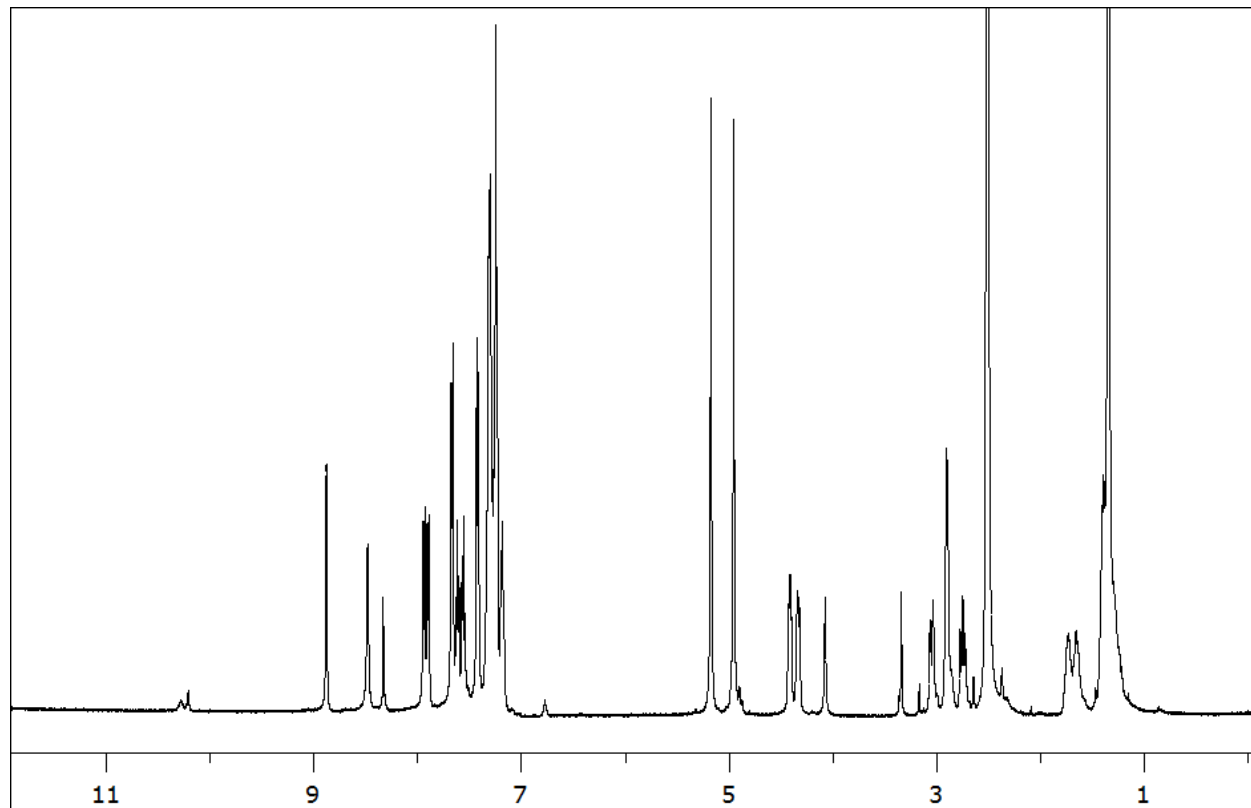
**Cbz-Phe-Lys(TFA)-PABA-6AMQ:**  $^1\text{H}$  NMR (500 MHz, MeOD):  $\delta$  8.93 (d,  $J$  = 5.1 Hz, 1H), 8.79 (d,  $J$  = 8.5 Hz, 1H), 8.43 (bs, 1H), 8.10 (d,  $J$  = 9.1 Hz, 2H), 7.99-8.03 (m, 2H), 7.84 (dd,  $J$  = 5.1, 8.5 Hz, 2H), 7.62 (d,  $J$  = 8.5 Hz, 2H), 7.44 (d,  $J$  = 8.7 Hz, 3H), 7.10-7.35 (m, 11H), 5.24 (s, 2H), 5.04 (dd,  $J$  = 12.5, 21.7 Hz, 2H), 4.47-4.52 (m, 1H), 4.39-4.45 (m, 1H), 3.13 (dd,  $J$  = 5.8, 13.9 Hz, 1H), 2.86-2.97 (m, 3H), 1.38-1.97 (m, 6H);  $^{13}\text{C}$  NMR (125 MHz, MeOD):  $\delta$  173.59, 171.05, 161.46, 161.18, 157.23, 154.24, 141.16, 141.13, 141.11, 138.21, 136.68, 133.73, 132.27, 129.52, 128.79, 128.71, 128.67, 128.19, 128.11, 127.72, 127.68, 127.59, 127.40, 125.25, 125.21, 124.89, 124.88, 119.87, 66.45, 66.41, 66.37, 65.51, 54.91, 53.65, 39.12, 39.06, 31.14, 31.08, 31.04, 26.71, 26.66, 26.63, 22.46, 22.34, 14.05

**Cbz-Lys(TFA)-Lys(TFA)-PABA-4AMQ:**  $^1\text{H}$  NMR (500 MHz, MeOD):  $\delta$  8.92 (d,  $J = 6.7$ , 2H), 8.72 (d,  $J = 6.7$  Hz, 3H), 8.63 (d,  $J = 8.7$ , 2H), 8.08-8.16 (m, 2H), 7.87-7.92 (m, 1H), 7.67 (d,  $J = 8.6$  Hz, 2H), 7.51 (d,  $J = 8.6$  Hz, 3H), 7.27-7.40 (m, 6H), 5.36 (s, 2H), 5.07-5.17 (m, 2H), 4.50-4.60 (m, 1H), 4.08-4.19 (m, 1H), 3.32-3.34 (m, 3H), 2.89-2.98 (m, 5H), 1.44-2.01 (m, 12H);  $^{13}\text{C}$  NMR (125 MHz, MeOD):  $\delta$  173.62, 161.75, 161.47, 157.25, 153.12, 151.73, 144.46, 139.17, 138.58, 136.68, 134.12, 131.33, 129.20, 128.52, 128.11, 127.68, 127.41, 122.72, 120.96, 120.93, 119.86, 119.79, 119.17, 107.48, 67.70, 66.37, 65.51, 54.94, 54.90, 53.64, 39.15, 39.12, 39.08, 39.05, 31.14, 31.07, 31.02, 26.67, 26.63, 22.46, 22.43, 22.41, 22.38, 22.32, 22.31, 14.06, 13.07

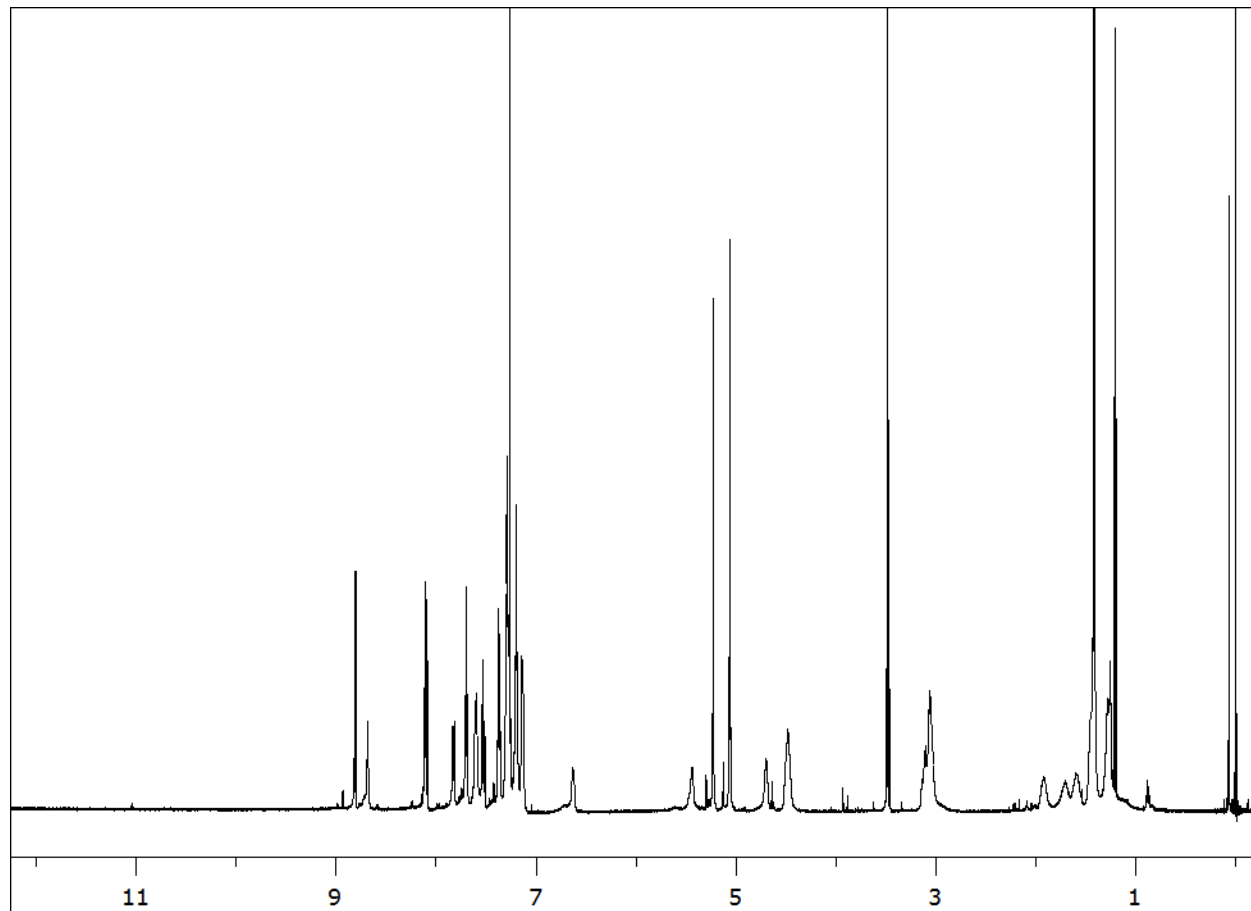
**Cbz-Lys(TFA)-Lys(TFA)-PABA-5AIQ:**  $^1\text{H}$  NMR (500 MHz, MeOD):  $\delta$  9.50 (bs, 2H), 8.51 (bs, 2H), 8.19-8.28 (m, 2H), 8.11 (d,  $J = 8.3$  Hz, 1H), 7.85 (t,  $J = 8.0$  Hz, 3H), 7.64 (d,  $J = 8.4$  Hz, 2H), 7.46 (bs, 3H), 7.29-7.39 (m, 6H), 5.25 (s, 2H), 5.07-5.16 (m, 2H), 4.52-4.57 (m, 1H), 4.09-4.19 (m, 1H), 3.37 (s, 2H), 2.88-2.97 (m, 4H), 1.46-2.00 (m, 12H);  $^{13}\text{C}$  NMR (125 MHz, MeOD):  $\delta$  173.53, 171.02, 161.31, 157.22, 155.35, 150.13, 150.12, 138.16, 136.68, 133.63, 132.49, 128.95, 128.68, 128.12, 127.70, 127.67, 127.49, 127.40, 125.47, 119.84, 117.78, 117.76, 66.51, 66.46, 66.36, 65.51, 54.84, 53.55, 39.14, 39.06, 31.23, 31.05, 27.39, 26.70, 26.66, 22.44, 22.35

**Cbz-Lys(TFA)-Lys(TFA)-PABA-6AMQ:**  $^1\text{H}$  NMR (500 MHz, MeOD):  $\delta$  8.93 (bs, 2H), 8.76 (d,  $J = 8.5$  Hz, 2H), 8.41 (bs, 2H), 8.10 (d,  $J = 9.1$  Hz, 3H), 7.98-8.03 (m, 2H), 7.83 (dd,  $J = 5.1, 8.4$  Hz, 1H), 7.64 (d,  $J = 8.5$  Hz, 2H), 7.44 (d,  $J = 8.6$  Hz, 3H), 7.28-7.39 (m, 6H), 5.23 (s, 2H), 5.11 (dd,  $J = 12.5, 18.2$  Hz, 2H), 4.50-4.56 (m, 1H), 4.12-4.19 (m, 1H), 3.31-3.35 (m, 2H), 2.88-2.97 (m, 4H), 1.43-2.01 (m, 12H);  $^{13}\text{C}$  NMR (125 MHz, MeOD):  $\delta$  173.59, 171.05, 161.68, 161.40, 157.23, 154.05, 144.19, 142.50, 139.6, 138.16, 137.61, 137.60, 137.59, 137.58, 137.56, 136.68, 132.38, 129.91, 128.60, 128.15, 128.11, 127.68, 127.39, 126.06, 123.53, 121.75, 119.87, 113.56, 66.37, 66.24, 54.92, 53.63, 48.47, 45.01, 39.11, 39.05, 31.15, 31.03, 26.67, 26.63, 22.45, 22.35

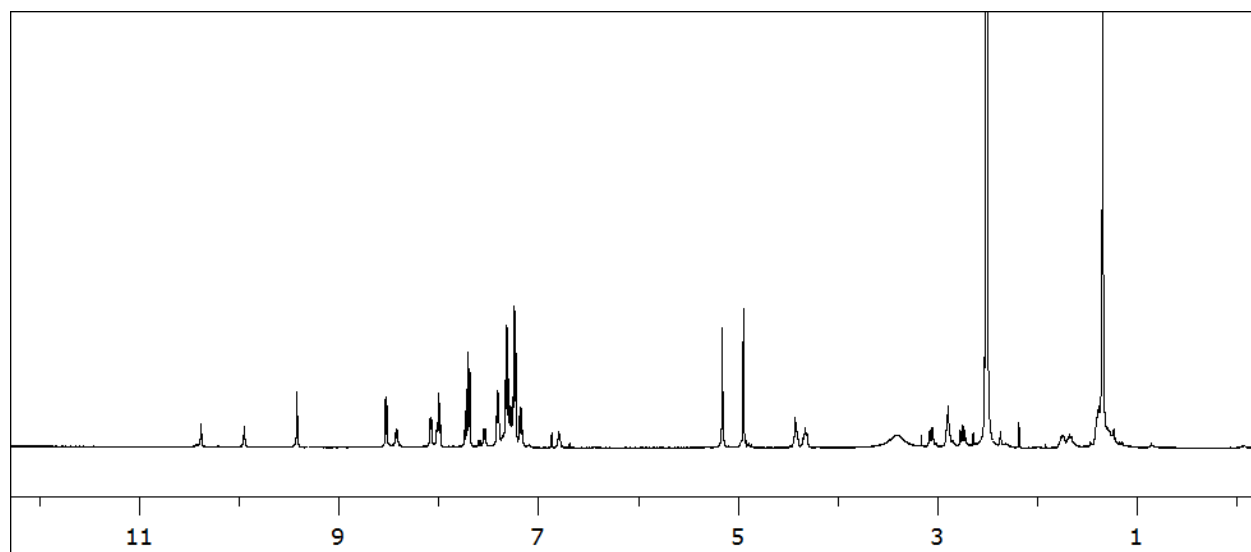
Cbz-Phe-Lys(BOC)-PABA-3AMQ (DMSO) - Proton



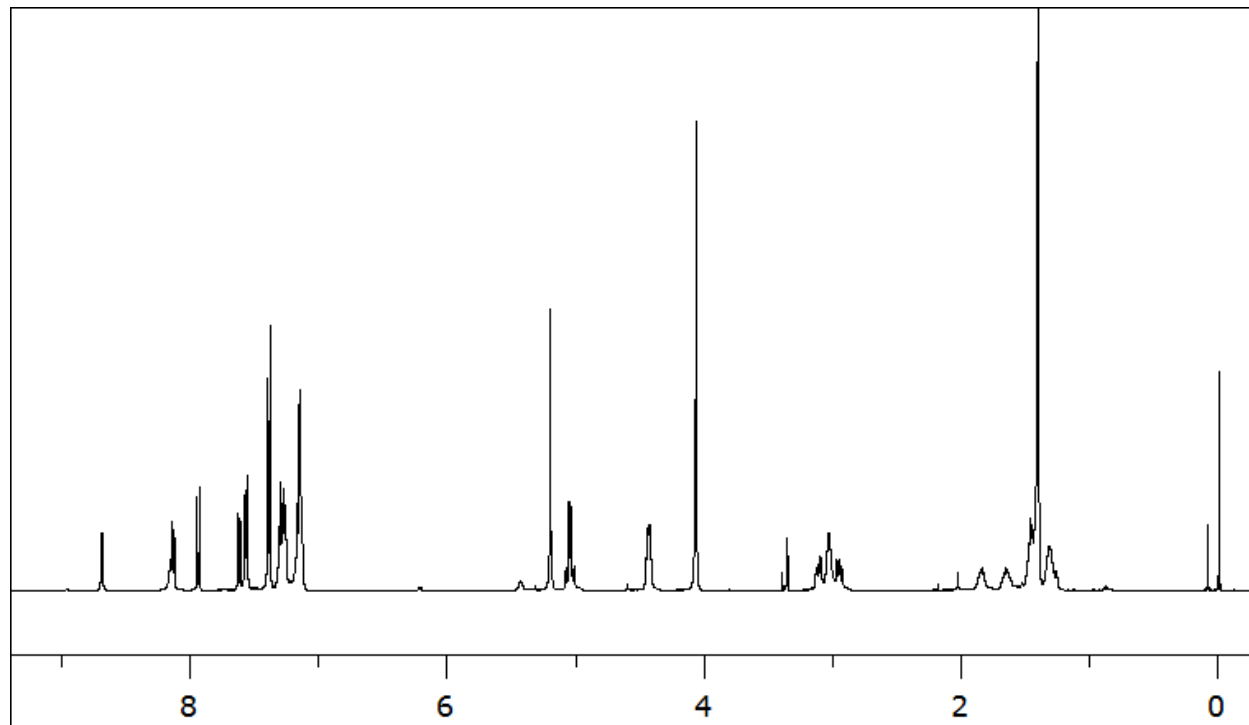
Cbz-Phe-Lys(BOC)-PABA-4AMQ (CDCl<sub>3</sub>) - Proton



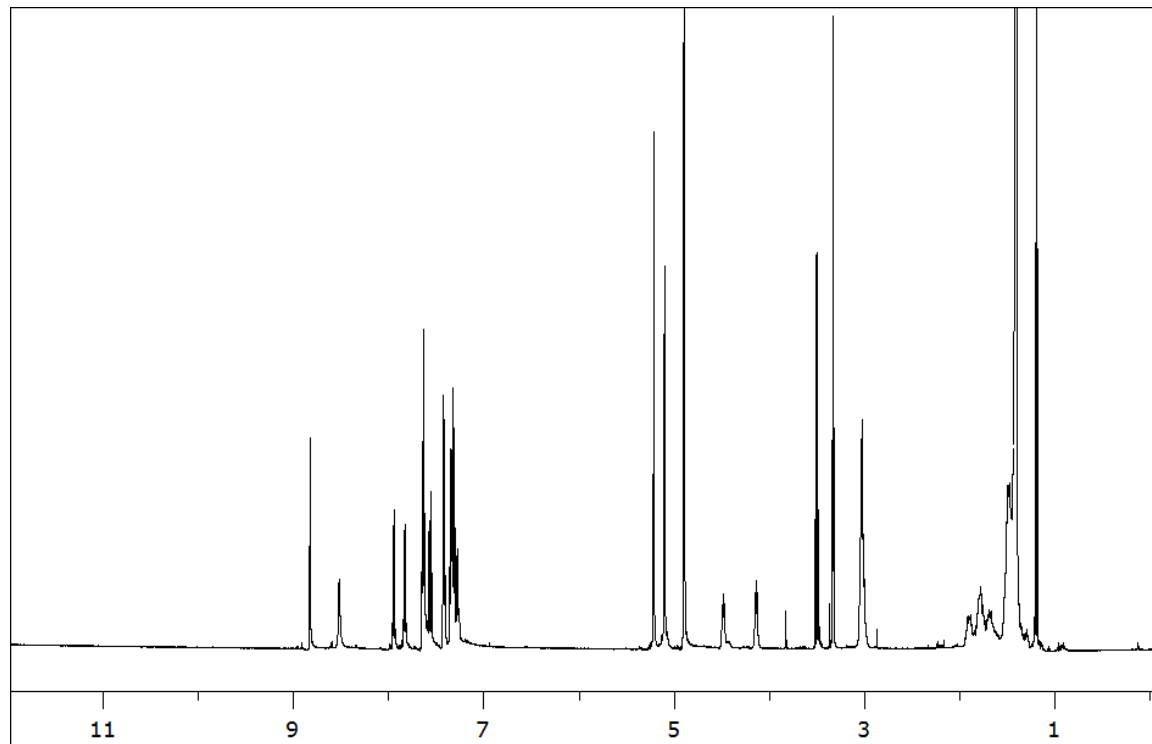
Cbz-Phe-Lys(BOC)-PABA-5AIQ (DMSO) - Proton



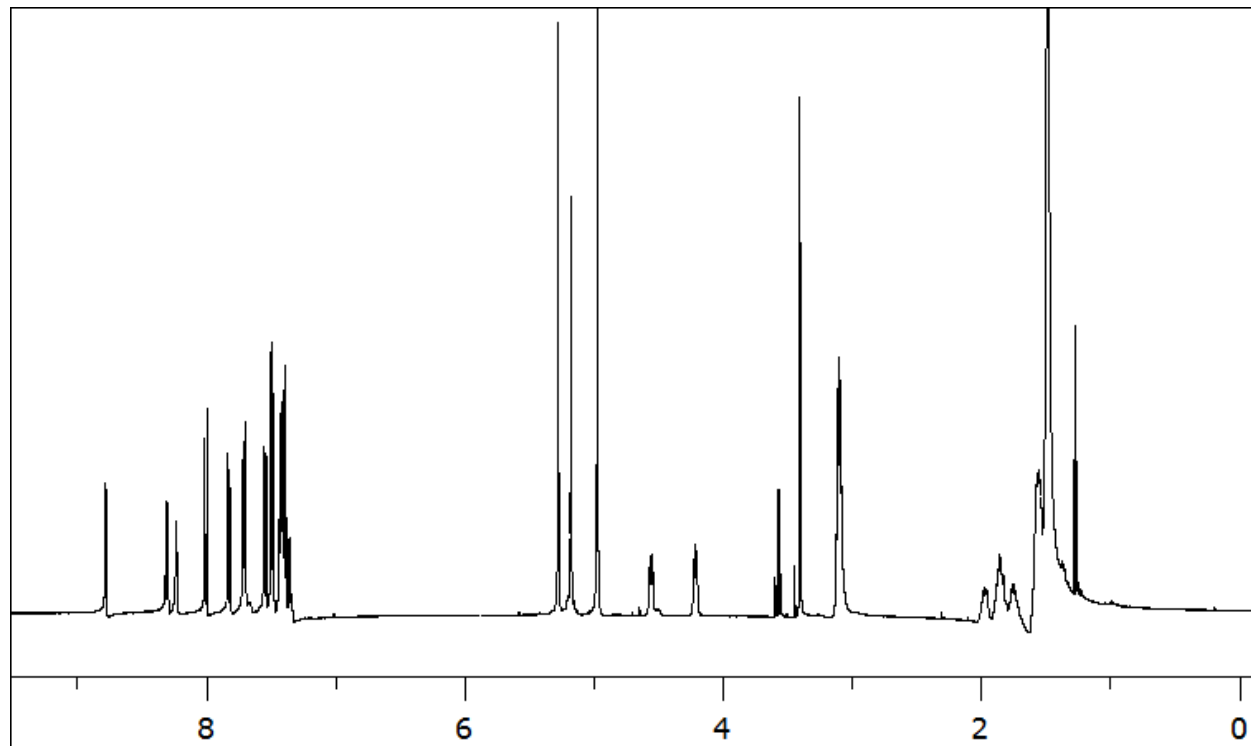
Cbz-Phe-Lys(BOC)-PABA-6AMQ (CDCl<sub>3</sub>, drops of MeOD) - Proton



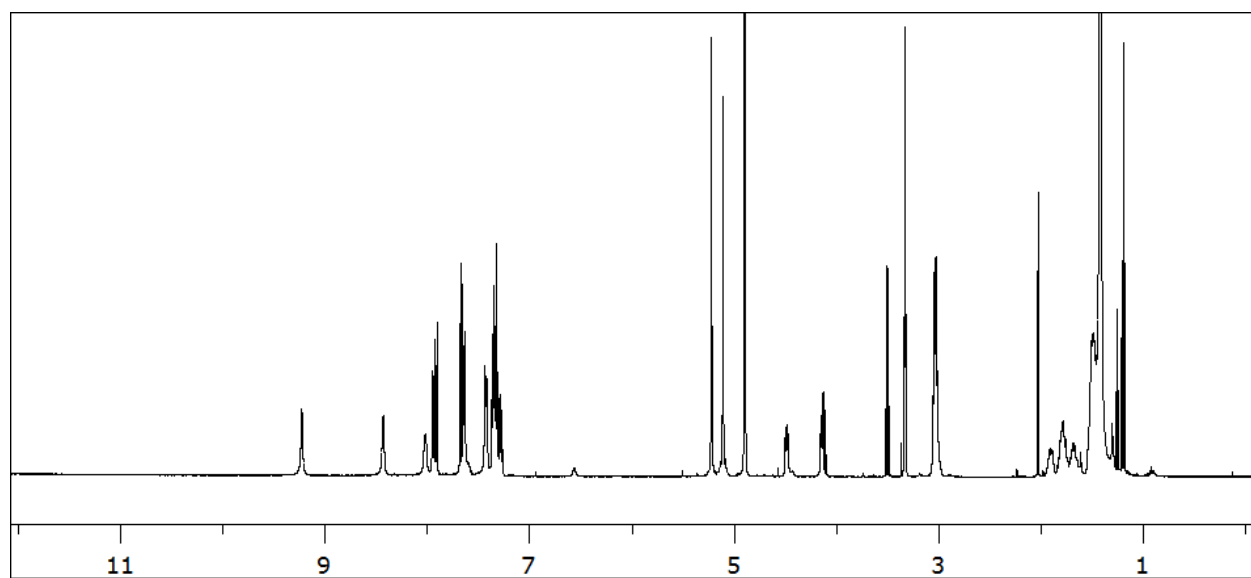
Cbz-Lys(BOC)-Lys(BOC)-PABA-3AMQ (DMSO) - Proton



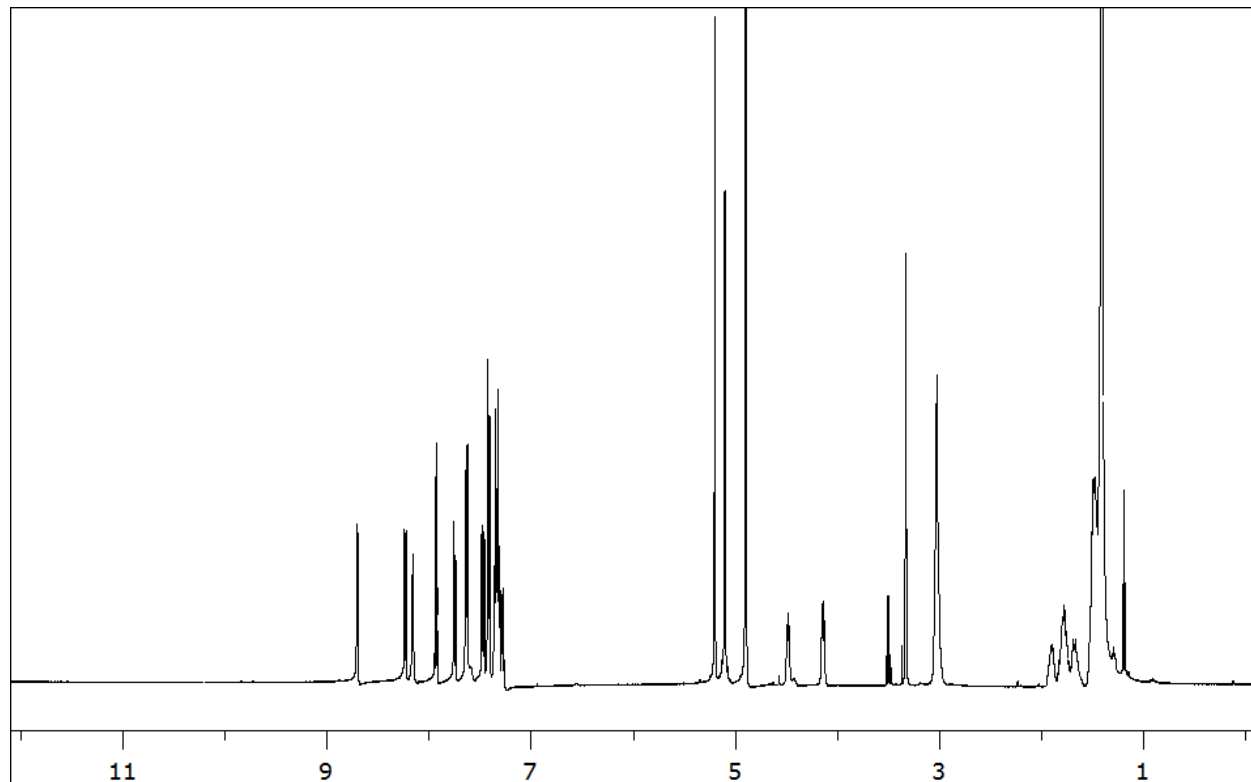
Cbz-Lys(BOC)-Lys(BOC)-PABA-4AMQ (CDCl<sub>3</sub>) - Proton



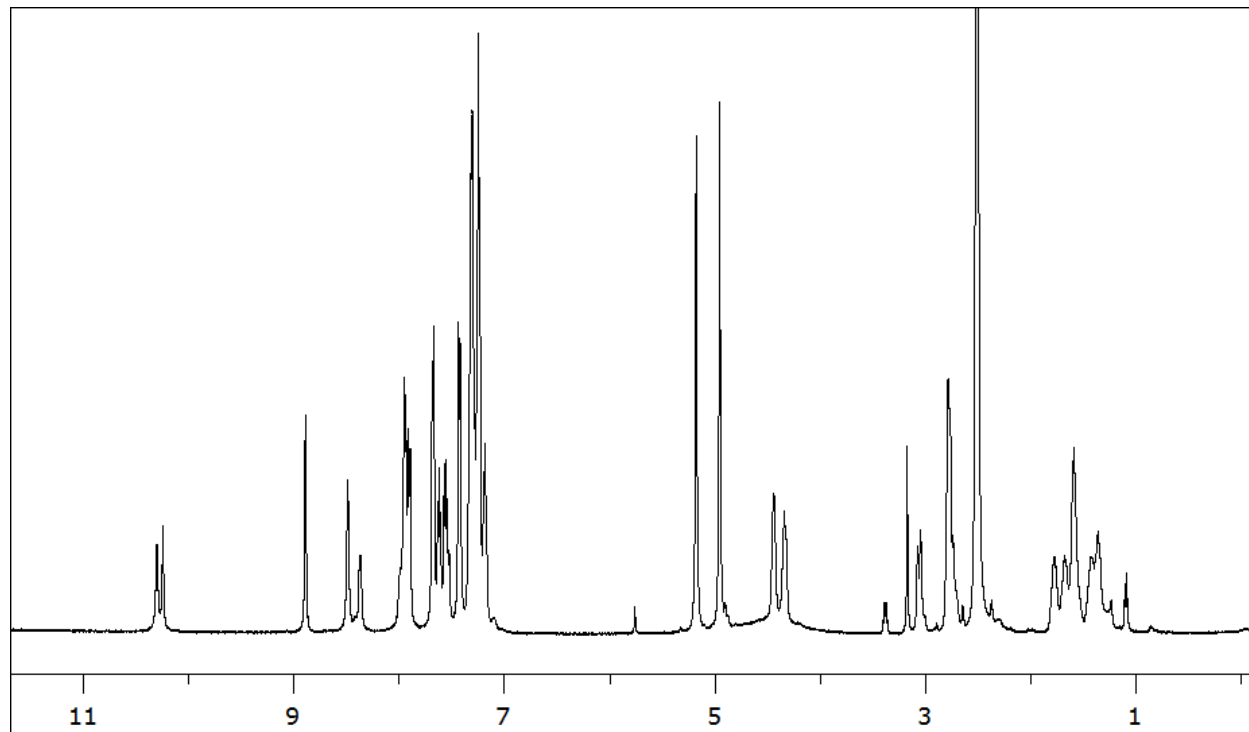
Cbz-Lys(BOC)-Lys(BOC)-PABA-5AIQ (MeOD) - Proton



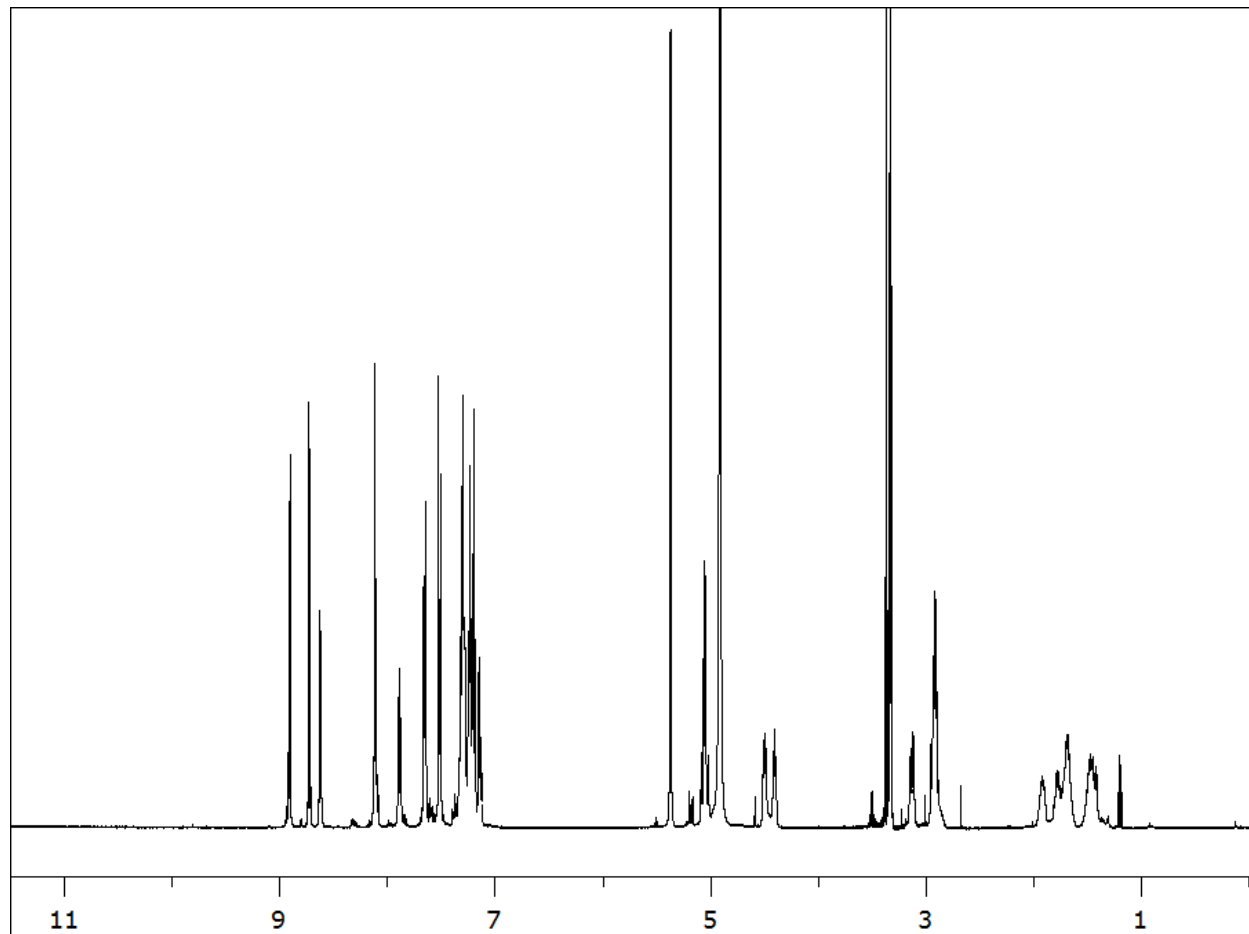
Cbz-Lys(BOC)-Lys(BOC)-PABA-6AMQ (MeOD) - Proton



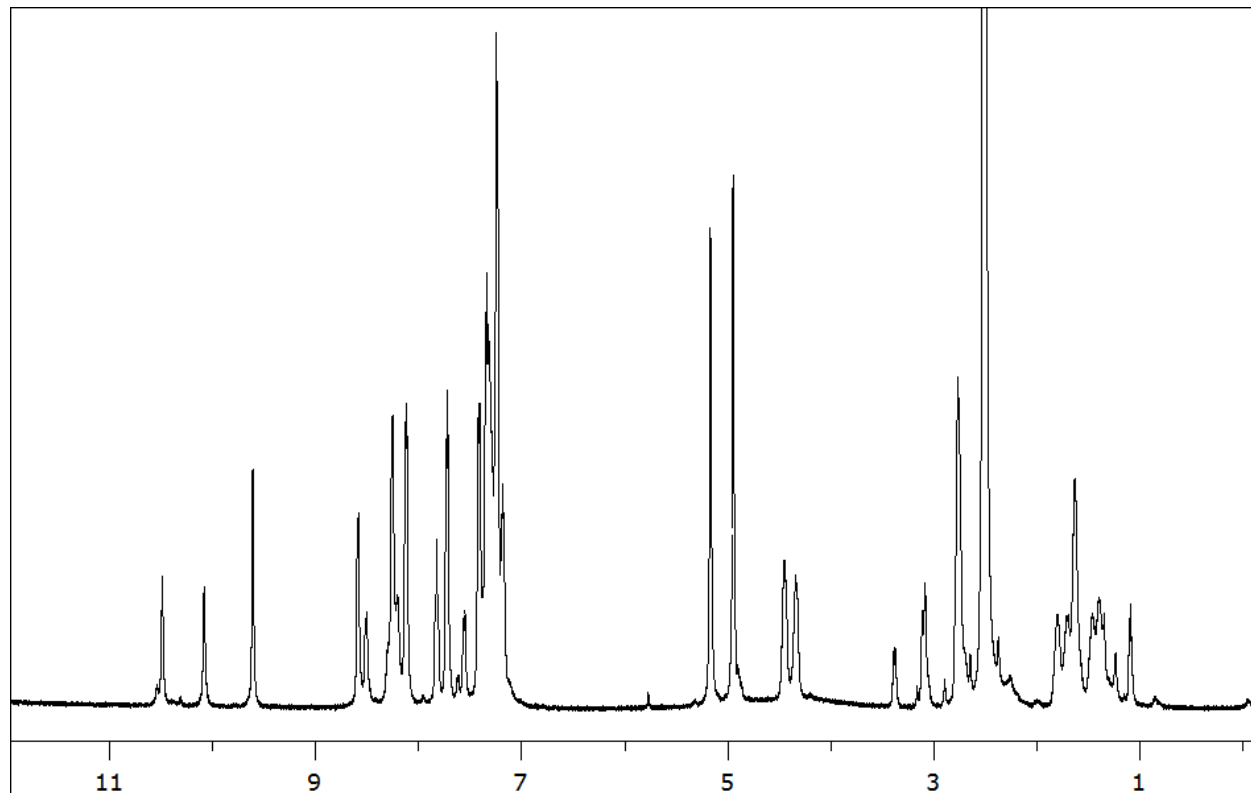
Cbz-Phe-Lys(TFA)-PABA-3AMQ (DMSO) - Proton



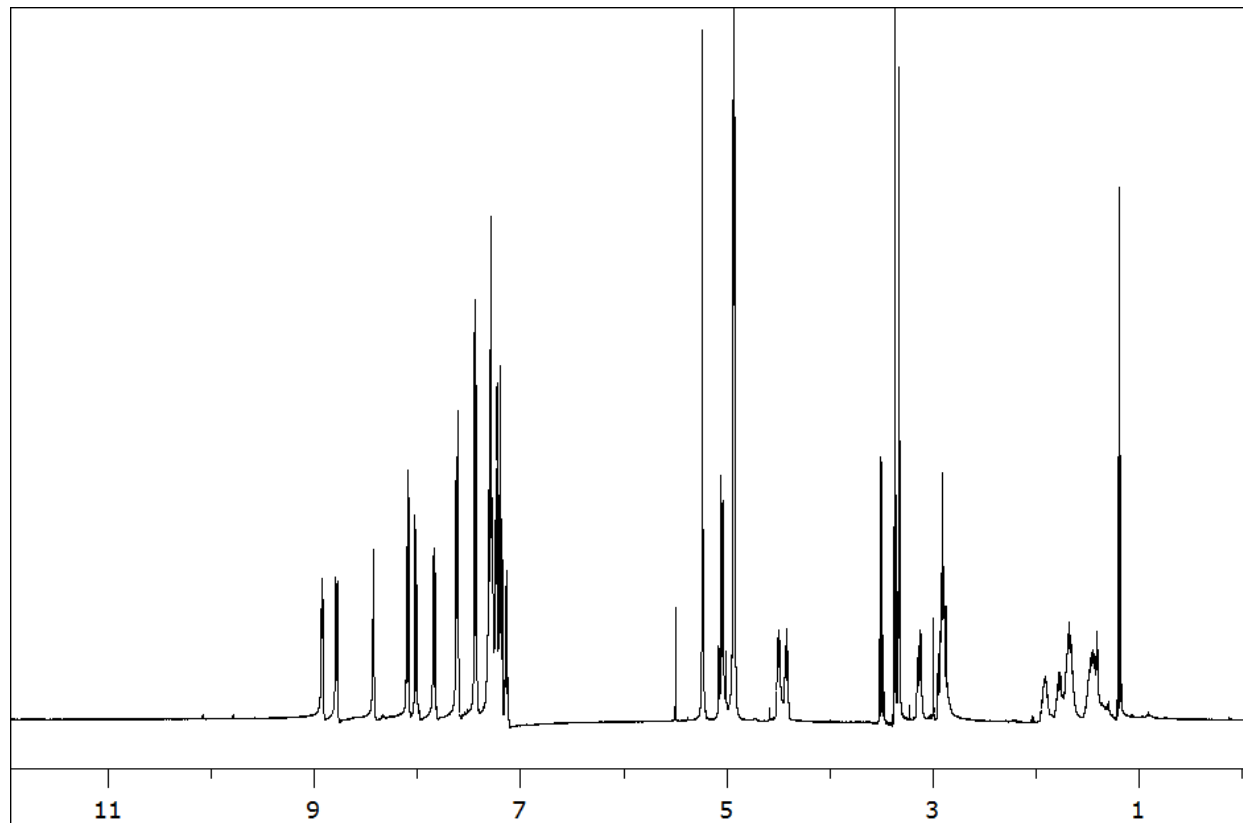
Cbz-Phe-Lys(TFA)-PABA-4AMQ (MeOD) - Proton



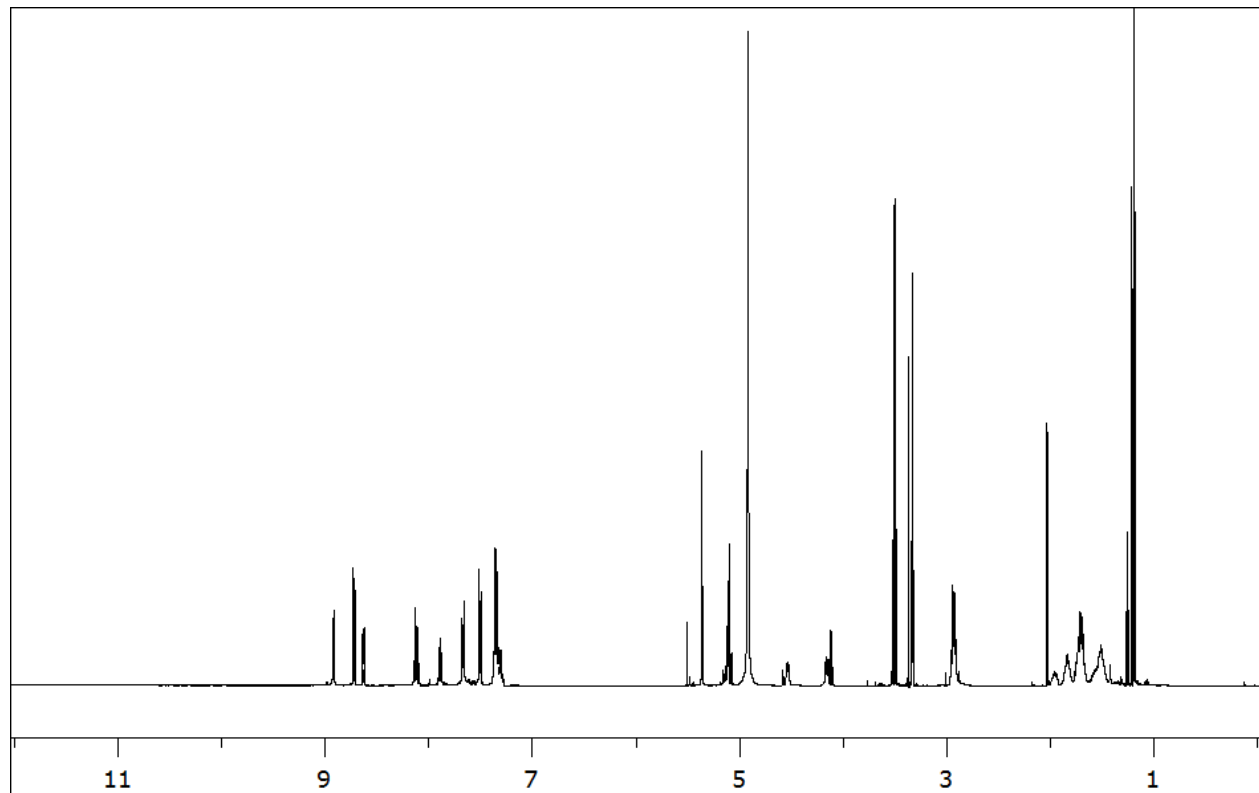
Cbz-Phe-Lys(TFA)-PABA-5AIQ (DMSO) - Proton



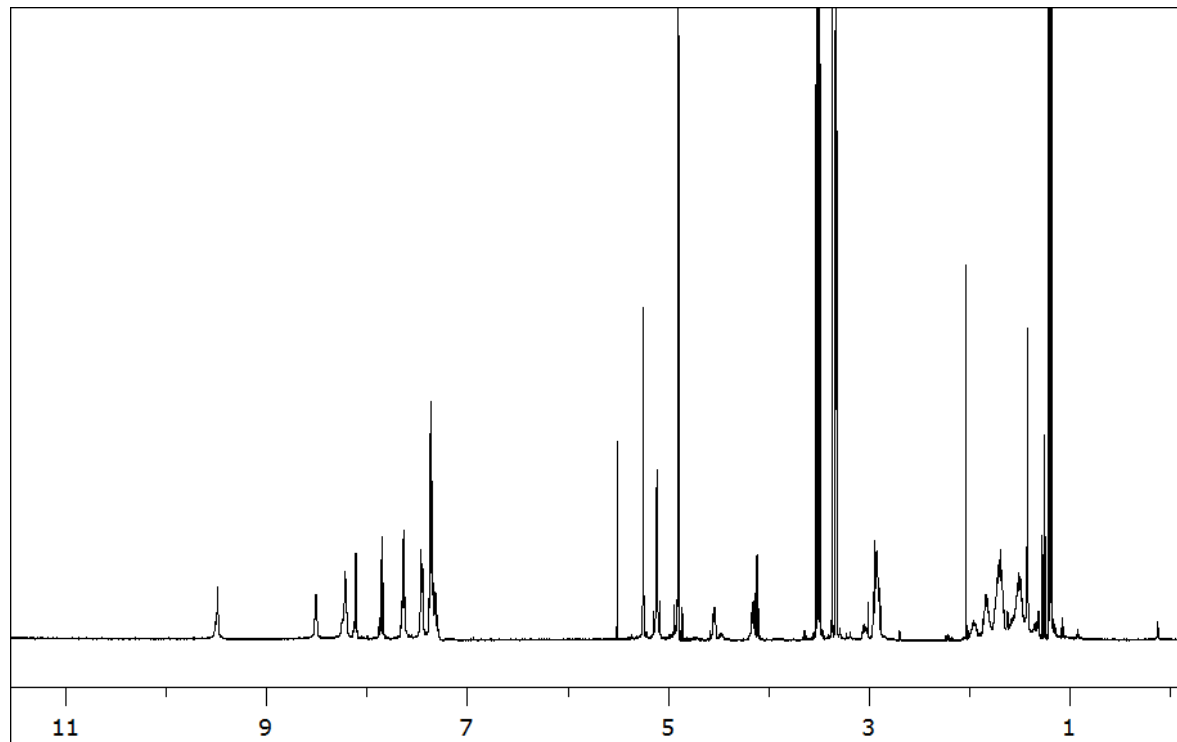
Cbz-Phe-Lys(TFA)-PABA-6AMQ (MeOD) - Proton



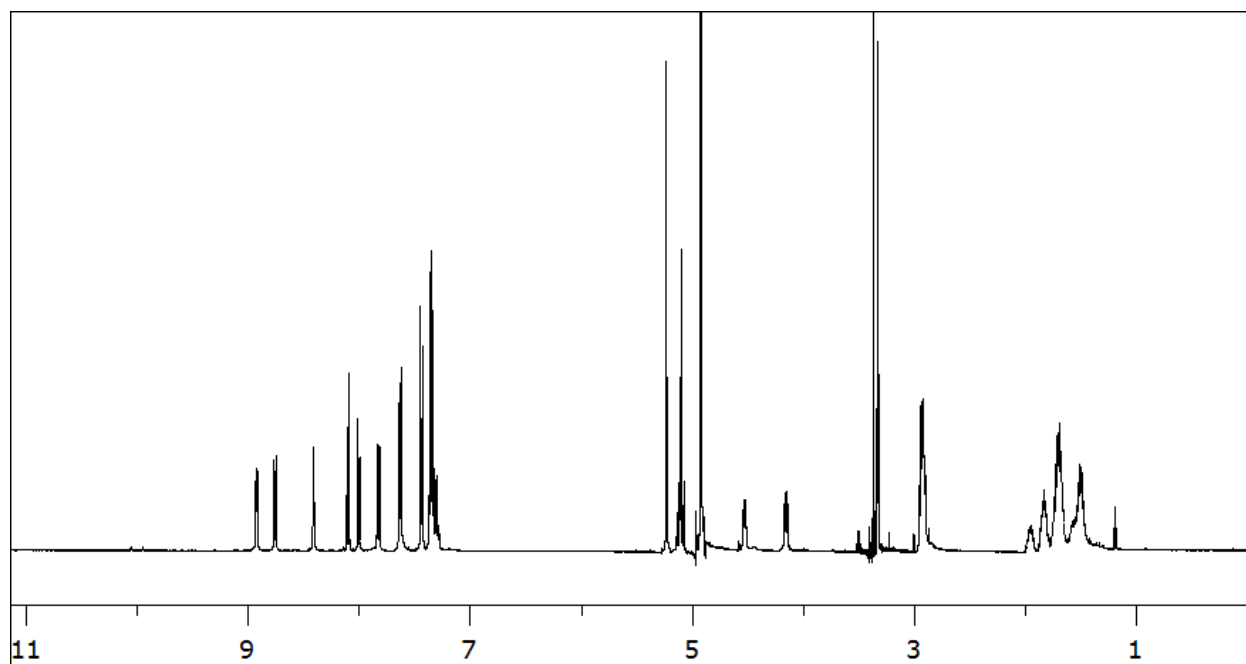
Cbz-Lys(TFA)-Lys(TFA)-PABA-4AMQ (MeOD) - Proton



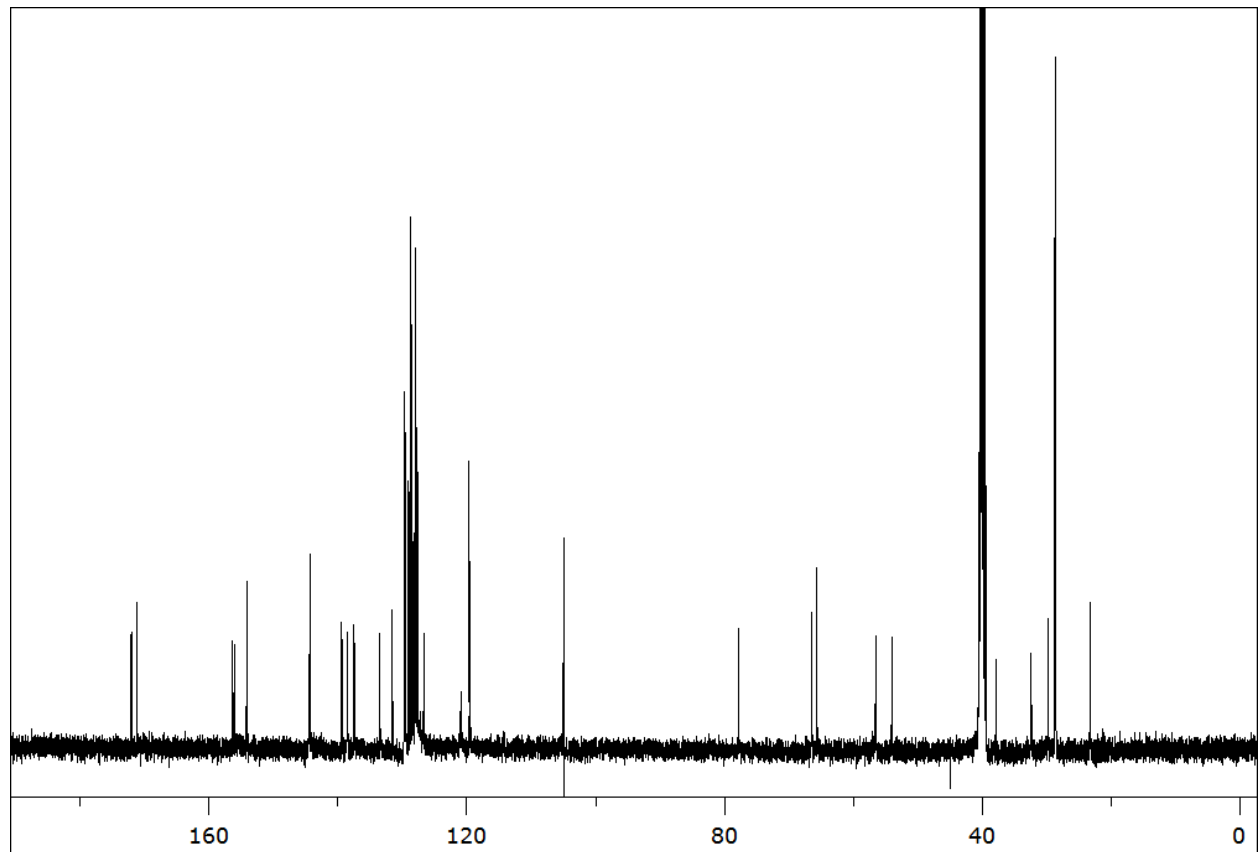
Cbz-Lys(TFA)-Lys(TFA)-PABA-5AIQ (MeOD) - Proton



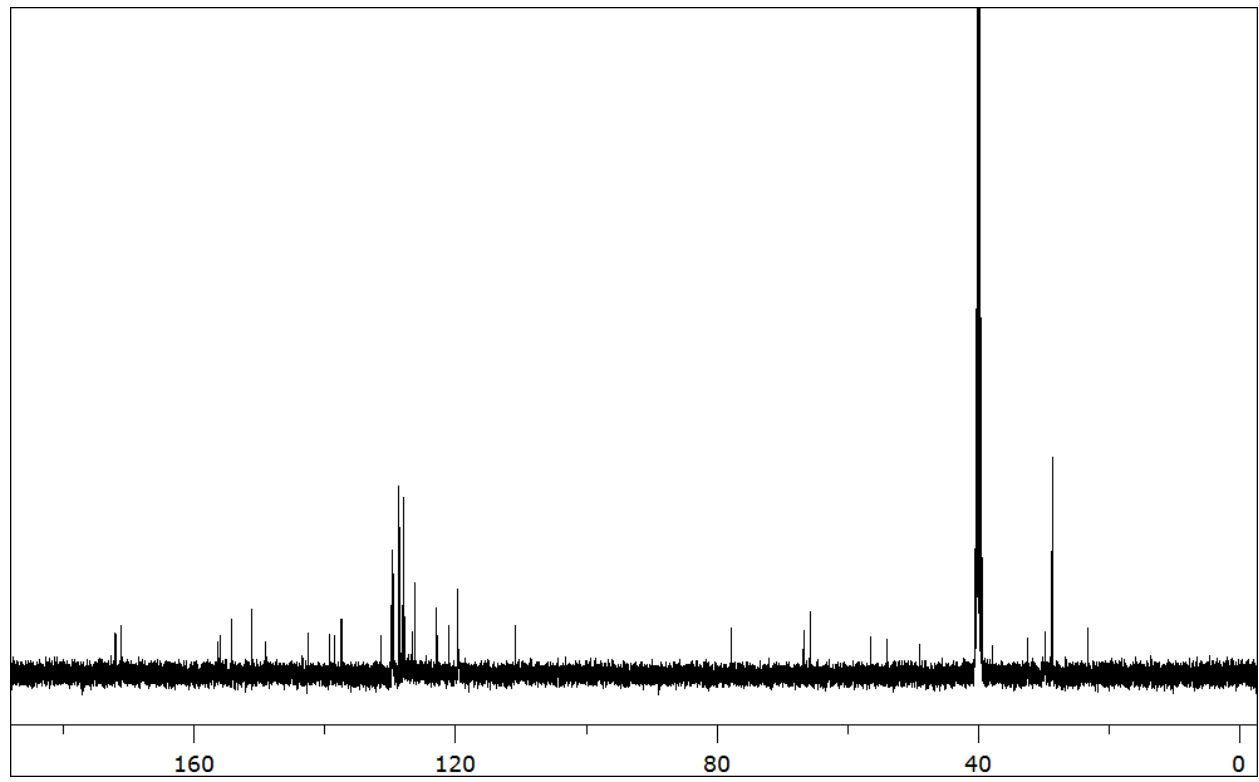
Cbz-Lys(TFA)-Lys(TFA)-PABA-6AMQ (MeOD) - Proton



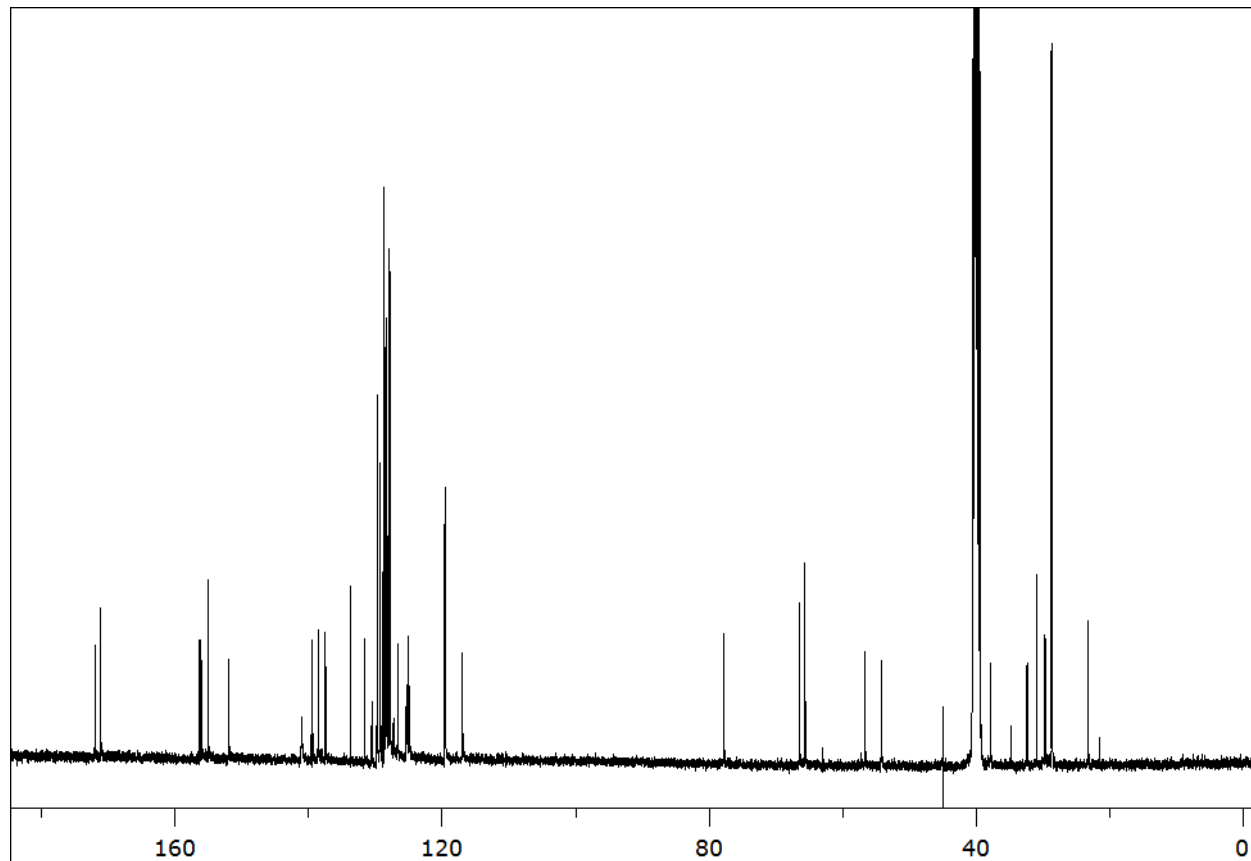
Cbz-Phe-Lys(BOC)-PABA-3AMQ (DMSO) - Carbon



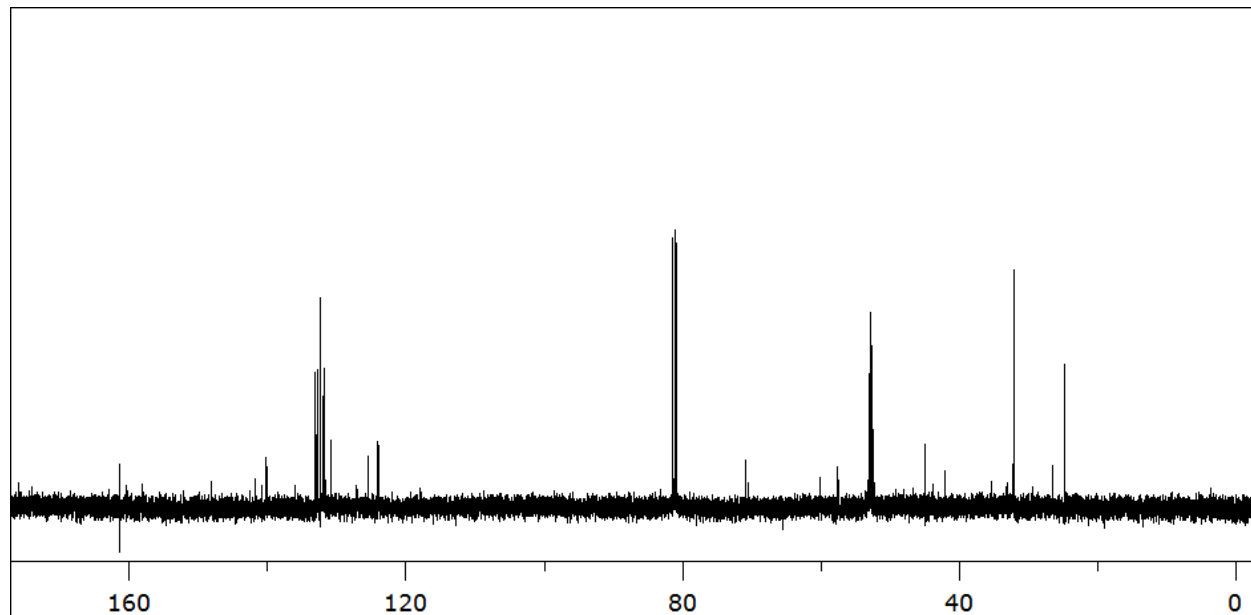
Cbz-Phe-Lys(BOC)-PABA-4AMQ (DMSO) - Carbon



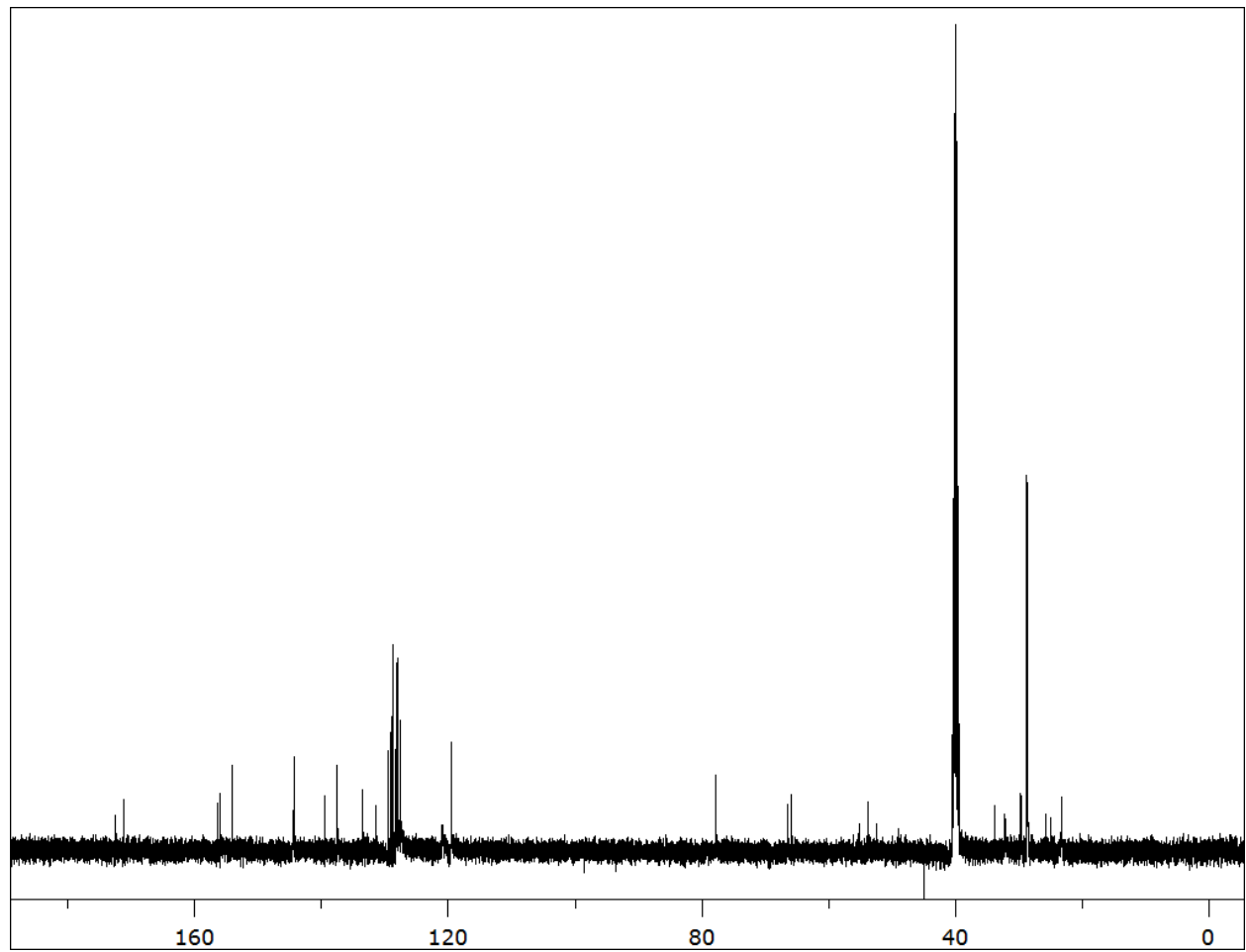
Cbz-Phe-Lys(BOC)-PABA-5AIQ (DMSO) - Carbon



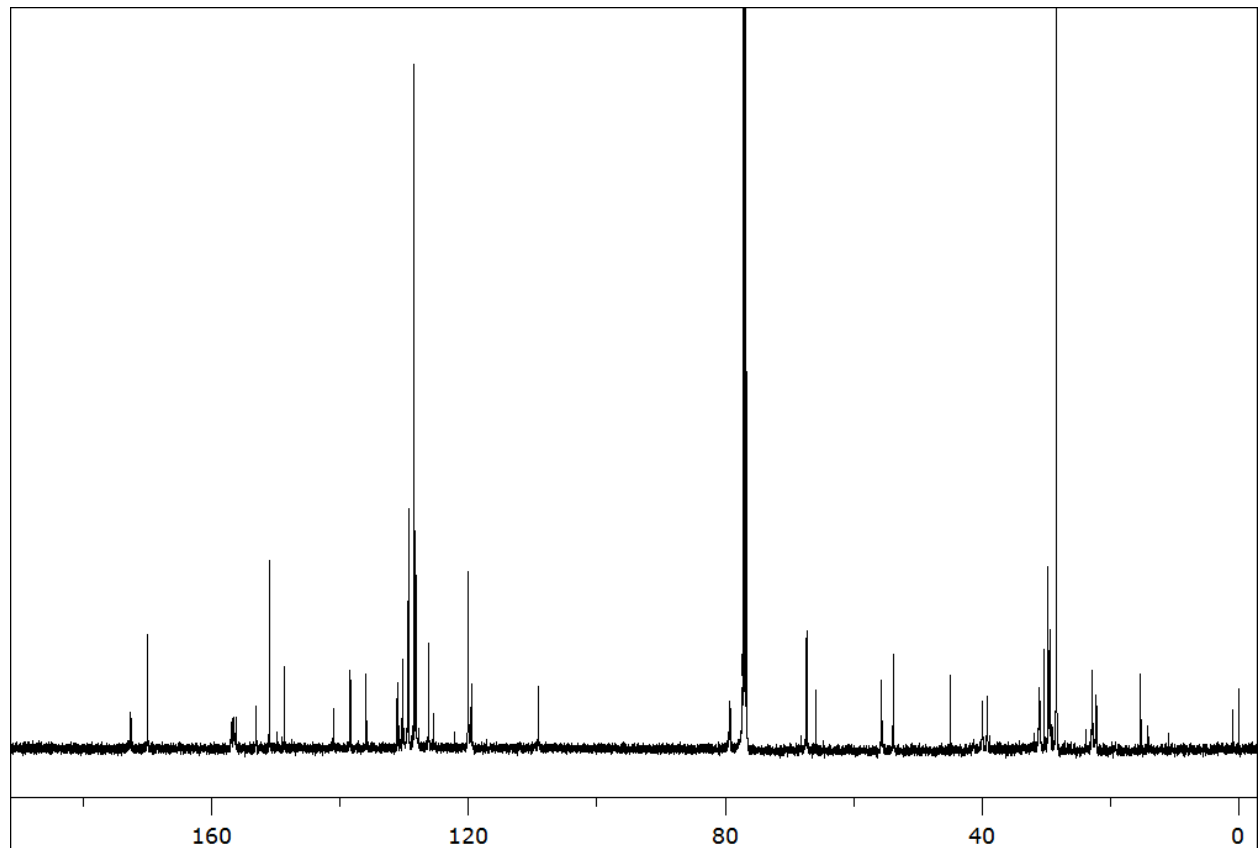
Cbz-Phe-Lys(BOC)-PABA-6AMQ (CDCl<sub>3</sub>) - Carbon



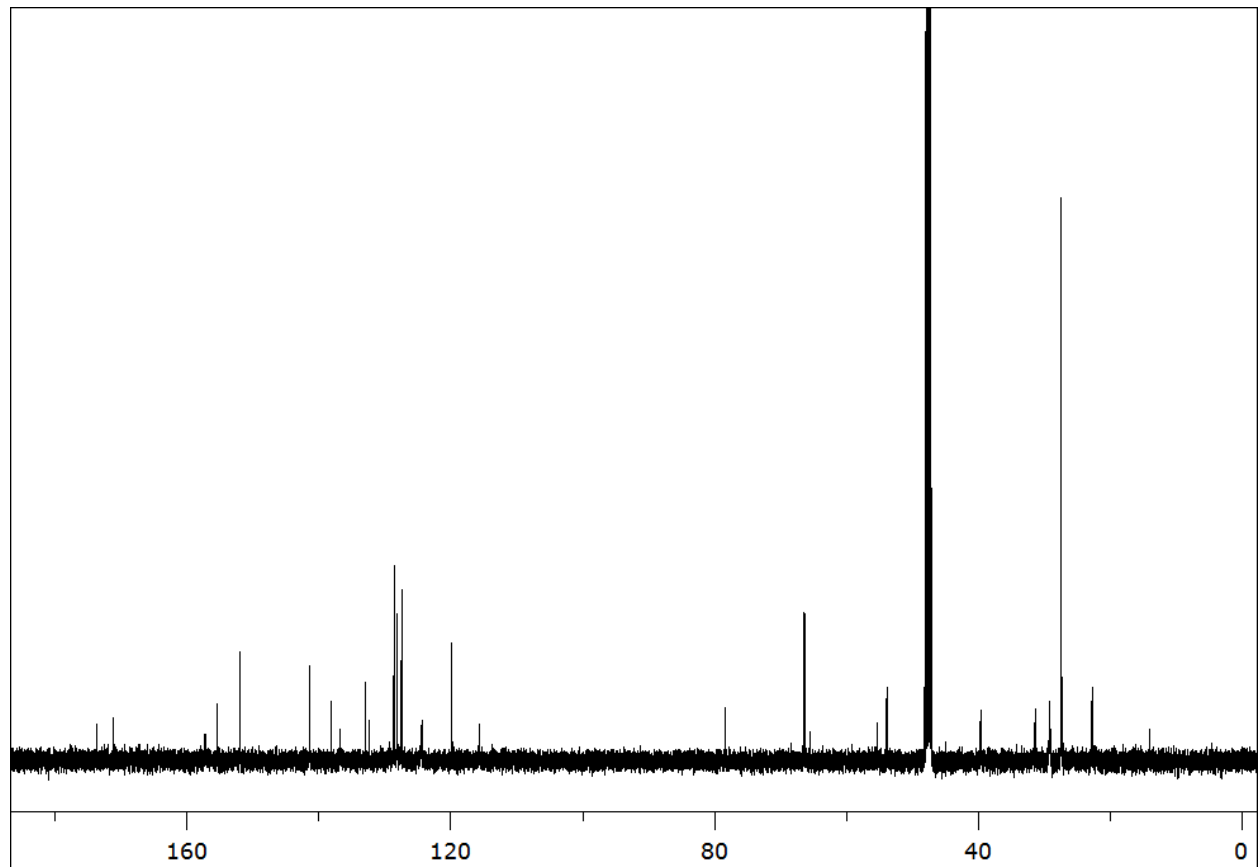
Cbz-Lys(BOC)-Lys(BOC)-PABA-3AMQ (DMSO) - Carbon



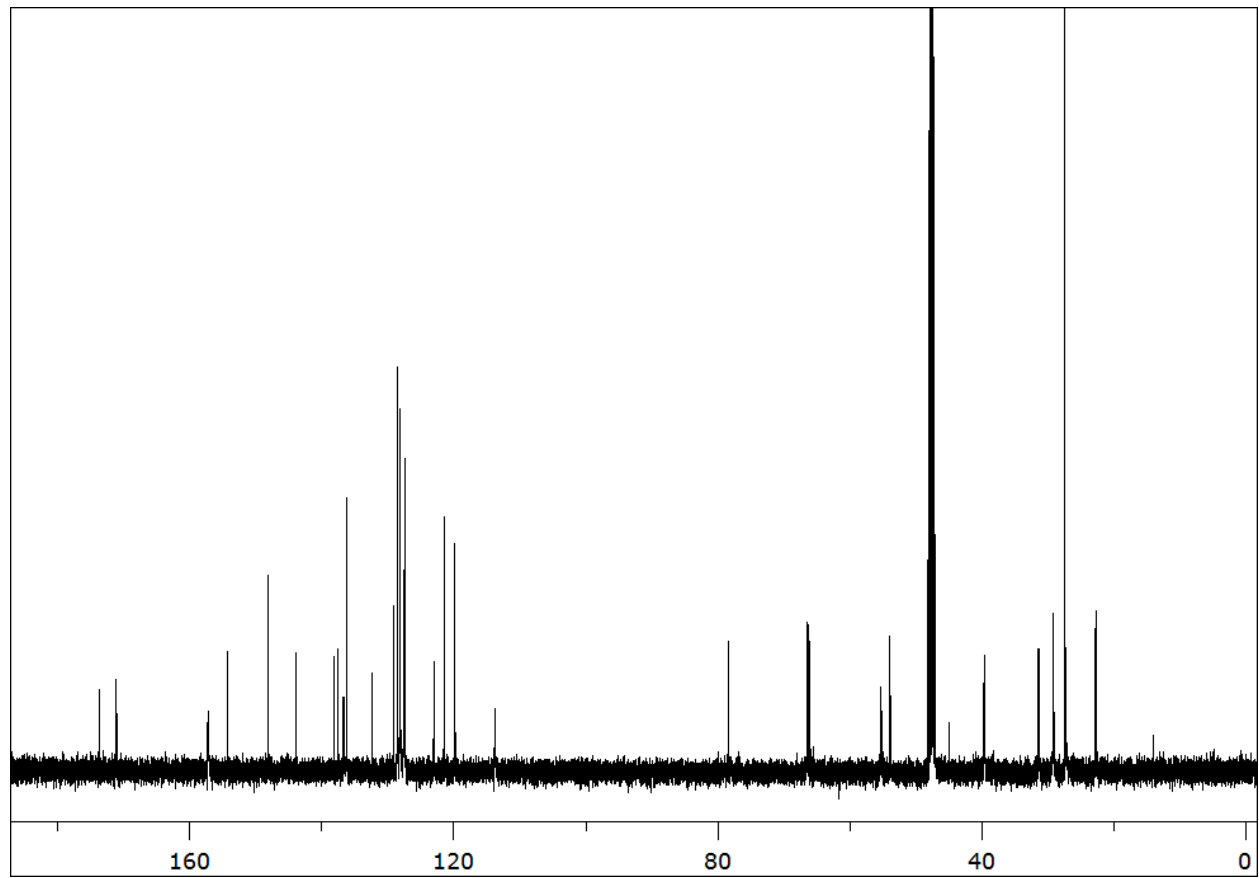
Cbz-Lys(BOC)-Lys(BOC)-PABA-4AMQ (CDCl<sub>3</sub>) - Carbon



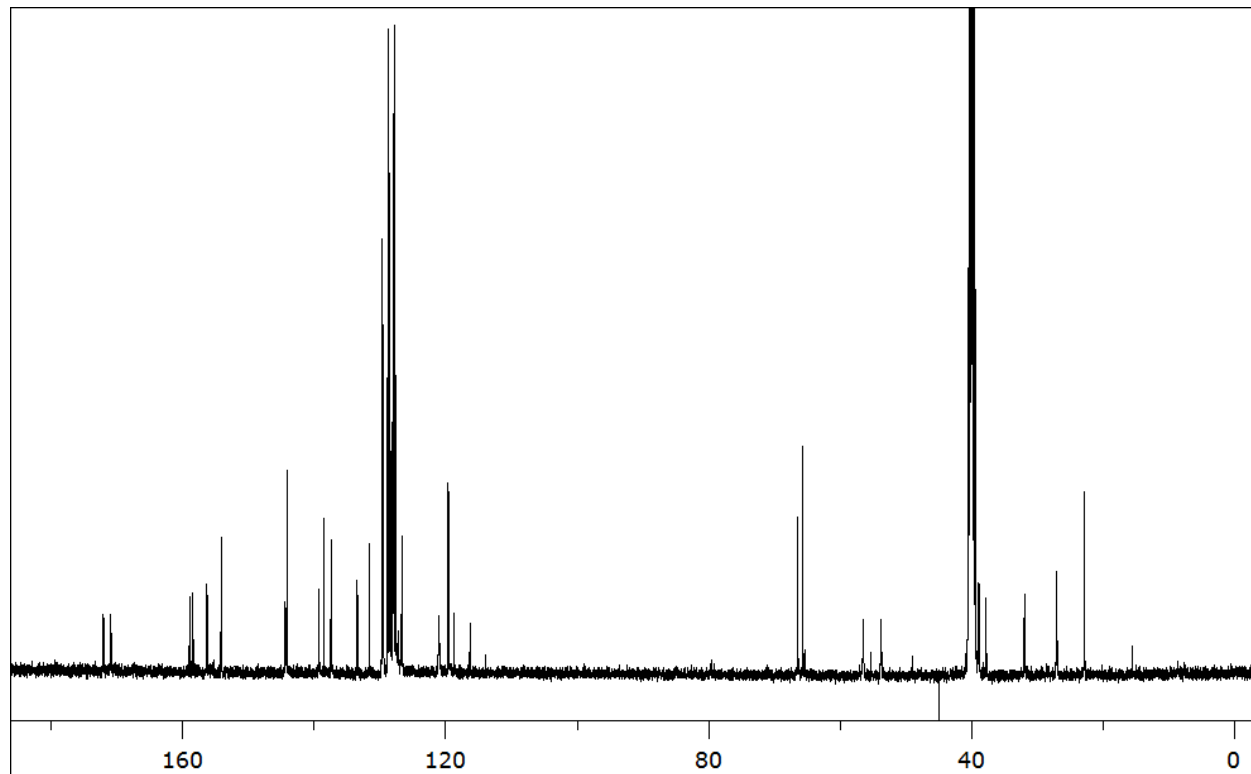
Cbz-Lys(BOC)-Lys(BOC)-PABA-5AIQ (MeOD) - Carbon



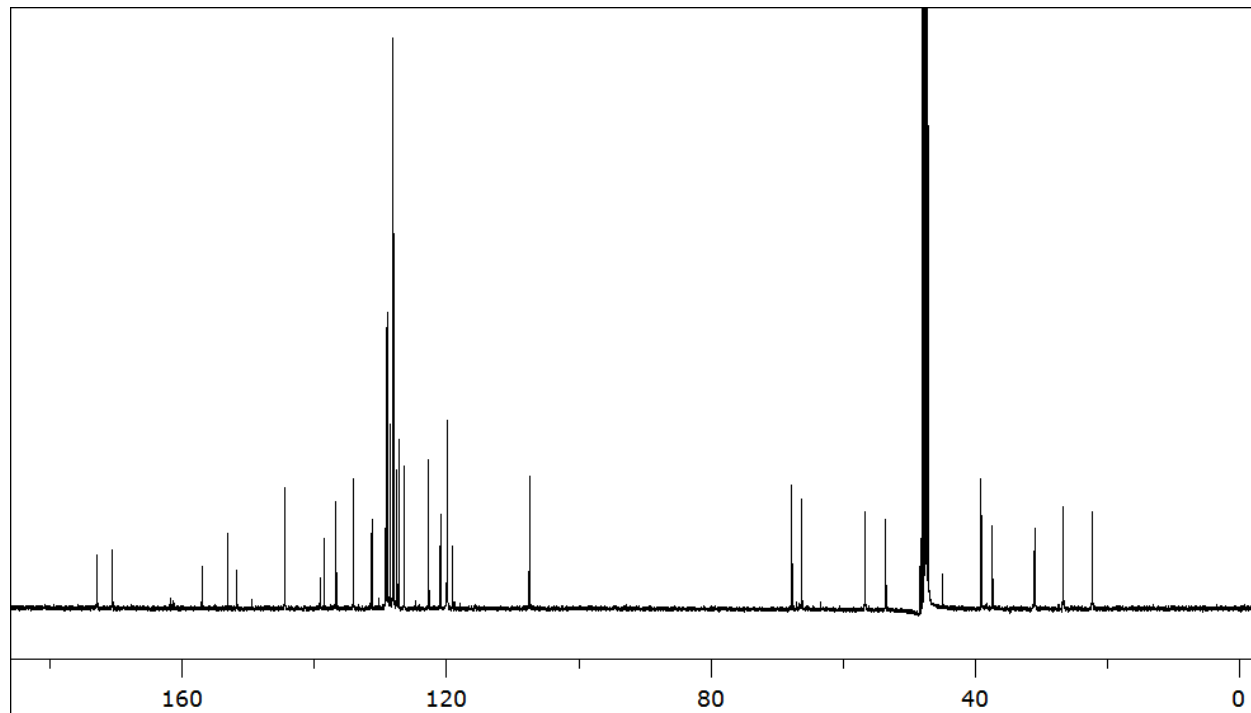
Cbz-Lys(BOC)-Lys(BOC)-PABA-6AMQ (MeOD) - Carbon



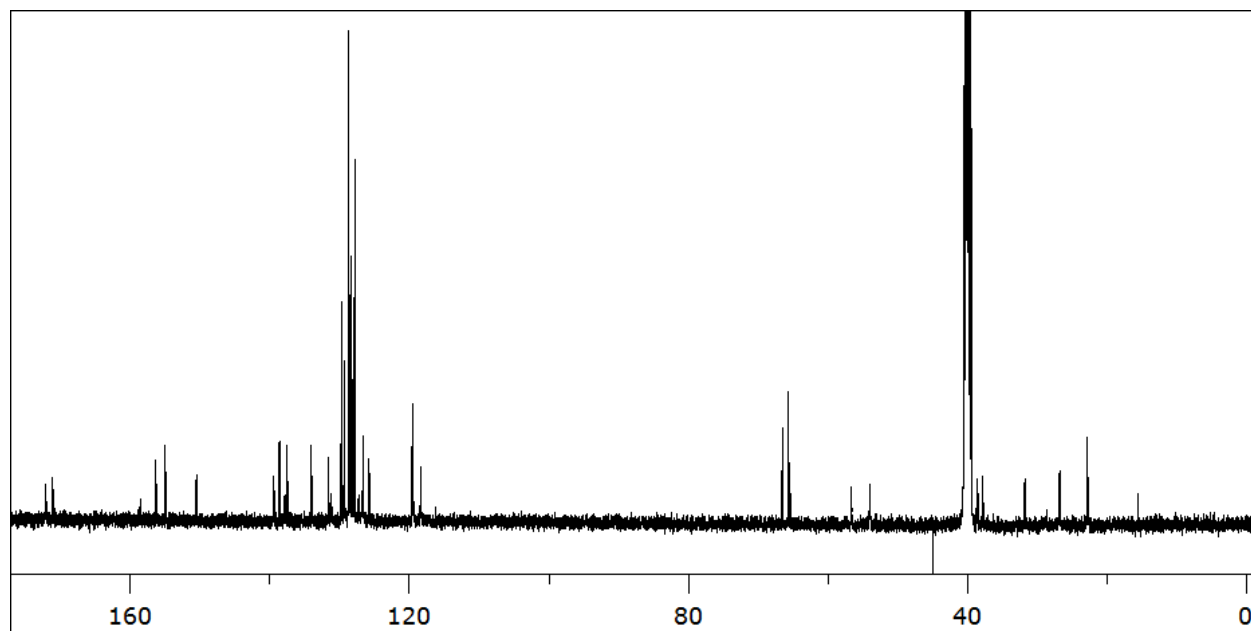
Cbz-Phe-Lys(TFA)-PABA-3AMQ (DMSO) - Carbon



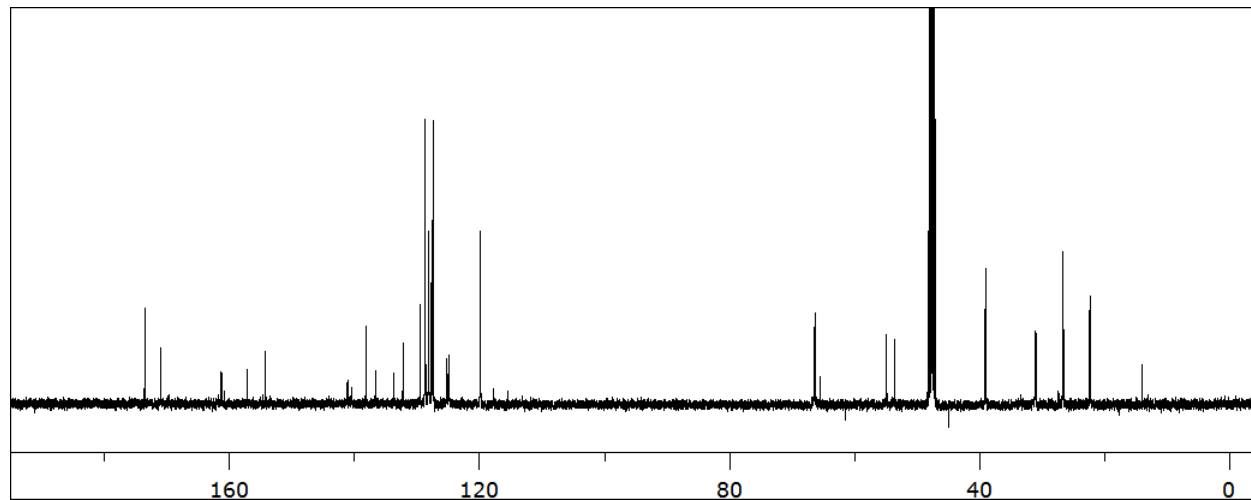
Cbz-Phe-Lys(TFA)-PABA-4AMQ (MeOD) - Carbon



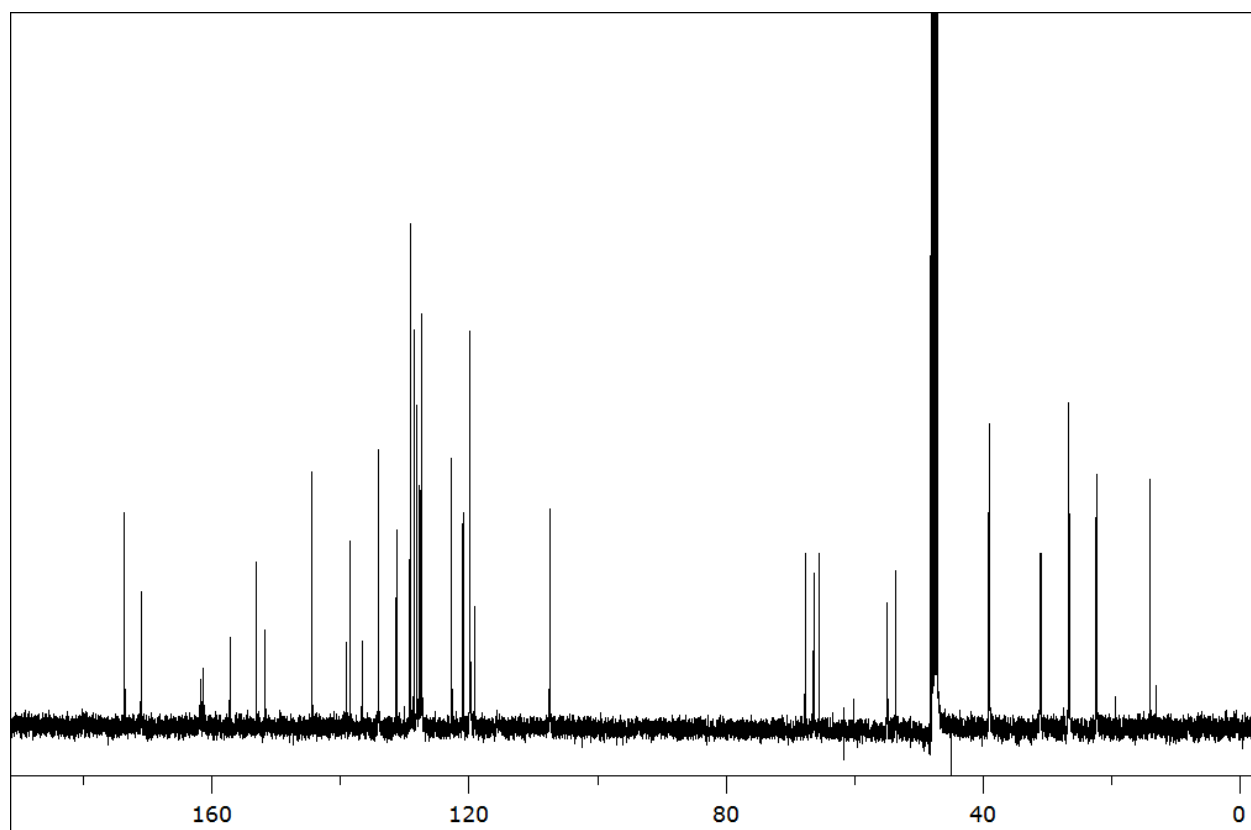
Cbz-Phe-Lys(TFA)-PABA-5AIQ (DMSO) - Carbon



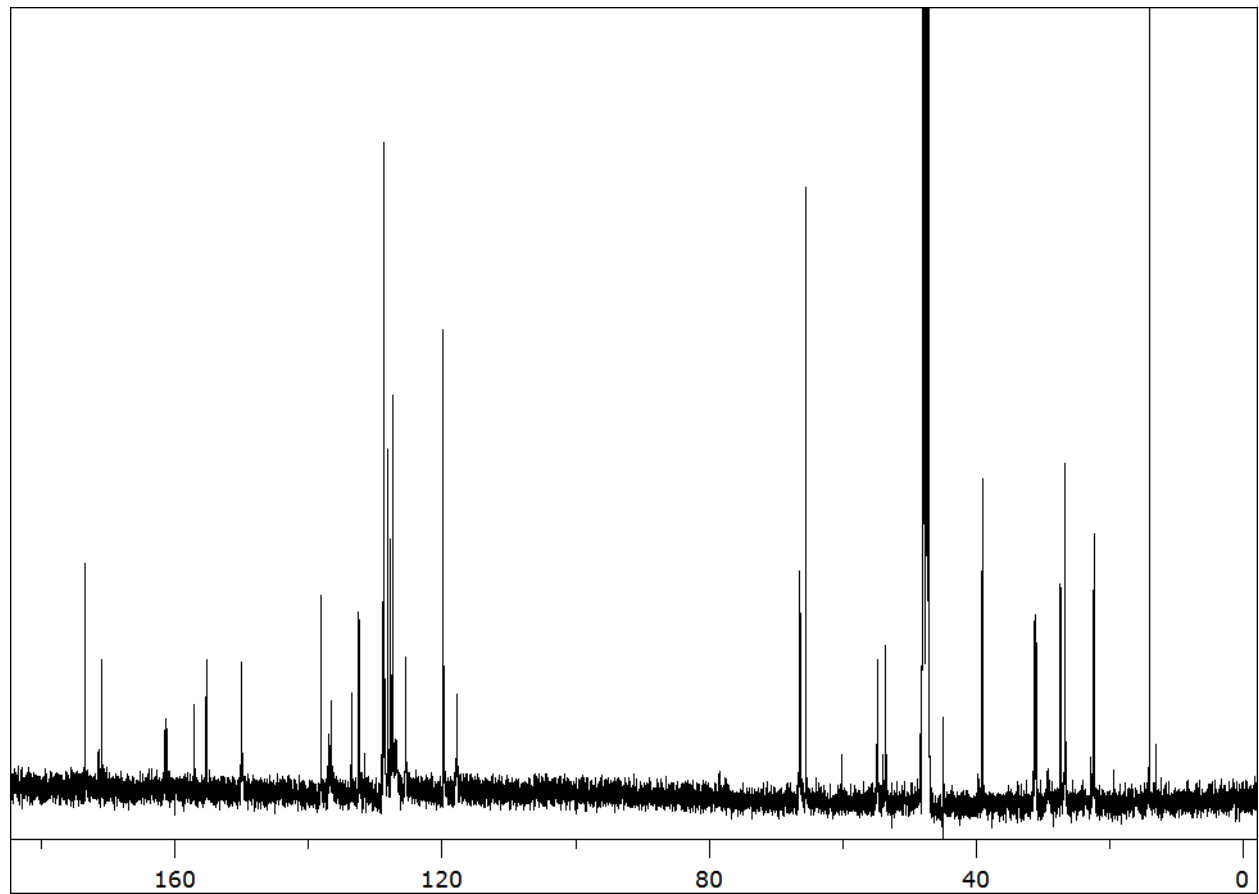
Cbz-Lys(TFA)-Lys(TFA)-PABA-3AMQ (MeOD) - Carbon



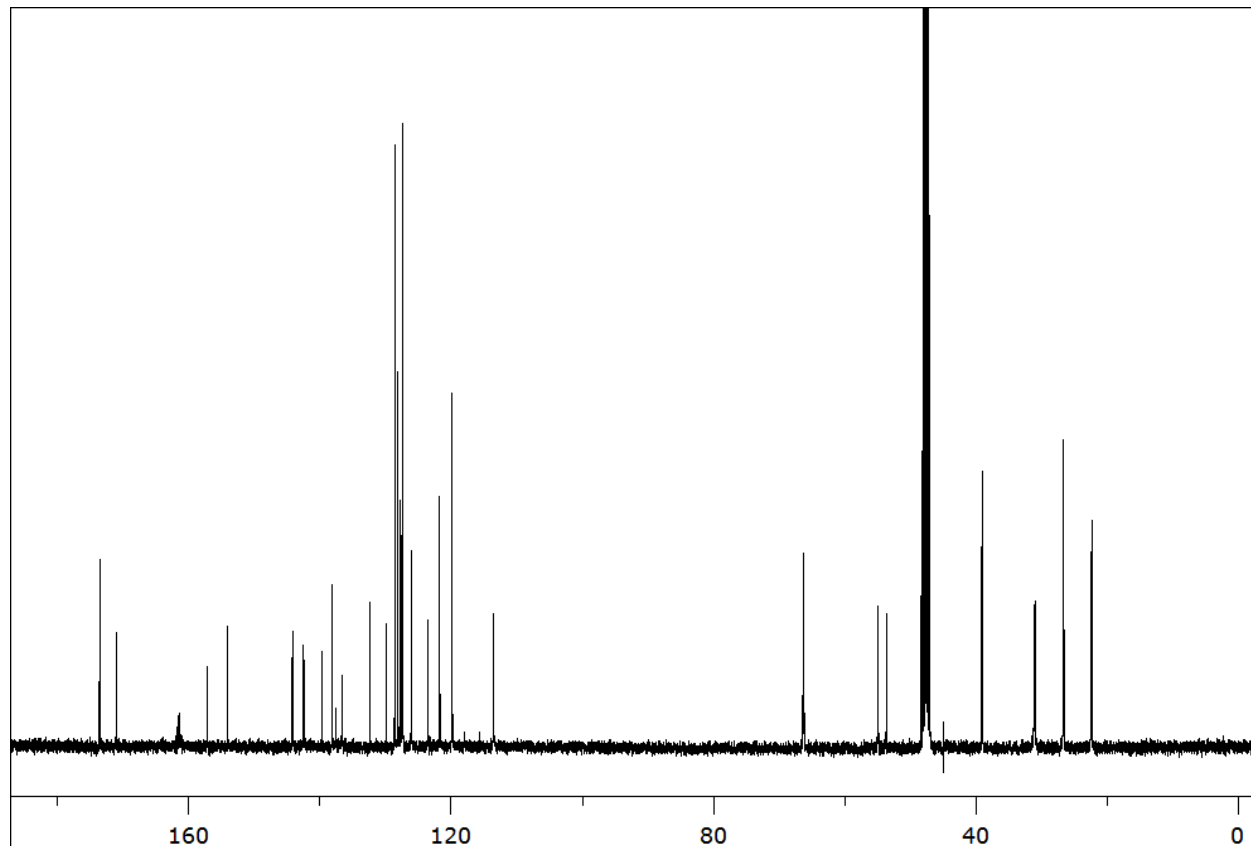
Cbz-Lys(TFA)-Lys(TFA)-PABA-4AMQ (MeOD) - Carbon



Cbz-Lys(TFA)-Lys(TFA)-PABA-5AIQ (MeOD) - Carbon



Cbz-Lys(TFA)-Lys(TFA)-PABA-6AMQ (MeOD) - Carbon



## Chapter 5: Conclusions and Future Work

We developed a convenient route to synthesize a series of probe candidates containing Z-FK-PABA and Z-KK-PABA recognition dipeptides conjugated to four different aminoquinolines intended as potential lysosomotropic reporter molecules. To estimate the enzyme kinetics values associated with each probe candidate, a convenient HPLC method was developed and used to estimate the  $k_{\text{cat}}/K_{\text{M}}$  values using recombinant CTB and CTL. Both the Z-FK-PABA-AQ and Z-KK-PABA-AQ peptides were efficient substrates of CTB. In contrast, CTL hydrolyzed the Z-FK-PABA-AQ probes with exceptionally high  $k_{\text{cat}}/K_{\text{M}}$  values. This suggests that a prodrug inspired approach using lysosomotropic reporters may have utility in detecting cysteine cathepsins activity in cell culture or *in vivo*. This is of particular importance toward the goal of developing substrate-based PET agents that release a radioactive reporter molecule in the lysosomes of cells expressing high levels of CTL. Future work would involve cell assays to determine the membrane permeability of the intact probes, specificity of each probe toward the cysteine cathepsins in cell lysates containing cellular enzymes, and experiments designed to quantify the retention of each quinoline reporter within the lysosome following treatment of cells with each probe candidate. Excitingly, the HPLC method developed for estimating the  $k_{\text{cat}}/K_{\text{M}}$  values in this thesis could be used to quantify the aminoquinoline isomers in each instance.

It is relevant to point out that a substrate-based approach using prodrug inspired chemistry designed to release a lysosomotropic reporter is applicable to various lysosomal enzymes including several aspartic and serine proteases. In addition, other enzyme classes that operate within the lysosome, such as phosphatases and glycosidases, may be excellent candidates using a similar approach.